An Ankle Robot for a Modular Gait Rehabilitation System

by

Jason W. Wheeler

Submitted to the Department of Mechanical Engineering
in partial fulfillment of the requirements for the degree of

Master of Science in Mechanical Engineering

at the

MASSACHUSETTS INSTITUTE OF TECHNOLOGY

May 2004 [June 2004]

Author .....
Department of Mechanical Engineering
May 7, 2004

Certified by.....
Hermano Igo Krebs
Principal Research Scientist
Thesis Supervisor

Accepted by.....
Ain Sonin
Chairman, Department Committee on Graduate Students

An Ankle Robot for a Modular Gait Rehabilitation System

by

Jason W. Wheeler

Submitted to the Department of Mechanical Engineering
on May 7, 2004, in partial fulfillment of the
requirements for the degree of
Master of Science in Mechanical Engineering

Abstract

Patients with neurological disorders, such as stroke survivors, can be treated with physical rehabilitation to regain motor control and function. Conventional therapy techniques are labor intensive and non-standardized. This is especially true in gait rehabilitation. The robotic therapy paradigm developed in the Newman Lab for Human Rehabilitation uses low impedance robots, such as the MIT-MANUS, to provide assistive therapy in a repeatable and measurable fashion. A system is now being designed to assist gait rehabilitation using a series of lower extremity and pelvis robots that can be used together or independently. The focus of this document is ankle rehabilitation. Ankle function is typically not targeted in conventional or other robotic therapy systems. The result is often that the patient is required to wear a brace or orthosis after therapy. The proposed module allows all normal ankle movements and is capable of driving the two most important movements in gait, dorsi/plantar flexion and inversion/eversion. It is designed to provide sufficient force to position the foot in swing phase while still being as lightweight and backdriveable as possible. The kinematics consist of two parallel two-link mechanisms. The robot is driven by two DC brushless motors with planetary gearheads to amplify the torque output.

Thesis Supervisor: Hermano Igo Krebs
Title: Principal Research Scientist

Acknowledgments

If you're wondering, as you should be, how I ever made it to this point, the answer is in this section. I have been extremely blessed to be surrounded by good and smart people, to whom I owe a great debt of gratitude.

I have learned so much in the past two year working in the Newman Lab. I'd like to thank Neville Hogan and Igo Krebs for their attention to detail and desire to produce only quality work. Their guidance has been invaluable in this work. The other students in the lab have also given insight and made this a more enjoyable place to work. Steve Buerger's expertise and creativity have been a resource that I have used over and over again. He has also done his best to dissuade me from staying for a Ph.D. Jerry Palazzolo was a great help to me in getting acclimated to the lab. He is a talented engineer and you have to get up pretty early in the morning to beat him to the lab. Mike Roberts is a great designer and has contributed to this work in a number of ways. James Celestino was always willing to help and was a great softball team captain (despite his allegiance to the evil empire). Who can forget the ISN students; Tom Bowers, Chan Rhyou, and Doug Eastman? Tom and I worked exact opposite schedules. I'm not sure he functions correctly during daylight hours. Sue Fasoli was a huge help with clinical issues and girl scout cookies.

Special thanks to Prof. David Krebs and Dov Goldvasser from the Biomotion Lab at the Massachusetts General Hospital for the use of their equipment and more importantly, their time and expertise. Fred Cote at the Edgerton Shop was very helpful in the building of mock-ups. Valuable insight into the clinical aspects of the design were given by Doctors Rich Macko, Larry Forrester, and Christopher Bever and their associates from the Baltimore V.A. Hospital. Dustin Williams at Interactive Motion Technologies contributed to the design and ordering of many of the mechanical and electrical components.

I would not be here if it were not for my parents. Their constant support and love means more to me than I think they realize. They have bailed me out of jams more than they can probably remember. Most of all, I have to thank Cecy. She is the

one who inspires me to work hard (but less) so I can come home before she's asleep, even if that's only 9:00. I can't thank her enough for following me on this crazy journey of ambition and adventure. I look forward to a lifetime and more of such adventures. Her family deserves credit for letting me steal her from them temporarily. Then there's little Anna. She wasn't around when we came here two years ago but we're sure glad she's here now. She brightens everything we do.

Contents

Chapter 1

Introduction

1.1 Motivation

There are millions of individuals who suffer from some kind of gait disability. Many of these people require either rehabilitation or prosthetic devices. Current rehabilitation methods are very labor intensive. Often, multiple therapists are required to perform strenuous physical tasks. There is also a high degree of variability and subjectivity in the current methods.

Robotic technology has proven effective in rehabilitation of the upper limb after stroke [1]. The use of robotic devices in gait rehabilitation could provide an accurate, repeatable method for assisting lower limb movement. It would also provide an accurate way of recording data for gait analysis and an objective measure of rehabilitation.

The goal of this research is to improve the gait rehabilitation process by employing robotic technologies. The scope of the project is to design a system that would support some or all of the patient's body weight while the robotic devices assist in lower limb movement. These robots could drive the patient's gait or be passively moved as the patient walks. These devices could be used either on a treadmill or as an ambulatory device on level ground. This document deals specifically with an ankle module for such a system.

1.2 Stroke

Stroke, or cerebrovascular accident, is one of the leading causes of gait disability. There are approximately four million people in the United States alone who are living with the effects of stroke and about 730,000 new strokes occur each year. About three quarters of these survive [3]. A common result of a stroke is hemiparesis, where part or all of the sensory and motor control in one side of the body is lost. The effect of the loss of control in the affected limbs can reduce or eliminate the hemiparetic patient's ability to walk or perform other everyday tasks. Another common effect of stroke is an increase in muscle sensitivity to stretch called spasticity. Spasticity can impair the yielding quality of eccentric muscles in the gait pattern, often resulting in altered or compensatory gait patterns [6].

Most stroke survivors recover some or all of their ability to perform essential tasks through rehabilitation [4]. The MIT-MANUS robot has been proven to be an effective tool for upper extremity rehabilitation in hemiparetic patients [1]. Many of the existing methods for gait rehabilitation, however, require multiple therapists to manually assist the patient's movements.

1.3 Other Causes of Gait Disability

In addition to stroke, Multiple Sclerosis, Cerebral Palsy, and Spinal Cord Injury are neurological disorders which can cause serious gait pathologies. Many of the pathologies resulting from these disabilities are similar to those caused by stroke but can be more severe. They often affect both lower limbs rather than a single side. The robotic devices should be able to attach to both legs simultaneously or to a single limb in the case of hemiparesis.

1.4 Ankle Rehabilitation

One of the most common pathologies experienced by patients with neurological disorders is a loss of ankle control called drop foot. Drop foot limits the ability of the

patient to progress their affected limb while walking and can cause injury if contact to the ground is made while the foot is improperly positioned. Another common pathology with similar complications is an inverted foot caused by spastic muscles. Most current rehabilitation methods are unable to address these problems. Often, the ankle is placed in an brace or orthosis simply to avoid injury. In many cases, the orthosis must be worn permanently after therapy is complete. A robotic device that attaches at the ankle would allow rehabilitation while still preventing injury to the patient.

Chapter 2

Background

This chapter will discuss the theoretical and experimental background of topics relevant to this thesis. The normal gait process will be described, as well as important physiological aspects of the lower limb. Common gait pathologies will also be discussed with an emphasis on ankle and foot deviations. Finally, a description of some of the prevalent methods currently being used for gait rehabilitation will be presented.

2.1 Normal Gait

2.1.1 Terminology

A review of some common terms is necessary before discussing the human gait cycle.

- Gait: "The manner of moving the body from one place to another by alternately and repetitively changing the location of the feet" [4]. This could include walking, running or a number of other types of movement. The focus of this thesis, however, is walking. Gait and walking will be used interchangeably throughout this document.

- Reference planes: These are the three, orthogonal, anatomical planes commonly used to analyze human movement. They include the Frontal, Transverse, and Sagittal planes, as shown in Figure 2-1.

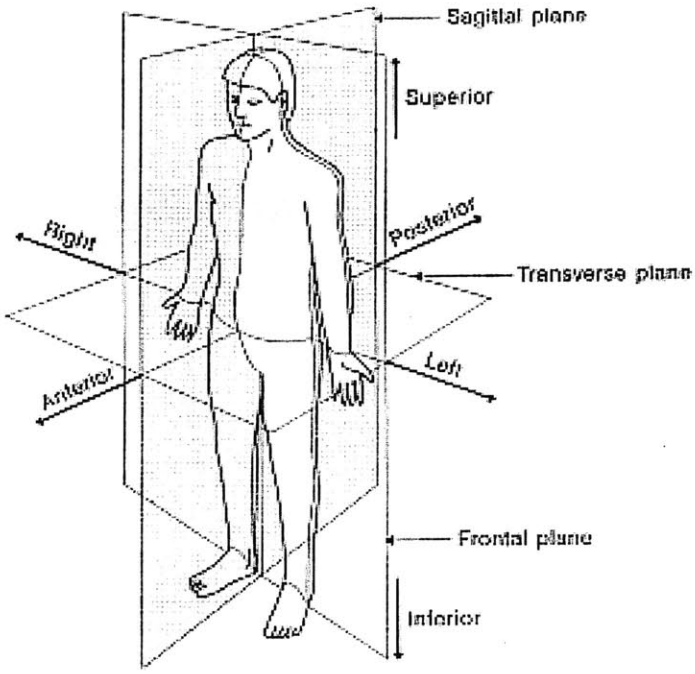

Figure 2-1: Reference planes for human movement [5].

- Stride Cycle: The interval between two successive occurrences of a repetitive event on the gait cycle. It is commonly measured from the time of heel contact of one foot until the next heel contact of the same foot [6].

- Leg Movements: These include the movements at the hip and knee joints. Each joint allows three movements; adduction-abduction (Frontal plane), flexion-extension (Sagittal plane), and internal-external rotation (Transverse plane). These movements are shown in Figure 2-2.

- Ankle and foot movements: These include movements at the ankle and foot joints. The ankle joint allows dorsiflexion and plantar flexion. The joints of the foot allow inversion-eversion and adduction-abduction. These movements are summarized in Figure 2-3.

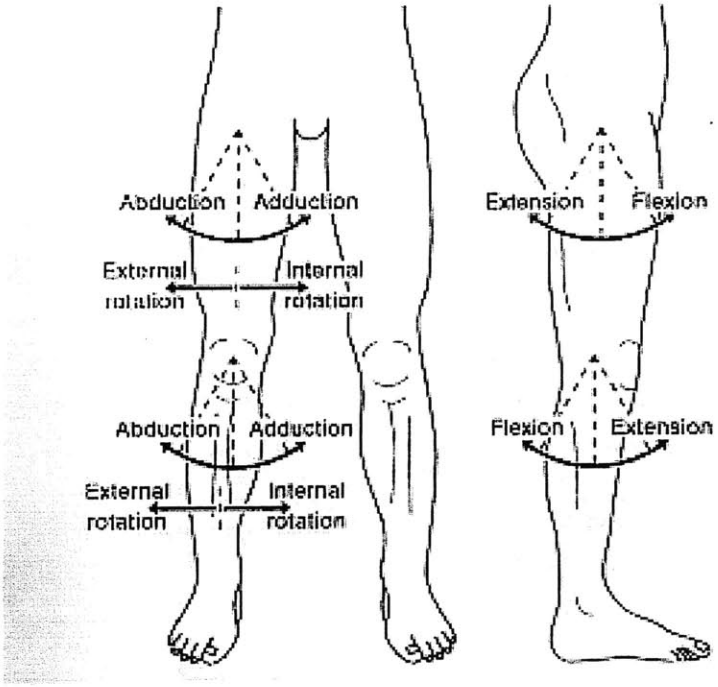

Figure 2-2: Allowable movements of the lower limb [5].

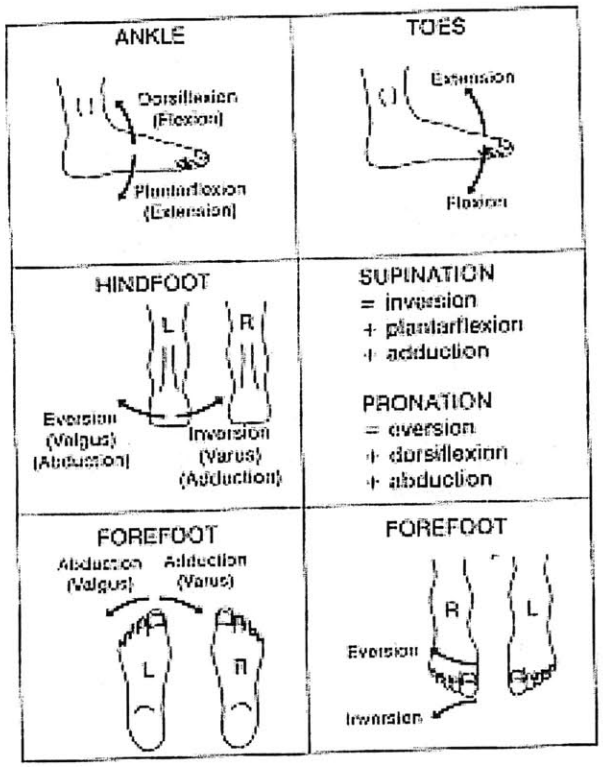

Figure 2-3: Allowable foot movements [5].

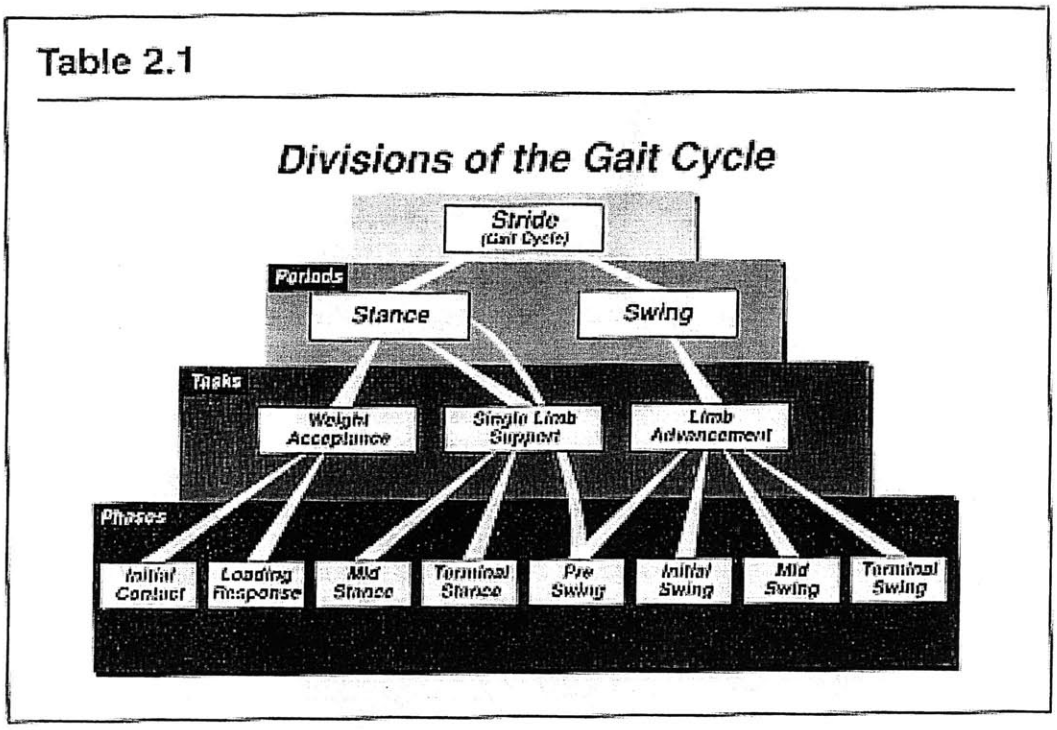

Figure 2-4: Hierarchy for gait analysis [6].

2.1.2 Phases of Gait

A convenient hierarchy for analyzing the phases of the gait cycle is given by Perry [6] (Figure 2-4).

The stride cycle is divided into two periods, stance and swing. Swing is the time that the foot is in the air and stance is the period that it is in contact with the ground. There is an overlap in the stance phases of the two legs called "double stance." Two such periods occur in each stride cycle. Stance comprises sixty percent of the gait cycle; forty percent for single limb support, and ten percent for each double stance phase. Swing phase comprises the remaining forty percent of the cycle [6] (Figure 2-5).

The gait cycle can be further divided into three primary tasks; weight acceptance, single limb support, and limb advancement. Finally, eight phases of the gait cycle can be identified which accomplish these tasks. These phases are shown in Figure

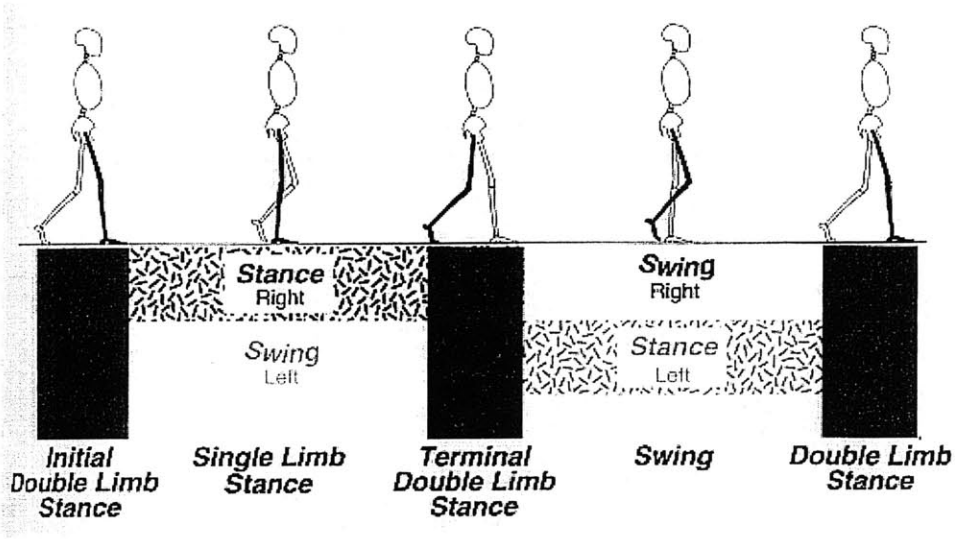

Figure 2-5: Typical stance and swing periods in a gait cycle [6].

2-6.

2.1.3 Gait Kinematics

A kinematic analysis of gait involves only the motion variables of the body segments such as position, velocity, and acceleration. These can be linear or angular motion variables. No attention is given to the forces or torques involved.

As with any kinematics problem, it is important to specify the frame of reference in which the variables of interest are defined. An absolute or inertial reference frame is one that is assumed to be at rest. A segmental reference frame can be defined as one that is fixed to a point in a body segment and constrained to move with that segment. Similarly, a joint reference system is one that is fixed to a point in a given joint and moves with that joint [7].

If the values of the motion variables in one of the reference frames mentioned above are known, it is possible to determine the value of the variables in another reference frame by using a linear homogeneous transformation matrix. This is a four by four matrix that transforms the coordinates by a series of translations and rotations. This transformation matrix, T, is of the form

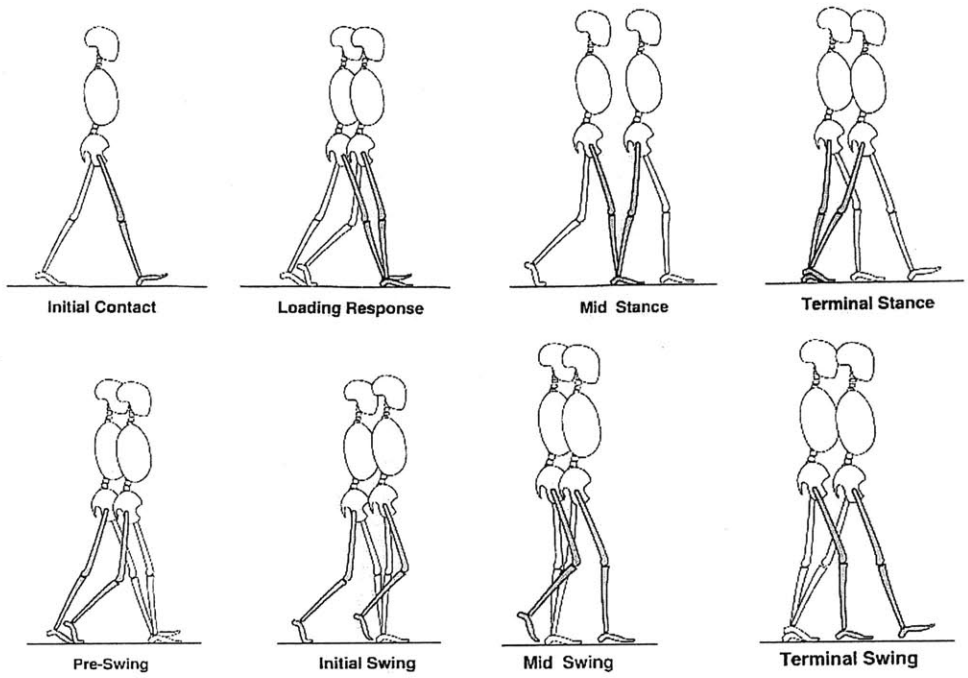

Figure 2-6: Phases of Gait [6].

$$T = \begin{pmatrix} c\phi c\varphi - s\phi c\theta s\varphi & -c\phi s\varphi - s\phi c\theta c\varphi & s\phi s\theta & x \\ s\phi c\varphi + c\phi c\theta s\varphi & -s\phi s\varphi + c\phi c\theta c\varphi & -c\phi s\theta & y \\ s\theta s\varphi & s\theta c\varphi & c\theta & z \\ 0 & 0 & 0 & 1 \end{pmatrix} \tag{2.1}$$

where c and s are shorthand for cosine and sine, respectively, ϕ, φ, and θ are the Euler angles, and x, y, and z are the offsets between the two frames [6]. This same procedure can be done using screw theory to describe the motion in each reference frame about a screw axis.

In gait analysis, data is most meaningful when presented in the terms of joint reference frames. This data discussed in this document will be relative to the joints being considered unless otherwise noted.

2.1.4 Gait Kinetics

Kinetics deals with the forces and torques that accelerate inertia to produce motion. The main external force involved in the walking cycle is the ground reaction force (GRF). In gait analysis, joint torques and powers are of primary interest. These variables can be calculated by performing an inverse dynamic analysis using the kinematic data present and the transformations described in the previous section.

The ground reaction force is the reaction force generated when the person's foot is in contact with the ground. It is due to the sum of the person's weight and the acceleration of the center of mass (CM). This force can be decomposed into three orthogonal components; vertical, lateral shear, and progressional shear [6]. The magnitudes of these forces over a stance period are shown in Figure 2-7. The two shear components are small compared to the vertical component.

The vertical component of the ground reaction force, F, can be expressed as

$$F = M(g + a) \tag{2.2}$$

where M is the mass of the person, g is the acceleration due to gravity, and a is the acceleration of the person's center of mass in the vertical direction [6]. Because M and g are constants, only the acceleration of the CM can change the value of this force. Faster walking speeds usually result in higher accelerations and thus higher ground reaction forces.

As seen in Figure 2-7, there are two peaks separated by a valley in the vertical ground reaction force. The first peak occurs during heel contact as weight is transferred to the limb. The valley occurs in late mid-stance as the body rolls over the stationary foot. The second peak occurs in terminal stance as the CM accelerates as the body falls forward.

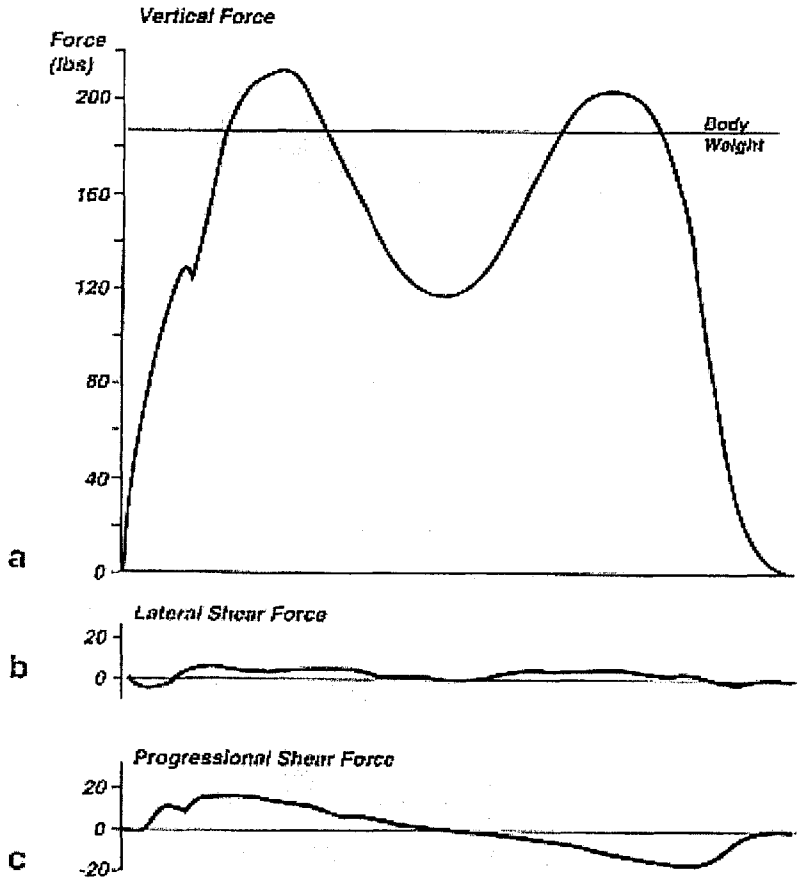

Figure 2-7: Components of ground reaction force in three planes over a gait cycle [6].

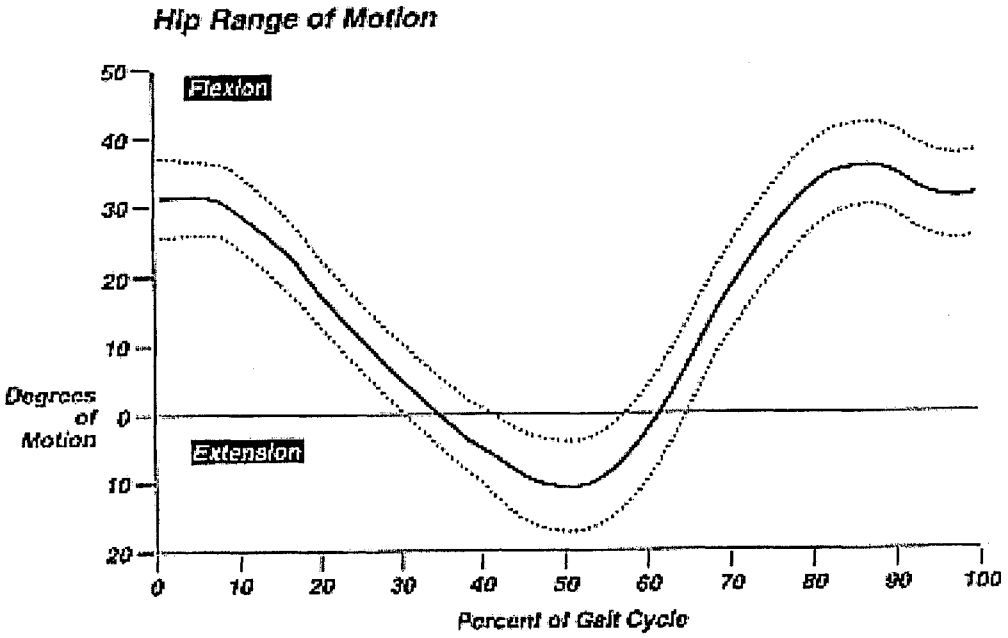

Figure 2-8: Hip range of motion in the Sagittal plane over a gait cycle [6].

2.2 Gait Physiology

A description of the relevant physiological aspects of the hip, knee, ankle, and foot will be presented here. The main focus will be on the ankle-foot complex as that is the subject of this research.

2.2.1 Hip

The hip represents the junction between the lower limb and the pelvis. Because of this, it requires more mobility and control in all three planes than the other joints of the lower limb. Hip flexion and extension in the Sagittal plane has the largest range of motion. Figure 2-8 shows the typical range of Sagittal plane motion over a gait cycle. This movement is necessary for forward progression. Adduction and abduction in the Frontal plane has a much smaller range but with higher muscular demand [6].

In the initial contact and loading phases of the gait cycle, the hip is in about 30 degrees flexion in the Sagittal plane (with respect to the vertical). The five hip

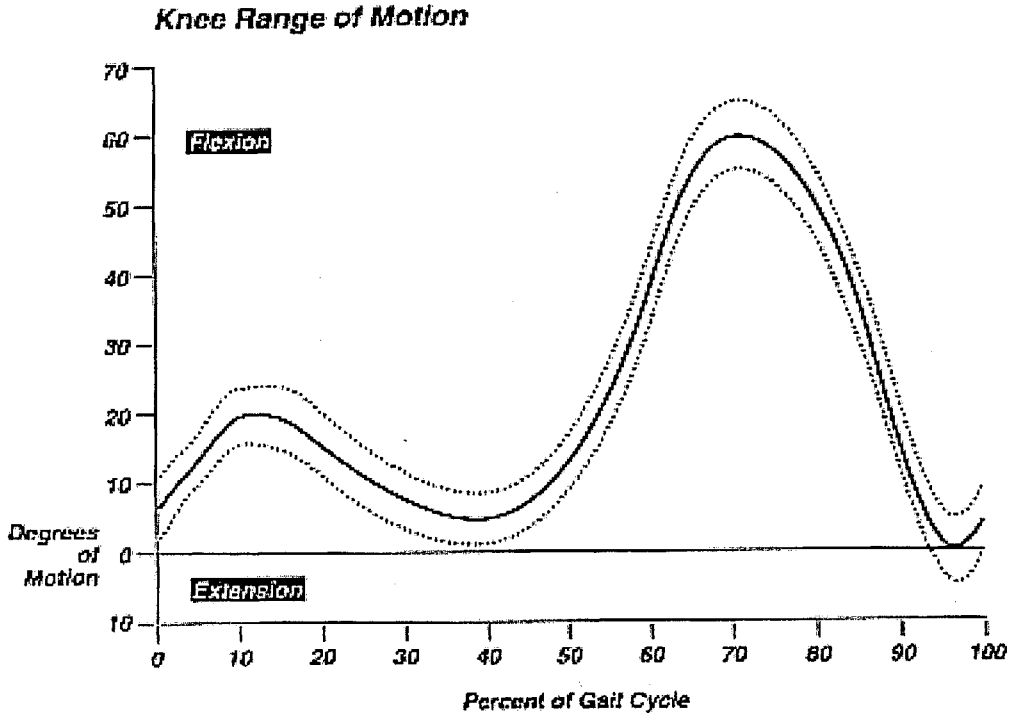

Figure 2-9: Knee range of motion in the Sagittal plane over a gait cycle [6].

extensor muscles are active to provide stability. As the leg goes into mid-stance, the hip gradually extends into the neutral (vertical) position. The hip then goes into slight extension in terminal stance and pre-swing before gradually flexing again through the swing phases to provide limb progression.

The abductor muscle group provides stabilization of the pelvis throughout the gait cycle [6].

2.2.2 Knee

The knee is the junction of the femur and tibia, which are the long bones of the major segments of the lower limb. The range of motion in the Sagittal plane is much larger that those in the other two planes. Motion in the Frontal plane provides vertical balance during the stance phase. Transverse rotations allow changes in alignment as the body swings around the support leg.

The typical flexion/extension behavior at the knee over a gait cycle is shown in

Figure 2-9. At initial contact, the knee is near its neutral position (tibia parallel to femur). The knee provides shock absorption and the flexor and extensor muscles provide stability in the loading response phase. The knee is flexed slightly as this process takes place and then returns to near neutral position through midstance to provide maximum weight bearing capacity. The knee then flexes again in terminal stance to allow the ankle to push off. The knee then moves into about 60 degrees of flexion during swing phase to provide foot clearance.

2.2.3 Ankle

The junction where the shank (tibia) meets the foot (calcaneus) is commonly referred to as the ankle joint. A more accurate description, however, involves not only the ankle joint but the subtalar joint as well which runs at an acute angle with the calcaneus. A small structure called the talus which lies between the tibia and the calcaneus, serves as a weight-bearing link between the leg and the foot. It also allows the two single axis joints (ankle and subtalar) to provide three degrees of freedom [6]. This complex mechanism is often separated into two separate joints for simplicity. This has proven adequate because, in gait, two of the degrees of freedom present (pronation-supination and adduction-abduction) behave as coupled degrees of freedom. This coupled movement is know as inversion-eversion [8]. This analysis will make this distinction as well and address the subtalar joint in the next section.

When considered independently, the ankle joint can be described as a single degree of freedom joint, providing motion only in the Sagittal plane. This motion is called dorsiflexion (rotation toward the tibia) and plantar flexion (motion away from the tibia). The typical range of motion of this movement in gait is shown in Figure 2-10.

Functionally, the ankle is critical for progression and shock absorption during stance and limb progression during swing. In stance the foot-ankle complex can be analyzed as three successive mechanisms or "rockers." These mechanisms are known as; heel rocker, ankle rocker, and forefoot rocker [6] (Figure 2-11).

At initial contact, the ankle is approximately in its neutral position (foot is perpendicular to tibia). To facilitate shock absorbtion, the ankle then plantar flexes

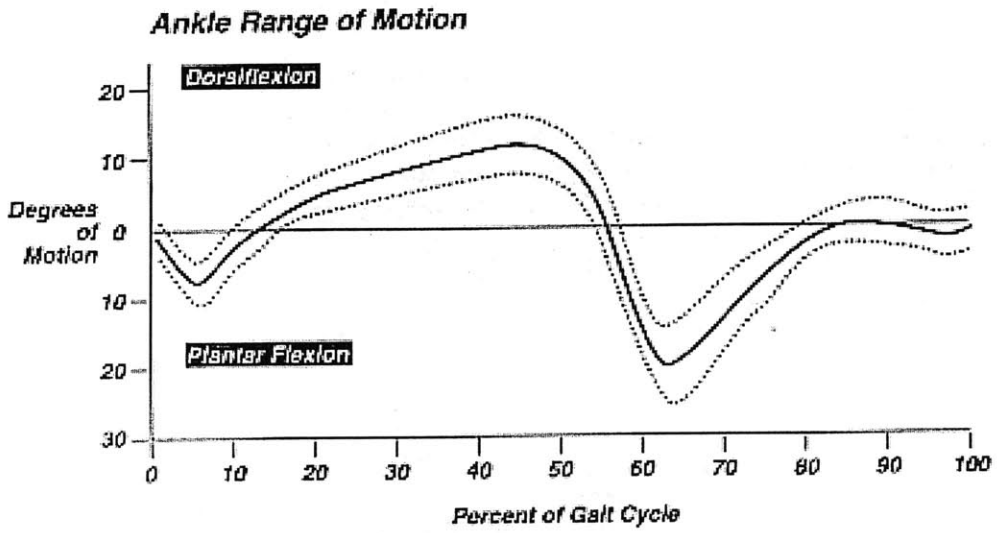

Figure 2-10: Ankle dorsi/plantar flexion range of motion for a gait cycle [6].

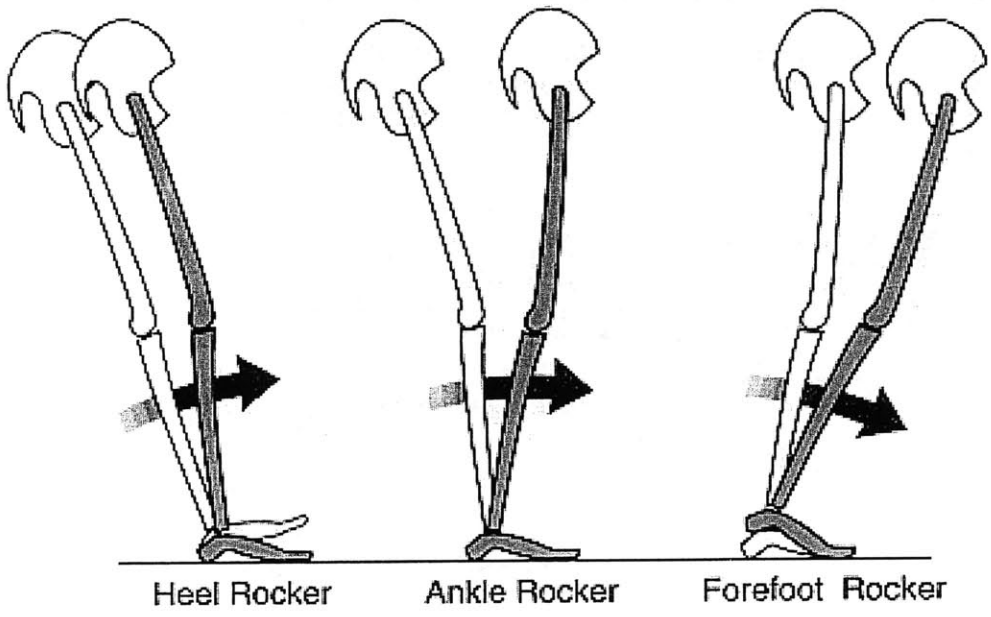

Figure 2-11: Heel, ankle, and forefoot rocker mechanisms for loading of a limb during stance [6].

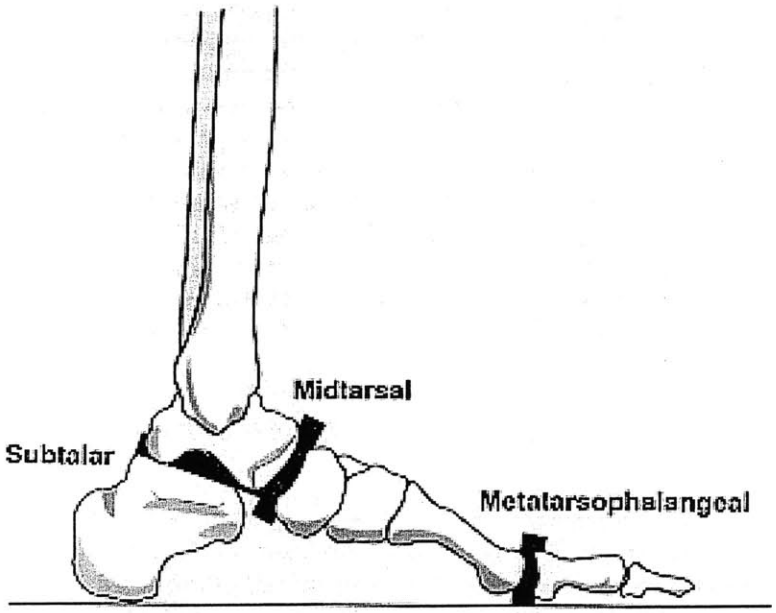

Figure 2-12: Main joints of the foot [6].

slightly and the heel rocker is initiated. A maximum of about ten degrees of plantar flexion is reached as the rest of the foot comes in contact with the ground. The ankle rocker is then initiated as the leg rolls over the foot in mid stance. When about ten degrees of dorsiflexion is reached, the forefoot rocker takes over in preparation for push off. In the pre-swing phase, plantar flexion occurs rapidly for progression, reaching a maximum of about twenty degrees shortly after toe-off. The ankle then returns to approximately neutral position to allow limb advancement and to prepare for contact again. Correct position at the time of heel strike is critical to avoid injury [16]

2.2.4 Foot

There are three main joints in the foot; the subtalar, midtarsal, and metatarsophalangeal joints [8]. These are shown in Figure 2-12.

The subtalar joint is the junction between the talus and the calcaneus. The joint axis is not parallel with the calcaneus, however. Movement allowed by the subtalar joint is an oblique tilting in both the frontal and transverse planes known as inversion

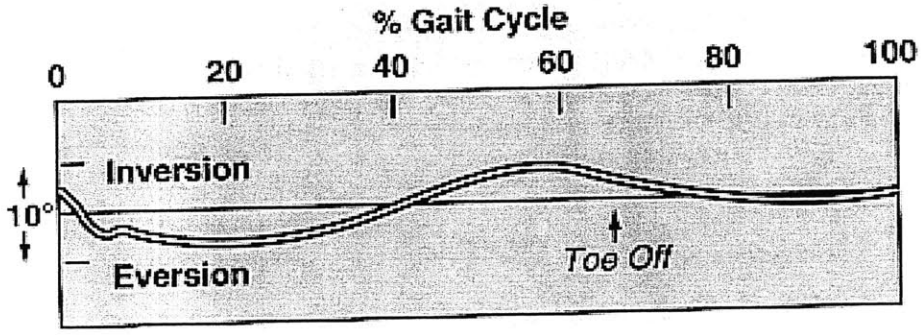

Figure 2-13: Typical inversion-eversion range of motion over a gait cycle [6].

and eversion [8]. While these movements are small in gait, they and the muscles associated with them are very important in weight bearing and balance during stance. Figure 2-13 shows the typical range of motion for inversion and eversion over a gait cycle.

The midtarsal joint allows only very small movements in the sagittal plane that have been observed but not measured. The metatarsophalangeal joint also allows motion in the sagittal plane. It plays an important role in the forefoot rocker mechanism [6].

2.3 Gait Pathologies

The number of recognized gait pathologies is too large to allow discussion of each of them here. For the purposes of this research, hemiparetic gait and some of the more common ankle and foot pathologies will be discussed.

2.3.1 Hemiparetic Gait

Hemiparetic patients typically have gait patterns that vary greatly from those of normal subjects. A number of studies have been done to identify specific deviations. A summary of some of the more common deviations will be given here. It should be noted that there is a large variability across patients. This is also true of normal gait

patterns. The results of these studies are general and not necessarily applicable to all patients.

The following deviations have been found in the distance and time aspects of walking in hemiparetic patients [9]:

- Reduced step length with unaffected limb
- Increased step length with affected limb
- Wider base of support
- Greater toe-out angles
- Increased periods of double support

A number of these characteristics have been attributed to a decreased gait velocity. The asymmetries in the affected and unaffected legs are not accounted for by this, however. Patients have shown considerable improvements in these aspects of gait with rehabilitation over the first six weeks to three months after stroke [10].

There are also significant deviations in hemiparetic gait with respect to joint kinematics. In most patients, the same joint phases that exist in normal gait are present in both the affected and unaffected limb. The range of motion, however, is often significantly reduced. Some of the specific pathologies in joint kinematics are listed below [9].

- Initial contact on the affected side is made with a flat foot. No ankle or forefoot rocker mechanisms are active.
- Irregular movement into dorsi flexion and excessive plantar flexion during stance have been observed.
- Reduced dorsi flexion or continued plantar flexion during swing can impede leg progression.
- Inverted foot during swing phase (increased inversion).

- Hyper-extension of the knee in stance due to impared muscles.
- Decreased flexion of the knee in the swing phase also impedes the forward progression of the leg.
- "Hip hiking" during swing is often used to compensate for the lack of ankle dorsiflexion and knee flexion.

In addition to these kinematic factors, a number of kinetic and energetic deviation are also common. The loading of the body weight at initial contact is not balanced in the vertical plane as it is in normal gait. There is a much greater variability in this weight distribution due to the lack of control of the ankle and foot muscles. This can result in a loss of balance and increased joint pain. The energy expenditure of hemiparetic gait can also be as much as 67 percent more than that of normal gait [9].

2.3.2 Ankle and Foot Pathologies

Most ankle and foot gait pathologies can be grouped into four categories; excessive dorsiflexion, excessive plantar flexion, excessive inversion, and excessive eversion [6]. These categories could also be described as reductions in movement. For example, excessive dorsiflexion could also be called reduced plantar flexion.

Excessive dorsiflexion commonly occurs in one of two action patterns (Figure 2-14). The first (curve A in Figure 2-14) involves an abrupt change from plantar flexion to about ten degrees of dorsiflexion during the loading response phase. This position is then maintained throughout stance.

The second pattern (curve B in Figure 2-14) involves a progressive increase of dorsiflexion throughout mid and terminal stance.

Both of these patterns tend to increase the demand on the quadriceps. This is due to an increased heel rocker effect and an increase in both rate and magnitude of ankle movement.

Excessive dorsiflexion is usually caused by either weakness of the soleus or the ankle being locked in the neutral position by a fused joint or corrective orthosis [6].

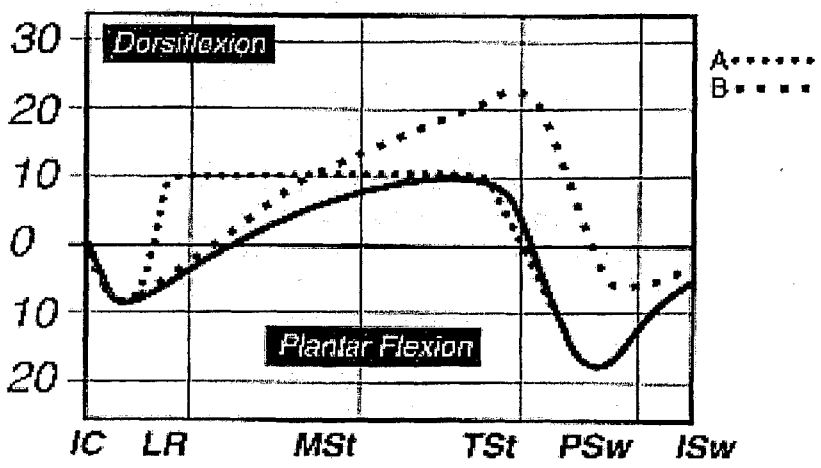

Figure 2-14: The two action patterns of excessive dorsiflexion [6]

Excessive plantar flexion most commonly affects five of the eight gait phases. Figure 2-15 shows these locations.

During initial contact, excessive plantar flexion can result in a low heel contact or the forefoot hitting the ground before the heel. In the stance phases, the result is a loss of progression and a reduced gait speed. The tibia can also be forced back resulting in hyper-extension of the knee. A diagram of these pathologies is shown in Figure 2-16.

During swing, excessive plantar flexion can impede the forward progression of the leg as the toe may drag on the ground. This can result in a number of compensatory gait patterns such as hip hiking and swinging or increased knee flexion.

Excessive inversion can be caused by either a static deformity or inappropriate muscle action. It results in the outside of the foot loading prematurely and more abruptly. The weight bearing capacity and balance of the affected limb can be significantly impaired during stance. There is usually no functional significance to excessive inversion during swing, except as it relates to the preparation for initial contact.

Excessive eversion has a similar effect, except the inside of the foot accepts a larger than normal loading response. The base of support and balance provided by the affected limb is impaired [6].

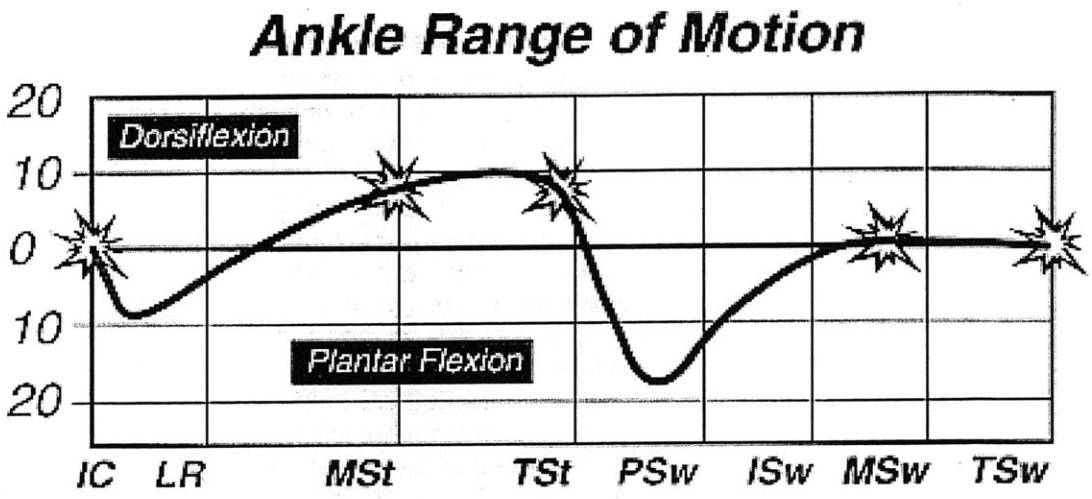

Figure 2-15: Gait phases where excessive plantar flexion is most significant [6].

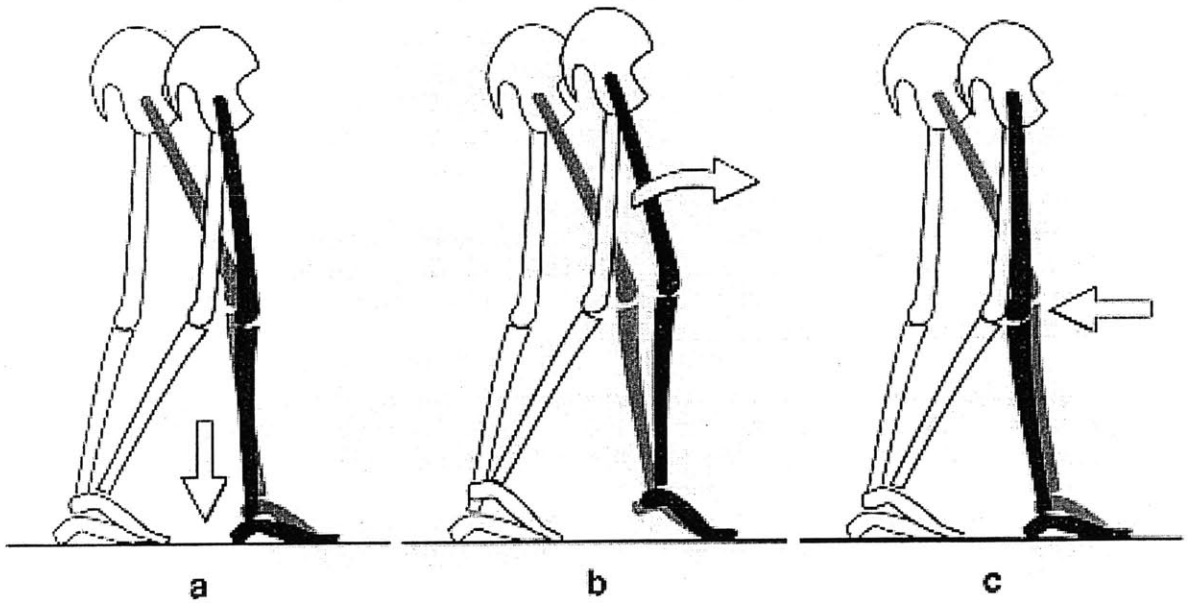

Figure 2-16: Loading response and stance gait deviations caused by excessive plantar flexion [6].

2.4 Current Technology

There are a number of important devices and techniques used to improve pathological gait. This section will discuss some of the most prominent technologies that are pertinent to this research.

2.4.1 Stretching and Strength Training

Stretching and strength training exercises are used, usually in the initial stages of rehabilitation, to restore some degree of mobility and/or muscle control to the affected limb. Very little attention is given to the actual functional task of walking. This discussion will focus on ankle training.

Usually, a therapist will stretch the joint a number of times manually or ask the patient to try to push or pull against some resistance provided by the therapist. These techniques have proven valuable in restoring mobility and strength to stroke patients. This can in turn improve the overall gait cycle [10].

There are some drawbacks to this method. The relationship between increased strength and mobility and the ability to perform functional tasks, such as walking, is still unclear. The exercises require a large amount of therapist time and effort and there is no way to objectively quantify results or progress.

Recently, intelligent devices have been developed to stretch spastic muscles to certain forced-based limits [11]. This provides a quantifiable way to perform these exercises. It does not, however, address specifically the functions of gait.

2.4.2 Braces and Orthoses

Often, therapists will fit patients with a corrective brace or other device to allow them to walk. Such devices are not typically used for rehabilitation but to stiffen a weakened joint or correct a specific misalignment. The most common type of such a brace is an ankle-foot orthosis (AFO). An AFO has been defined as "a medical mechanical device to support and align the ankle and foot, to suppress spastic and overpowering ankle and foot muscles, to assist weak and paralyzed muscles of the

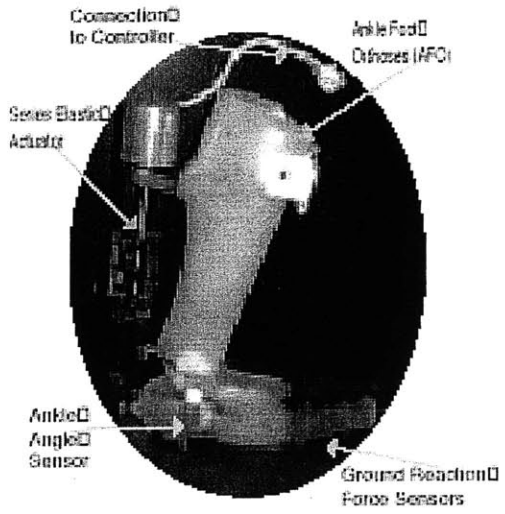

Figure 2-17: Single DOF active ankle foot orthosis [13].

ankle and foot, to prevent or correct ankle and foot deformities, and to improve the functions of the ankle and foot [12].

AFOs are not rehabilitation devices. They often encourage irregular, compensatory gait patterns. They are discussed here because they are commonly used to treat gait pathologies after stroke or other diseases. Most AFOs limit the range of ankle motion to prevent excessive dorsiflexion or plantar flexion. Many have no range of motion at all. Generally, only one degree of freedom is allowed if any at all.

Recently, impedance based AFOs have been developed. An active ankle foot orthosis (AAFO) was designed in MIT's Leg Lab that uses a linear series elastic actuator to vary impedance at the ankle joint [13] (Figure 2-17). This device assists only one degree of freedom, movement in the sagittal plane. As with other AFOs other ankle and foot movements are restricted.

2.4.3 Treadmill Training

Treadmill training is used to assist in the gait rehabilitation of patients after stoke and other neurological diseases. There are various methods for doing this. A common method used for hemiparetic patients is described here.

The patient's weight is either fully or partially (as in the case of stroke) supported as he or she stands on a treadmill by an overhead lift system that attaches to a harness that the patient is wearing. Three therapists then assist the patient as he or she walks on the treadmill. One therapist stands behind the patient and holds the trunk erect. Another moves the affected leg of the patient by pushing near the lower hamstring during swing and on the tibialis anterior during stance. The third therapist ensures that the unaffected leg moves correctly. In the case of Spinal Cord Injury or other disorders where both legs are affected, it becomes even more difficult for the therapists. If the patient suffers from excessive plantar flexion, a brace is used to avoid toe drag during limb progression.

Treadmill training sessions are usually short due to therapist fatigue. This process is highly labor intensive. There is also a large degree of variability in each training session. A robotic device that could perform these tasks would be a significant improvement over this method.

Recently, devices has been developed to control patient movement on a treadmill or pedals [18][17]. One such device, called the Lokomat, was developed by Colombo et al and is shown in Figure 2-18. These devices support the patient's weight and move the pelvis and/or limbs in a walking motion. They are high force and high impedance devices so they cannot be driven by the patient. The limbs are simply moved in prescribed patterns. These devices are also limited to use on a treadmill (or pedals). Another limitation of these devices is the lack of ankle training. The Lokomat system has a passive ankle support but no current device actively addresses ankle rehabilitation. It is likely that an AFO would still be required after therapy.

The goal of this research is to develop a group of independent but compatible devices to control all of the major movements during gait. The device should be able to move the patient or be driven with low impedance as the patient moves, as with the MIT-MANUS robot. It should also work on a treadmill or over ground. This document will specifically discuss the design of an ankle module for such a system. The ankle module could be used in conjunction with other modules or independently during conventional therapy.

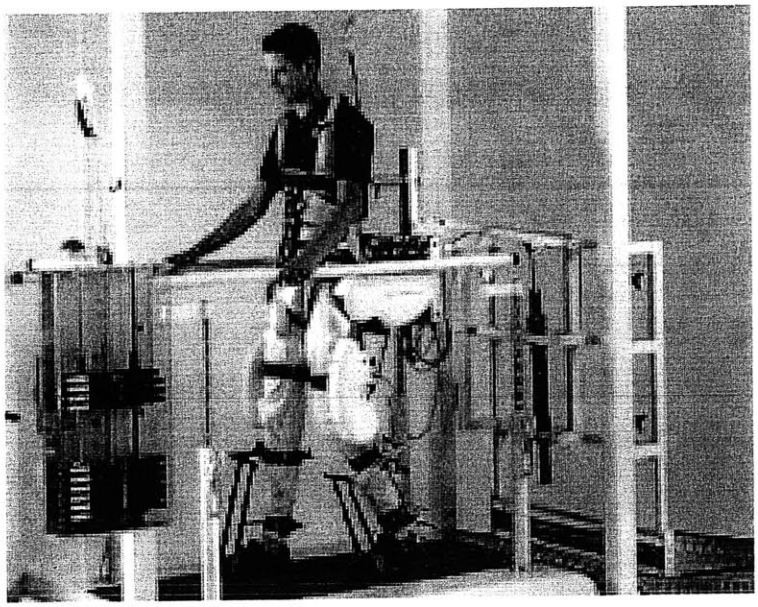

Figure 2-18: Lokomat treadmill trainer [17].

Chapter 3

Functional Requirements

This chapter will explain the specifications which the ankle robot was designed to meet. The functional requirements discussed are target specifications. To what degree the final design meets these requirements is detailed in subsequent chapters.

Generally speaking, the device was designed to provide adequate and appropriate kinematic assistance while being safe and modifying the normal gait cycle as little as possible. The specifications below were derived from the physiological and experimental data presented in the previous chapter.

3.1 Kinematic Requirements

As discussed in the previous chapter, the ankle joints provide three degrees of mobility. The device should assist those movements that are critical to gait and necessary to avoid injury. It is also important that the device not impede motion in any direction. The device should allow at least 25 degrees of dorsiflexion, 45 degrees of plantar flexion, 20 degrees of internal or external rotation, 25 degrees of inversion and 15 degrees of eversion. These limits are greater than the normal gait ranges of motion (see Chapter 2) and are closer to maximum physiological limits.

The most important ankle movement in gait is dorsi/plantar flexion. Inversion and eversion are also important for balance and proper foot positioning at impact. An inverted foot at the time of heel strike could cause injury. The most common ankle

pathologies cased by stroke are drop foot (excessive plantar flexion) and excessive inversion [16]. The device will assist these two movements. The third degree of mobility, internal and external rotation, is less important in gait. In addition, the rotation of the foot in the transverse plane is controlled to a greater degree by rotations of the upper leg and knee, which will not be controlled by the device [8]. A mechanical benefit of actuating fewer degrees of freedom than are actually present is that it eliminates the need for precisely locating the patient axes.

3.2 Mechanical Requirements

From a mechanical standpoint, the device must provide sufficient force to assist movements and still be backdriveable. Ankle torques can be very large near the end of stance phase as the body weight is propelled forward (100-200 N-m). Supplying torques of this magnitude would either require large motors, which are heavy, or a large gear reduction, which adds weight and endpoint impedance. The device was designed to supply torques needed to position the foot during swing phase and provide some assistance during stance phase. Specifically, the device will provide at least 17 N-m of torque to the ankle joint in any degree of freedom. This value is higher than that required for foot positioning in swing phase for normal subjects [25]. It is anticipated that more torque will be required to position the foot for stroke patients due to increased tone.

Every effort was also made to minimize endpoint friction and inertia. The target specification for maximum viscous friction is 65 oz-in. It was also desired to keep the endpoint inertia below 35 $lb - in^2$.

3.3 Safety and Functionality Requirements

It is important that the device be safe and easy to use for both the patient and therapist. The functional requirements listed below address these concerns.

- The entire device will weigh less than 8 lbs.

- The weight should be placed as close to the knee as possible.
- The device can be used with other modules (e.g. pelvis) or independently.
- It can be used on a treadmill or over ground.
- It will take less than 5 minutes to attach/detach from the patient.
- It can be installed on either leg.
- There will be no hardware between the patients legs that could impede limb advancement or cause injury.
- Stops, switches and limits will be included as needed to ensure patient safety.
- It should be aesthetically pleasing and comfortable.

The weight requirement is critical. The reason for placing the weight near the knee is that the patient's perception of the added inertia will be less if it is closer to the knee and hip muscles. This is due both the the shorter lever arm and the stronger proximal muscles [32]. This was verified qualitatively on normal subjects in tests described in Chapter 5.

Chapter 4

Kinematic Selection

This chapter will discuss the kinematic concepts that were considered to provide the necessary mobility and torque transmission detailed in the functional requirements.

4.1 Mobility

As discussed in Chapter 2, there are two joints in the ankle separated by a bone. This configuration results in a joint with three effective degrees of freedom. For the purposes of this analysis, the ankle will be modelled as a single joint with three degrees of freedom. This is not a completely accurate physiological model, such is not required for this analysis. The kinematics of the mechanism must allow the same number of degrees of freedom with the robot attached as are present without it.

To allow free mobility to the patient, the linkage consisting of the leg, foot, and ankle robot should have the same number of degrees of freedom (mobility) as the ankle joint itself. The mobility, M, of some linkages can be expressed using Gruebler's Equation,

$$M = 6(n - j - 1) + \sum_{i=1}^{j} f_i \tag{4.1}$$

where n is the number of links, j is the number of joints and f_i is the mobility of joint i [14].

To meet the functional requirements, the linkage must have a mobility of at least 3. In fact, a mobility of exactly 3 (not including benign degrees of freedom) is required for a controllable device. The kinematic configuration of the mechanism must also allow the actuator torques to be properly transmitted to the ankle joint.

4.1.1 Kinematic Components

In designing a kinematic mechanism, it is important to understand the function and theory behind some commonly used joints and other components. This section will define a few components that are related to the concepts that were considered for the ankle robot.

- **Revolute Joint** - A revolute joint allows rotation about a single axis only. No translational mobility is allowed. Ball or roller bearings are commonly used to implement such a joint.

- **Prismatic Joint** - A prismatic or sliding joint allows translation in one direction only. No rotational movements are allowed. Linear sliding or rolling element bearings can be used for such an application.

- **Spherical Joint** - A spherical joint allows rotation in all three directions but allows no translation. These joints are normally implemented by assembling a greased ball in a socket.

- **Differential** - A differential allows rotation about two perpendicular axes. The third rotational degree of freedom is fixed, as well as all translational movements. A differential can be implemented using three bevel gears mounted as shown in Figure 4-1. This allow torque to be transmitted in both directions. For kinematic purposes, the mechanism can be modelled with two perpendicular revolute joints.

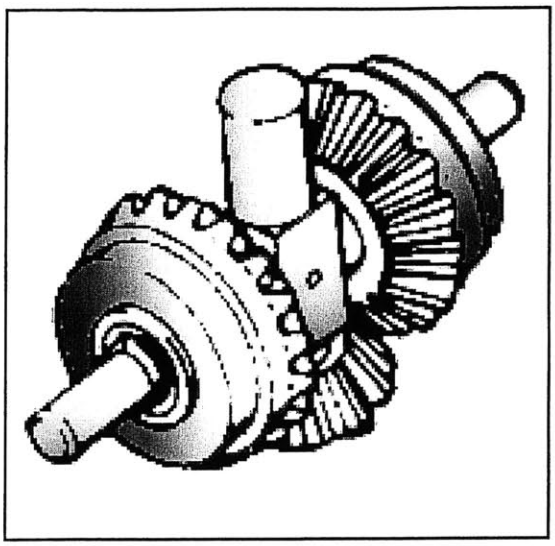

Figure 4-1: Geared differential [15].

4.2 Mechanism Concepts

A number of mechanism concepts were considered for the device. Those concepts which were analyzed in detail are discussed in this section. The concepts are shown as simple solid models.

4.2.1 Differential with Prismatic Joint on Foot

One of the first concepts considered consists of a differential attached to the shank and a sliding joint on the foot. They are connected by a two links and a spherical joint. The concept is shown in Figure 4-2.

This mechanism has a total of 4 links; the leg, foot, L-shaped link, and the link connecting the spherical joint to the slider. It has 4 joints; the ankle joint (M=3), the differential (M=2), the spherical joint (M=3), and the sliding joint (M=1). These joints provide a total mobility of 9. Gruebler's equation predicts a mobility of 3 for this system, as desired.

While this mechanism has the correct mobility, it has some problems. To get the required travel in dorsi/plantar flexion, the sliding joint on the foot would need to be over 12 inches long. This could interfere with either the ground or leg and would be

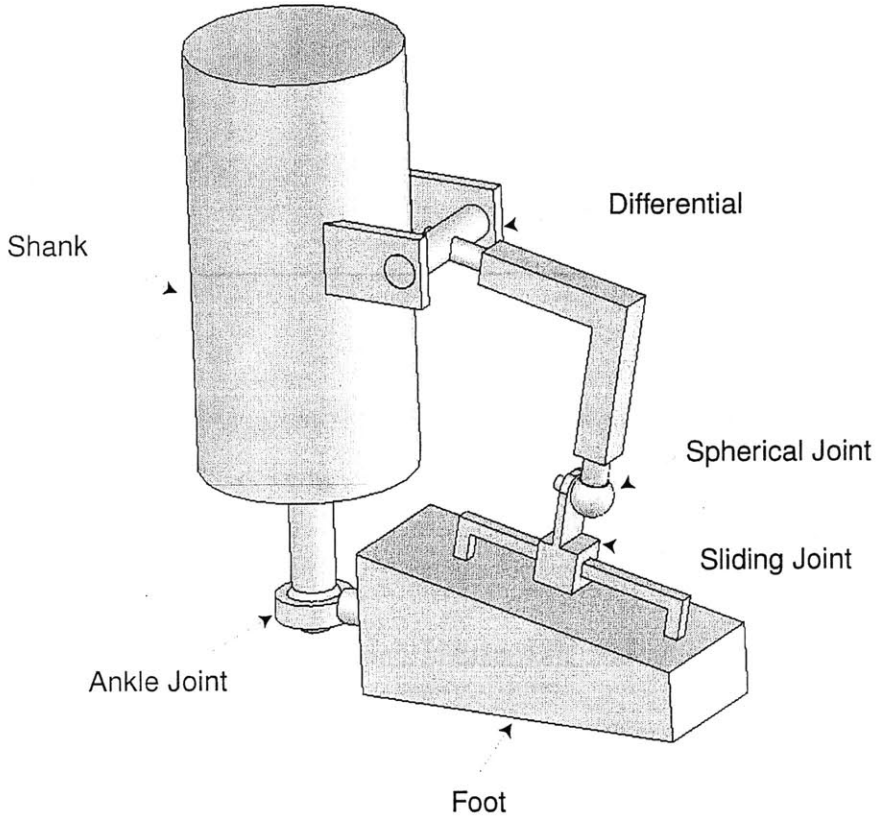

Figure 4-2: Mechanism concept with differential on shank and slider on foot.

heavy. Another potential problem is the torque transmission to the ankle joints. The actuators would be placed on the shank and drive the differential degrees of freedom. The torques transmitted through the mechanism to the ankle would primarily produce moments corresponding to dorsi/plantar flexion and internal/external rotation. As discussed in Chapter 3, it is desired to actuate inversion/eversion rather than internal/external rotation.

4.2.2 Curved Sliding Joint with Prismatic Joint Behind Shank

This concept consists of three sliding joints (see Figure 4-3). One is placed behind the leg and would be actuated to provide dorsi/plantar flexion moments. It is connected to the heel with a spherical joint. The other two sliding joints are in front of the leg and would provide moments for inversion and eversion. The sliding joint on the foot has a curved rail to allow rotation about the foot axis.

This mechanism has 5 links and 6 joints which provide a total mobility of 14. The total mobility of the system is then 2, which is not sufficient to meet the functional requirements for the ankle robot. It would also require a motor on the foot, adding to the inertia felt by the ankle joint.

4.2.3 Differential with Serial Linkage

This concept consists of a simple, two-link serial mechanism connected to the shank with a differential and to the foot with a spherical joint (see Figure 4-4).

This concept has 4 links and 4 joints which provide a total mobility of 9. This results in a mechanism mobility of 3, as desired. This concept is very simple, lightweight, and compact. However, as with the concept with the slider on the foot, the projected torques at the ankle do not correspond to inversion and eversion. The primary moments will be produced in the dorsi/plantar flexion and internal/external rotation directions.

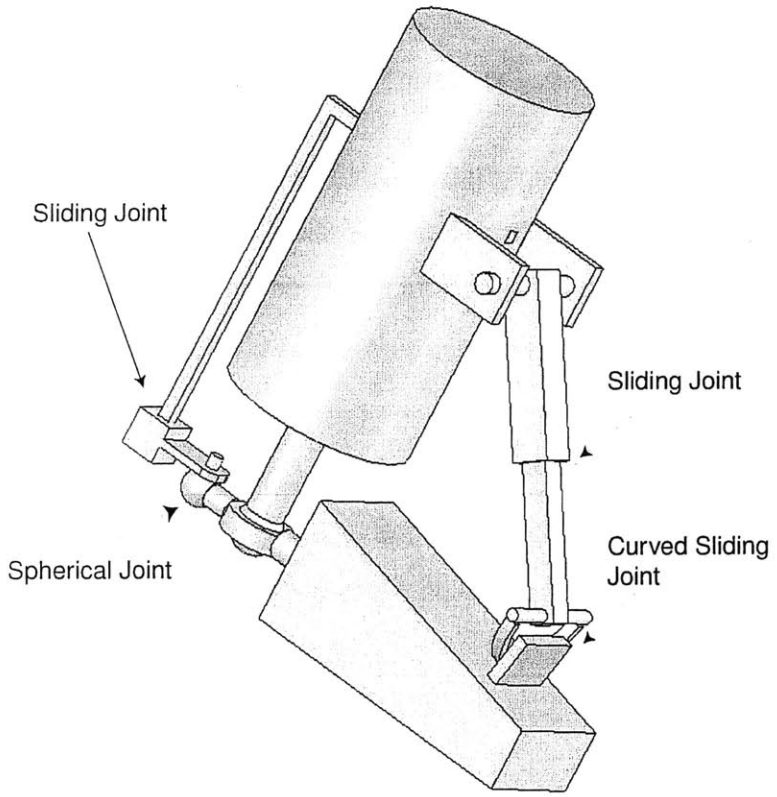

Figure 4-3: Mechanism with curved slider on foot.

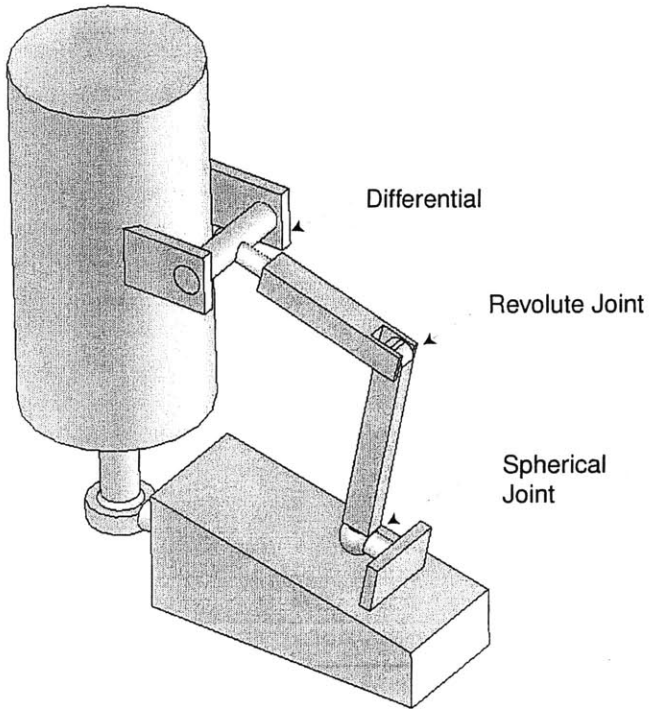

Figure 4-4: Concept with serial linkage on a differential.

4.2.4 Dual Sliding Joints

Another concept considered consists of two sliding joints or actuators mounted in parallel with spherical joints on either end (Figure 4-5).

This mechanism has 6 links and 7 joints which provide a total mobility of 17. Gruebler's Equation predicts a mobility of 5 for the system but two of these degrees of freedom are benign rotations of the sliding members. The desired mobility of 3 is achieved if these are disregarded. This mechanism is simple and compact. The challenge was to find actuators of reasonable weight that could supply sufficient force and were backdriveable. No linear actuator that met these criteria was found.

4.2.5 Differential with Parallel Linkage

This concept involves a single link mounted between a differential and two rods that connect to the foot as shown in Figure 4-6. Spherical joints are mounted at either end of these rods.

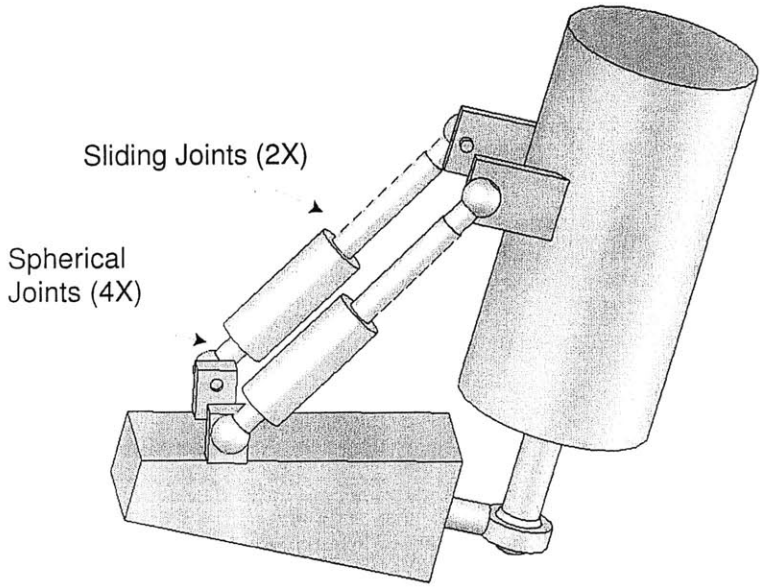

Figure 4-5: Concept with dual sliding joints.

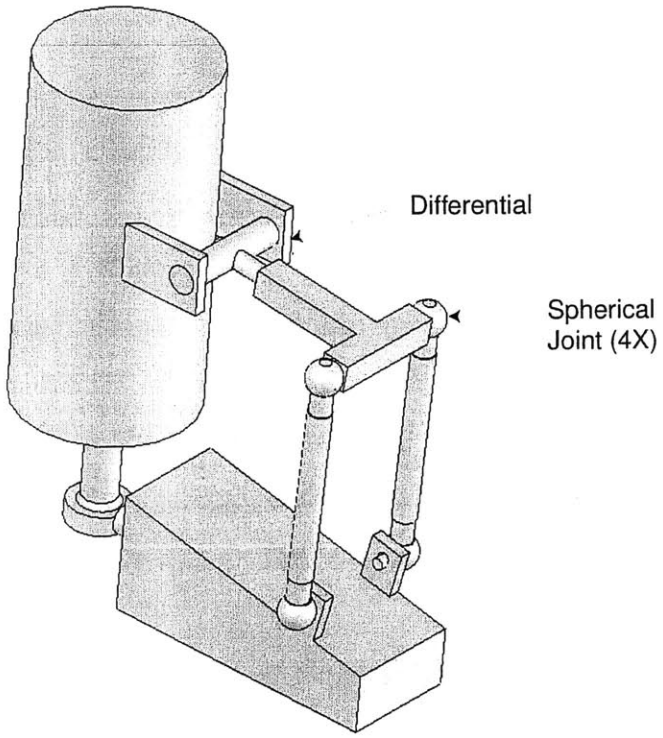

Figure 4-6: Concept with parallel linkage on a differential.

This mechanism has 5 links and 6 joints which provide a total mobility of 17. The predicted mobility of the system is 5. As with the previous concept, two of these degrees of freedom are benign (rotation of the rods). Disregarding these gives the desired mobility of 3. This mechanism not only has the correct mobility to meet the functional requirements but allows the torques to be transmitted from the actuators on the differential to the foot, providing dorsi/plantar flexion and inversion/eversion.

4.3 Mechanism Overview

The kinematic concept that was chosen is a slight variation of the parallel linkage mounted on the differential. The main link was converted to two links, each with a single degree of freedom, by essentially turning the differential "inside out" to create two independent revolute joints (Figure 4-7).

The kinematics for this mechanism are nearly identical to that with the differential. The effective mobility is 3 (6 links, 7 joints, total mobility of 17). The advantage is that one less set of gears and bearings are required. This reduces the weight and backlash of the robot.

Motion is produced by actuating the links on the shank. If both links move in the same direction, a moment is created at the ankle to produce dorsi/plantar flexion. If the links move in opposite directions, the resulting moment produces inversion/eversion. Locating the patient axes is not required using this approach. The rods produce forces on the foot which project to the patient axes.

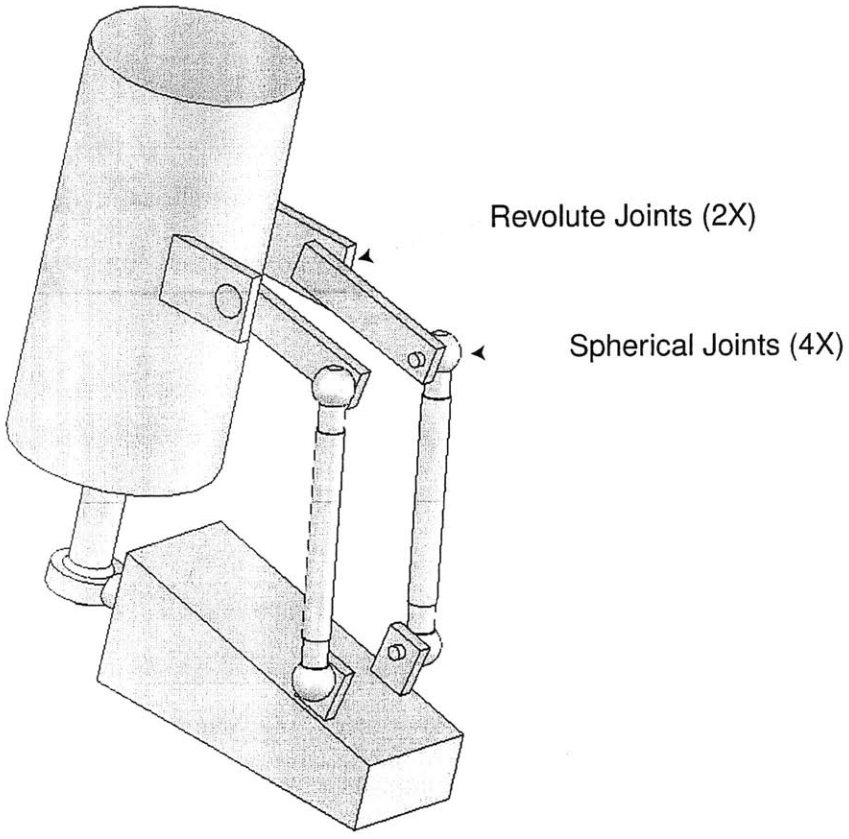

Figure 4-7: Selected kinematic configuration.

Chapter 5

Mock-ups and Testing

Throughout the design process of the ankle robot, proof of concept hardware was constructed. This chapter will discuss some of the relevant testing and verification procedures to the final design.

5.1 Mock-ups

Three kinematic mock-ups were constructed to determine if the concepts presented in Chapter 4 were viable. This section will focus on the mock-up of the concept most similar to the chosen design configuration, the parallel linkage mounted on a differential. As discussed in the previous chapter, the kinematics of this mechanism are nearly identical to that of the concept with the differential essentially turned "inside-out."

Photos of the mock-up are shown in Figure 5-1. The device connects to the shank using a modified baseball catcher's shin-guard. The shoe is secured into a modified snowboard binding. The differential is mounted in ball bearings to aluminum bars connected to the shin-guard. A machined, T-shaped link is connected to the output gear of the differential. Threaded aluminum rods connect this link to the snowboard binding via rod end spherical joints.

The snowboard binding was modified by removing the front half so only a single strap over the hind-foot remained. Aluminum pieces were added to either side to

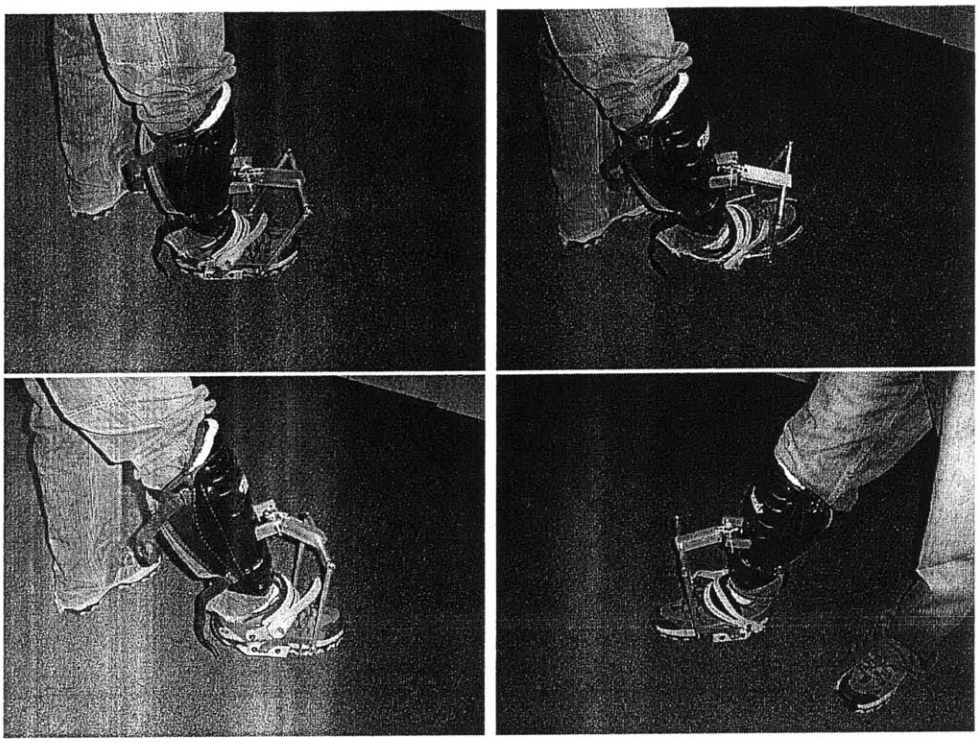

Figure 5-1: Kinematic mock-up in different configurations.

allow connection to the rods. The shin-guard has a semi-rigid foam interface that rests on the front of the leg. A solid plastic covering is offset from this foam a small distance. The machined parts were mounted to this plastic covering. The weight of the mock-up is 3.0 lbs. It was not designed to be actuated or carry significant loads, only to verify that the kinematic configuration met the functional requirements and did not significantly affect gait.

It was observed that the mock-up does not impede motion in any direction. Complete range of motion was allowed. Subjects noted that the interface was not uncomfortable and the friction and inertia in the mechanism were not noticeable.

5.2 Bio-Motion Lab Testing

To determine the effect of the mock-up on the gait pattern of normal subjects, tests were done at the Bio-motion lab at the Massachusetts General Hospital. Due to the limited time available to complete the testing, statistically significant evidence

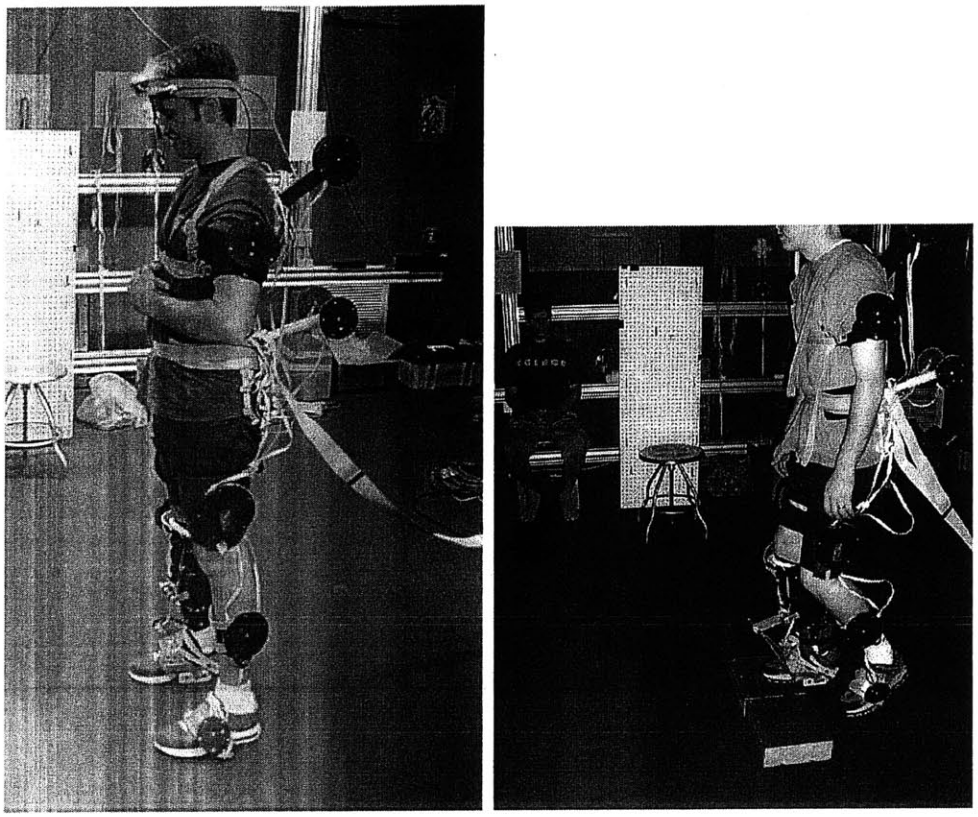

Figure 5-2: Bio-motion lab tests.

was not sought. The main goal of the tests was to see if the data showed any large deviations in the normal gait pattern that would advise changes to the design.

5.2.1 Description of Experiment

The test system uses LEDs mounted on the subject's limbs with 4 cameras to detect movements of the LEDs. Photos of the subjects with the LEDs mounted are shown in Figure 5-2.

Two male subjects were tested under three conditions:

1. **Normal Walking** - No mock-up or loading.

2. **Asymmetric Loading** - Ankle mock-up and weights to simulate actuators and transmission on right leg (7 lbs total weight).

	Free	Asymmetric	Symmetric
Trial 1	115 cm	127 cm	132 cm
Trial 2	133 cm	133 cm	140 cm
Average	124 cm	130 cm	136 cm

Table 5.1: Stride length, Subject 1, slow walking.

	Free	Asymmetric	Symmetric
Trial 1	65	60	57
Trial 2	59	61	63
Average	62	60.5	60

Table 5.2: Percent right foot stance, Subject 1, slow walking.

3. **Symmetric Loading** - Ankle mock-up and weights on right leg with dummy weights on left leg (7 lbs).

For each condition three tests were done:

1. **Comfortable Speed** - Self-selected speed of the subject.

2. **Slow walking** - Paced walking to a metronome at 60 beats per minute (bpm).

3. **Paced Stepping** - Stepping up and down on a 3 inch stair at 100 bpm.

Each test was done twice. The data was sampled at 152 Hz and filtered at 9 Hz by the data collection system. The data was analyzed and plotted in Matlab. It was normalized to percent gait cycle so the trials could be better compared. Some data dropout and wrapping had occurred in the data collection. These points were removed from the data set. Because of the small sample size, statistical significance is not inferred by this analysis. However, there are a number of conclusions that can be drawn.

5.2.2 Comparison of Selected Gait Parameters

A number of characteristic gait parameters were measured from the data and compared across testing conditions. These results are presented in Tables 5.1-5.5.

These data show little deviation in gait parameters based on the loading. In many cases, the variability between trials with the same loading is greater than the

	Left foot	Right foot
Trial 1	10.5 cm	9.5 cm
Trial 2	9.5 cm	10 cm

Table 5.3: Foot height, no loading, Subject 1, slow walking.

	Left foot	Right foot
Trial 1	11 cm	9.5 cm
Trial 2	10.5 cm	9 cm

Table 5.4: Foot height, asymmetric loading, Subject 1, slow walking.

variability between trials with different loading conditions. For stride length, for instance, there is a 18 cm difference between the first and second trials with no loading (115-133 cm) and both trials with asymmetric loading fall within this range of values. This is true with percent stance as well. The only possible effect apparent in these data is in the step heights of the left and right foot in the asymmetric loading case. In both trials, the right foot step height was 1.5 cm less than the left foot step height. This difference was not present in the other loading cases.

5.2.3 Plots of Selected Kinematic Variables

Looking at the actual data of different kinematic parameters is insightful in determining the effect of the different conditions on gait. Figure 5-3 shows the right foot position in the x-direction (forward/back) of Subject 1 during slow walking as a function of gait cycle. Note that forward is actually down on the y-axis of this plot. This plot shows the relative stride lengths for each of the trials. The first asymmetric case has a slightly larger slope just after toe off. This indicates an increased velocity for a short period of time. It then returned back to a similar pattern as the other trials. This trend was not evident in the second asymmetric trial. This could have been due to the fact that the subject was not yet fully accustomed to the weight and by the

	Left foot	Right foot
Trial 1	10 cm	10 cm
Trial 2	9.5 cm	10 cm

Table 5.5: Foot height, symmetric loading, Subject 1, slow walking.

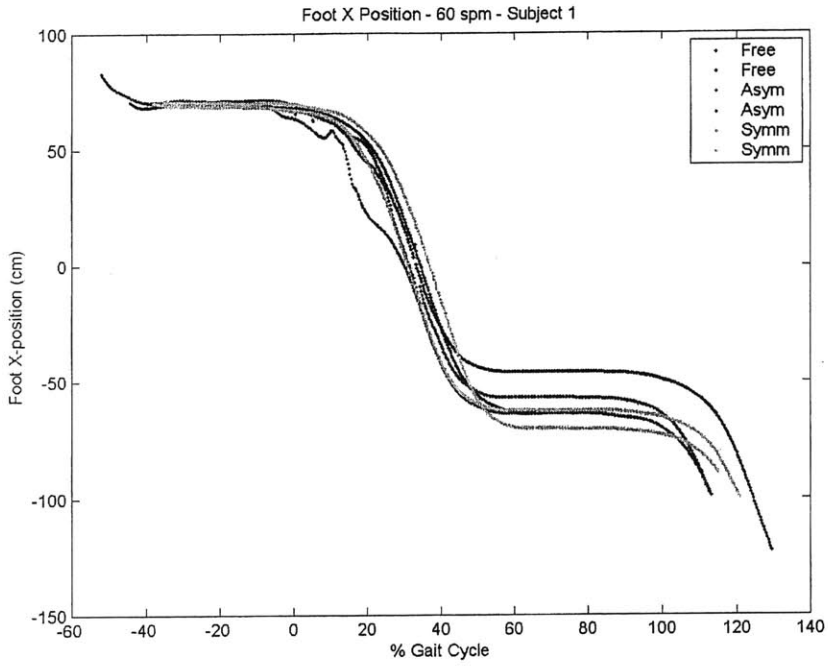

Figure 5-3: Foot x-position, Subject 1, slow walking.

second trial was able to compensate. As was noted earlier, it is evident here that the variability between trials with the same loading is often greater than the variability between trials with different loading conditions. This suggests that the device does not significantly influence these parameters.

Figures 5-4 through 5-6 show the angles of the foot, shank and thigh respectively, in the sagittal plane for Subject 1 during comfortable speed walking.

In each case, the general patterns and overall magnitudes of the rotations are very similar. The maximum rotation angle of the shank and thigh are nearly identical in all cases. There is a slight reduction in the foot angle in both the asymmetric and symmetric case (about 7-8 degrees) as compared to the no loading condition. This could be due to the restriction on ankle flexion imposed by the ankle weights, which were worn on the right foot in both cases. If this is the cause of the decreased magnitude of rotation, it should not be present in the ankle module final prototype.

These data suggest that the gait cycle is not significantly altered by the addition of the ankle module and ankle weights in normal subjects. As noted, however, some

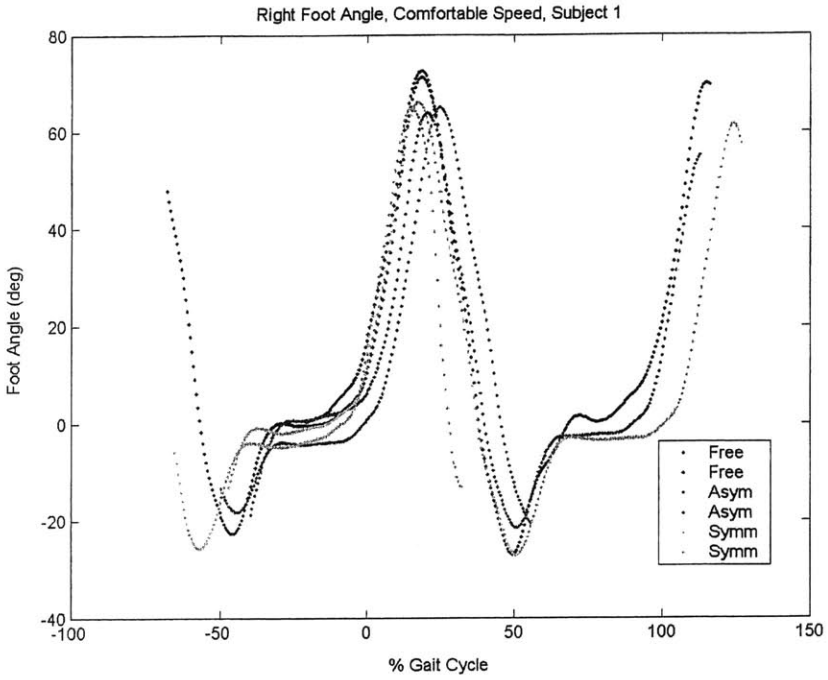

Figure 5-4: Foot angle, Subject 1, comfortable speed.

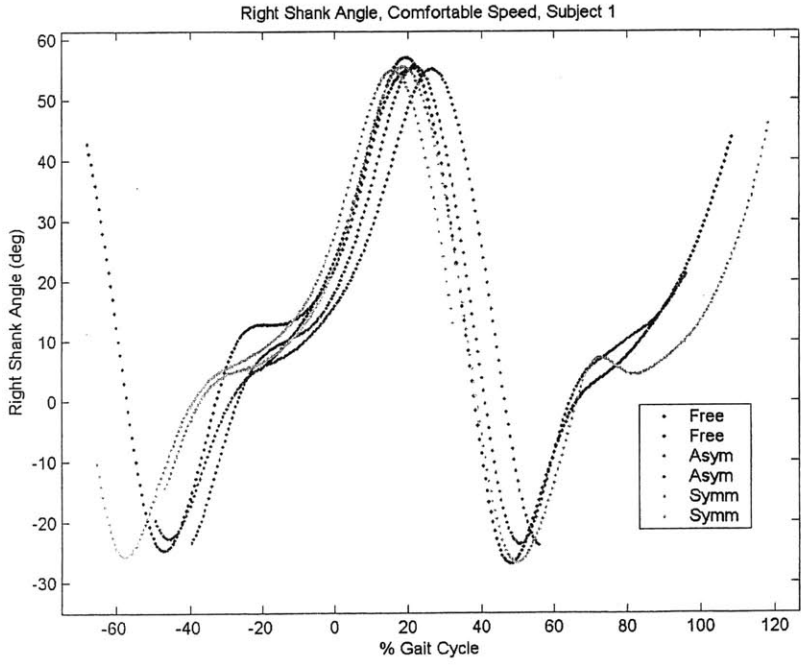

Figure 5-5: Shank angle, Subject 1, comfortable speed.

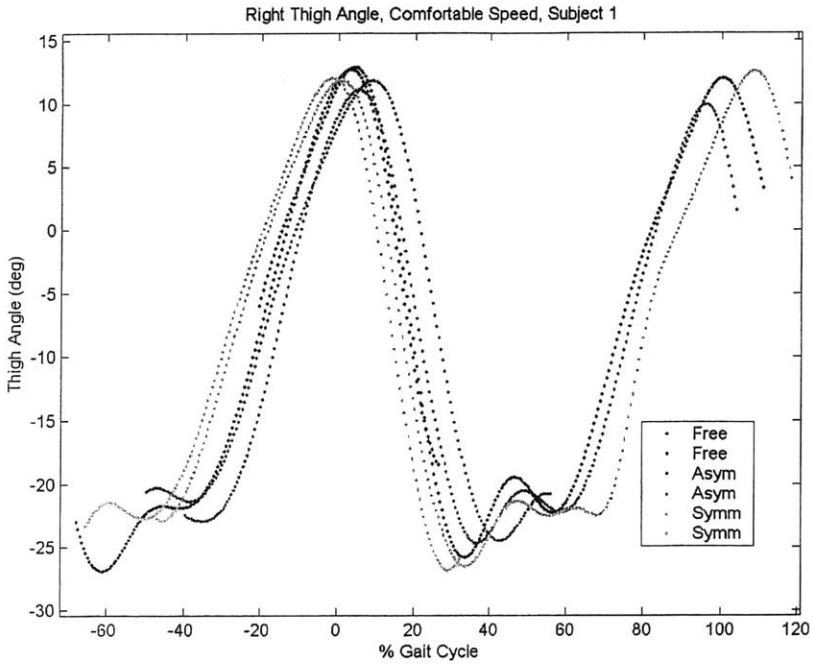

Figure 5-6: Thigh angle, Subject 1, comfortable speed.

small variations were present. In this set of tests, the weight was added right above the ankle in order to accommodate for the placement of the LEDs and other hardware. In the final prototype, the weight will be distributed much closer to the knee. This would reduce the perceived inertia that the subject feels and the effect on the gait pattern should be even less than is shown here.

Nothing is this data suggests that the current design would have any effect on gait patterns that would make it impractical. It also suggests that symmetric loading and allowing the subject to become accustomed to the device may further reduce any effects. Based on these promising results, it was decided to continue with the design of the prototype as planned.

Chapter 6

Actuator and Sensor Selection

This chapter discusses the different actuators that were considered for the ankle module. The rational for actuator selection is also explained. Due to the symmetric kinematics of the chosen design, two identical motors will be used.

6.1 Actuator Requirements

A number of performance characteristics can be considered when selecting an actuator for a given application. Those characteristics which are important for this application are discussed briefly here. Note that these characteristics relate to rotary actuators. Linear actuators were also considered but none were found that could provide sufficient force at a reasonable weight. Among those options explored were; solenoids, linear electric motors, and ball screws mounted to a rotary actuator. For example, assuming a moment arm of 15 cm, a force of about 55 N from each actuator (110 N total) would be required to produce an ankle moment of 17 N-m. Solenoids capable of producing this force with an appropriate range of motion would weigh approximately 4 lbs each.

6.1.1 Continuous Stall Torque to Weight Ratio

The most critical requirement for the ankle robot actuators is that they be lightweight. If the device becomes too heavy, it could become completely unusable for this application. A target weight for each actuator was set at about 1 lb. It must also, however, provide sufficient force to assist patient movement. The continuous stall torque of a motor is defined as that which results in a steady-state temperature rise. The motor can produce this torque continuously at zero speed if the ambient temperature is below a specified value [23].

Because of the high torque and low speed requirements for the device, it was anticipated that some gear reduction would be needed to minimize the overall weight of the device. An actuator of reasonable size was sought with a high ratio of continuous stall torque to weight and the transmission components were selected to minimize overall device weight.

6.1.2 Backdriveability

To allow the patient to move freely with the device attached, the motors must be backdriveable. The three factors that limit the backdriveablity of an actuator are, friction, inertia, and cogging torque. These should be as small as possible.

Motor friction can include static and viscous components. Viscous friction can be compensated for to some extent with a closed loop controller but increasing the controller gains to do this can compromise coupled stability when attached to the patient. Static friction is more difficult to compensate for.

Motor inertia includes the rotational inertia of the motor shaft and rotor. This becomes more important when a gear reduction is used because the inertia felt at the output of the gear train is equal to the inertia of the motor multiplied by the gear ratio squared.

Cogging torque is a position dependent torque felt when backdriving the motor. It results from the alignment of the magnet and lamination tooth edge in a brushless motor. It is especially problematic for controllers at low speeds. It can be minimized

by slanting the motor windings or increasing the air gap. Stall torque and efficiency can be compromised however by making these modifications [23]. Its effect can also be mitigated by using a gear reduction which effectively increases the number of poles felt at the gear output.

6.2 Types of Rotary Actuators

Characteristics of a number of rotary actuator are discussed in this section.

6.2.1 DC Brushed Servomotors

A DC brushed motor has permanent magnets on the stator and windings on the rotor. The motor is commutated mechanically via brushes which slide on a segmented slip ring on the rotor. The rotating magnetic field produced by the rotor is constantly trying to align itself with the stationary magnetic field induced by the stator. As the rotor turns to align, however, the brushes contact a new set of windings and create a new field.

An advantage of brushed servomotors is that they are easy to control due to the mechanical commutation of the brushes. Only an analog output and an amplifier are needed. It is also easier to decrease cogging in a brushed motor by increasing the number of slots.

Brushed motors also have several disadvantages. The brushes tend to wear out quickly when used in high torque applications due to the high currents drawn. They can also give off sparks generated at the brush interface. Heat generated in the windings is generally conducted through he rotor into the motor shaft and machine components. Experience has also shown that they may interfere with EMG signals if used nearby.

A variation on conventional brushed motors is an axial pole (e.g. ServoDisc) motor. These motors have virtually no cogging. The configuration and performance of such an actuator is shown in Figure 6-1. They are also typically larger in diameter and shorter than conventional brushed motors [23].

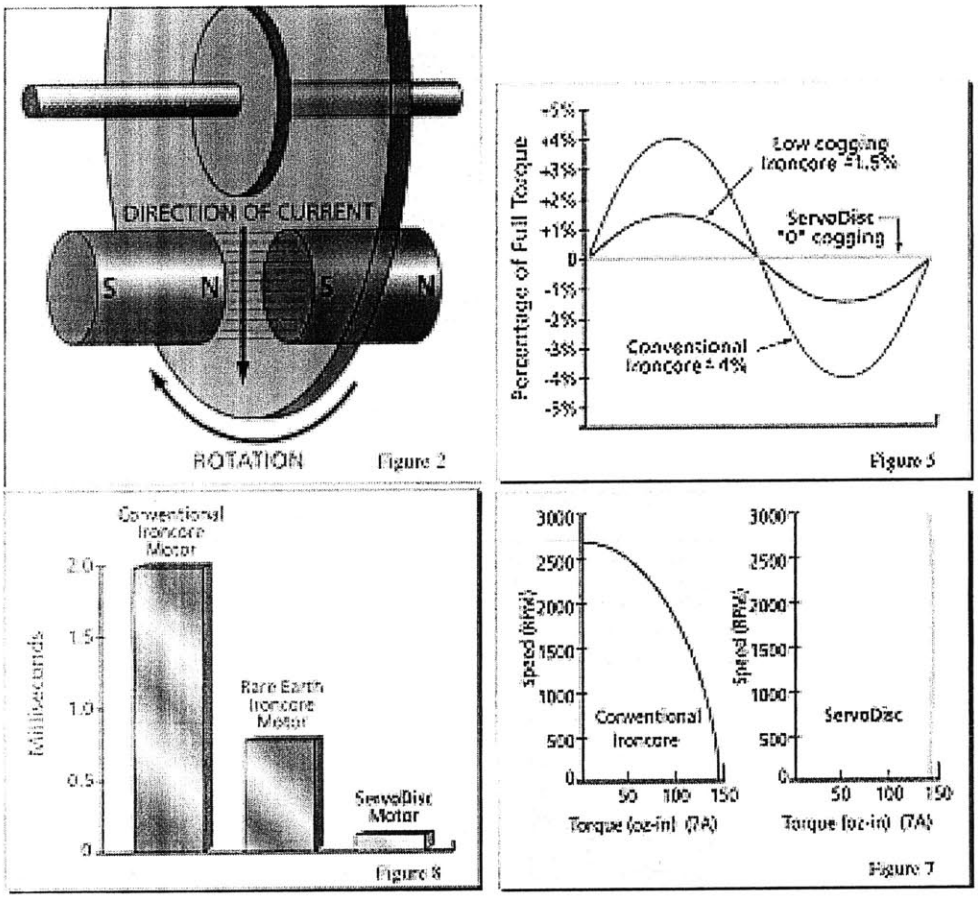

Figure 6-1: ServoDisc motors [26].

6.2.2 DC Brushless Servomotors

DC brushless motors have windings on the stator and permanent magnets on the rotor. Position information (e.g from Hall Effect Sensors) can be used to signal a motor driver which creates a rotating field in the stator. The rotor tries to follow this field.

Because the heat generated in a brushless motor can be dissipated through the stator, they can be operated at high torques and low speeds for a longer period of time. This is a major advantage for robotic applications.

The major disadvantages of brushless motors are increased controller complexity and the difficulty in reducing cogging. Cogging can be compensated for with a suitably fast controller [23].

6.2.3 Synchronous Reluctance Servomotors

These actuators work on the principle of magnetomotive force. When an iron object is placed in a magnetic field, a magnetic field is induced in the object. A torque is produced as the two fields try to align. This torque is called a reluctance torque because when the fields are aligned, reluctance in minimized. In synchronous reluctance actuators, a rotor with a radial configuration of iron bars tries to follow a rotating field induced in the stator. The torque produced is proportional to the lag in the fields.

These motors generally produce high torque at low speeds for direct drive applications. Such an actuator would be ideal for this application. However, no motor of acceptable weight was available. Specifically, the lightest motor of this type found was the NSK Megatorque AS4008 which has a mass of about 6.5 kg. A DC motor with a transmission to produce similar torque was still lighter and had similar impedance properties to a comparable reluctance motor [23]. A family of actuators that function using similar principles also exist. These include induction and switched reluctance motors.

6.2.4 Other Actuators

A number of other types of actuators were considered, including solenoids, Ultimag Rotary actuators and hysteresis motors. None of these options had available models that could provide sufficient force and range of motion at an acceptable weight. The actuator selection process was limited to some extent to motors that were readily available. For a future device, an actuator could be specifically designed to meet the requirements of the ankle robot.

6.3 Actuator Selection

Based on the above descriptions and available models, DC brushless servomotors were chosen as the best option. A number of companies manufacture a wide variety of models of these motors. An exhaustive search was done to find models that meet the criteria detailed above. Among the manufacturers who's models were considered were; Pittman, Parker, Bayside, Kollmorgen, and Maxon. The most appropriate model for each of these manufacturers, as well as the relevant specifications are shown in Table 6.1. Also listed in the table is the gear reduction ratio that would be required for the actuator to provide sufficient torque to meet the functional requirement. Figure 6-2 shows the ratio of continuous stall torque to weight for all five actuators. Figures 6-3 and 6-4 show the inertia and damping respectively that would be added to the system after the required gear reduction.

As can be seen in the figures, the Kollmorgen motor has the largest ratio of stall torque to weight. It also has the least viscous damping after reduction. The only actuator with lower inertia than the Kollmorgen motor after reduction is the Bayside BM060 which weighs 1.5 kg. This is due to the fact that the inertia felt after gear reduction is proportional to the square of the gear ratio. The bayside motor requires the smallest reduction but is still too heavy. These results suggest that the Kollmorgen motor is the clear choice. However, it does have a higher cogging torque than the Parker and Maxon motors, which feature "slotless" designs to reduce or eliminate cogging. Because of the critical weight requirement, the Kollmorgen RBE 00714 was

Motor	Cont. Stall Torque (N-m)	Inertia ($g - cm^2$)	Mass (kg)
Bayside BM060	0.54	93	1.5
Pittman 44X2	0.135	57	0.51
Parker SM161A	0.18	110	0.50
Kollmorgen RBE00714	0.249	32	0.39
Maxon EC40	0.125	85	0.39
	Visc. Damping (N-m/RPM)	Cont. Stall/Mass	Ratio Reqd.
Bayside BM060	1.5E-6	0.36	13.0
Pittman 44X2	2.9E-6	0.26	51.9
Parker SM161A	1.99E-6	0.36	38.9
Kollmorgen RBE00714	1.41E-6	0.64	28.1
Maxon EC40	3.36E-6	0.32	56

Table 6.1: Performance characteristics of five motor options.

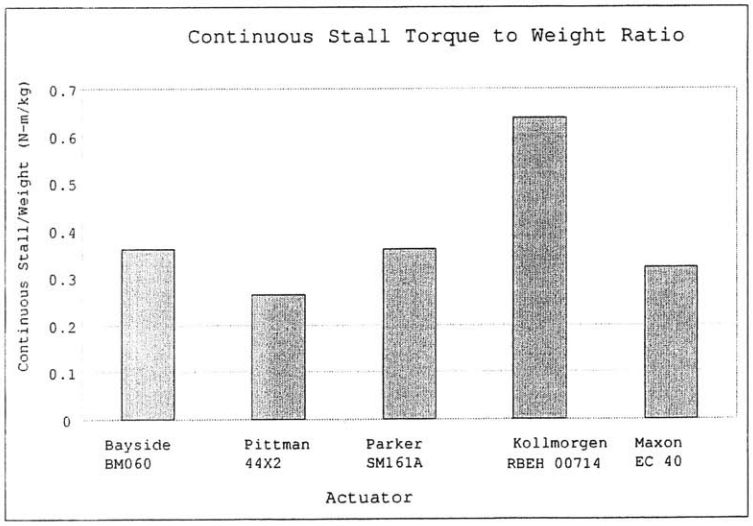

Figure 6-2: Continuous stall torque to weight ratio for 5 actuators.

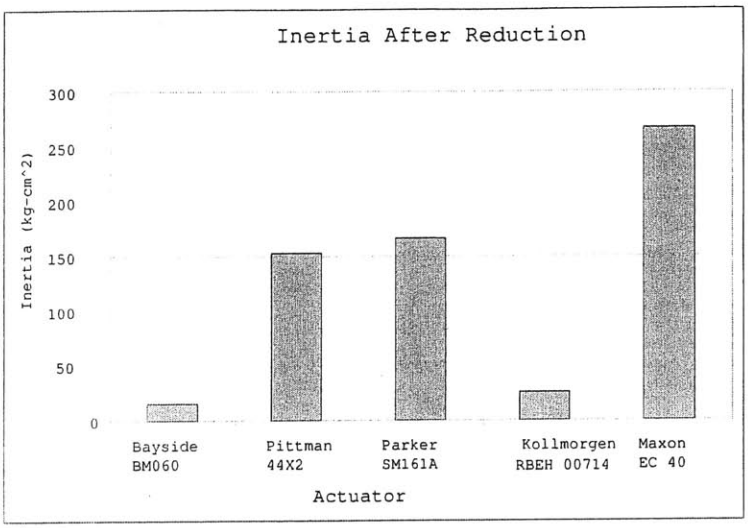

Figure 6-3: Inertia added after gear reduction for 5 actuators.

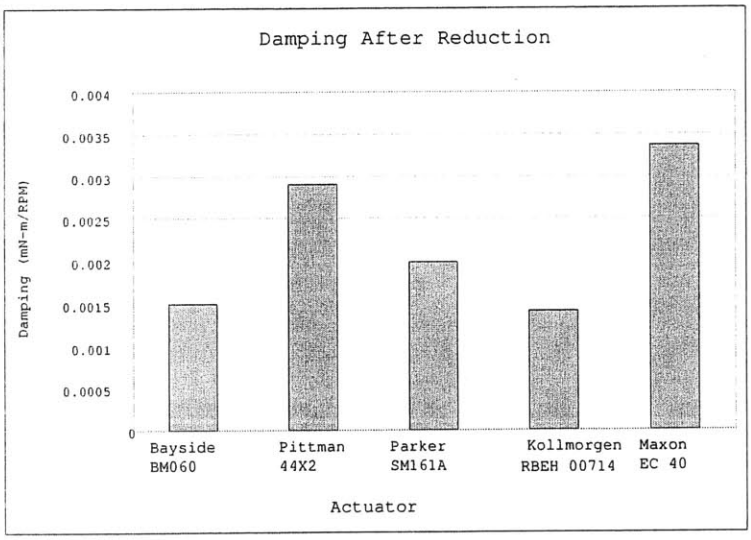

Figure 6-4: Viscous damping added after gear reduction for 5 actuators.

still selected for the ankle module. As mentioned previously, the gear reduction will mitigate the cogging effect by effectively increasing the number of poles.

6.4 Sensors

Sensors are needed to give position, velocity, and possibly force information to the controller and for measurement purposes. A number of options were available for sensing position and velocity information, including encoders and resolvers.

6.4.1 Incremental Encoders

Incremental encoders work by outputting two offset square wave pulses. The direction of rotation can be determined by which square wave is leading. An index bit is also output once per revolution and the angular position of the encoder shaft can be determined by counting the number of periods from the index bit. The resolution of the encoder can be increased by some factor using interpolation. Additional resolution can be obtained using quadrature decoding, which allows the edges between the waves, as well as the pulses to be counted. The advantages of incremental encoders are that they are small, lightweight and work well will existing hardware in the lab. They do need to be indexed each time they are turned on however. Another disadvantage is that they can be damaged if subjected to impact loads.

6.4.2 Absolute Encoders

Absolute encoders output a digital "word" using a pattern on a coded disk. A set of light sources shine through the disk and the light is detected on the other side by a set of photodiodes. These encoders do not require indexing at startup but are more expensive than incremental encoders.

6.4.3 Resolvers

Resolvers are constructed using two stationary sets of windings and a set of rotor windings. The two stationary sets of winding are offset from one another by 90 degrees and the rotor windings sit between them. The resolver operates by exciting the rotor with a sinusoidal voltage. The amplitude of the voltage on the stator windings varies as a function of the angle of the rotor. Resolvers also give absolute position information and do not need to be indexed. They are also much less susceptible to failure due to impact loads, which are likely to be encountered with this application. However, they are typically more expensive than encoders.

6.5 Sensor Selection

Incremental optical encoders have been used on other robots in the lab and work well with electrical equipment that is commonly used for controlling the motors. They were chosen for this reason and their low cost. The problem of impact loads was addressed by mounting them on a flexible coupling supplied by the manufacturer. If these sensors prove inadequate in initial testing, they can be replaced with resolvers without significant redesign of the electrical equipment.

The encoders are mounted to the rear shaft of the motor. Measuring position before gear reduction gives added resolution. The main requirement for the encoders is that they provide a reasonable resolution in a small, compact package. Gurley R120 encoders were the smallest encoders found with a high resolution. These were chosen for the design (Figure 6-5).

An important consideration with encoder selection is maximizing the resolution while ensuring that there are no counts lost. If the servo amplifiers have an input frequency of 2 MHz (a conservative estimate), at no time should the encoder send out pulses at a higher frequency than this. The maximum line count on the R120 encoder is 1024. This can be increased up to 16 times with interpolation. Interpolation is available at 1x, 2x, 5x, 10x, or 16x. An additional 4x resolution is gained by using quadrature decoding. The highest possible resolution for this encoder is then 65,536

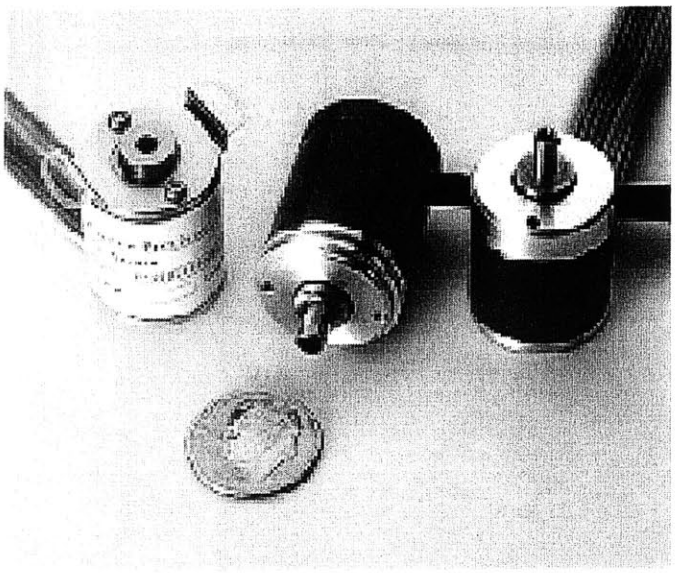

Figure 6-5: Gurley R119 and R120 optical encoders.

counts per revolution. This translates into a resolution of 0.0002 degrees. To produce an output of 2 MHz, the motor would need to rotate at a speed of 192 radians per second. This would require a movement at the ankle of approximately 6.4 radians per second. It is possible for movements faster than this to occur during operation. For this reason, 16x interpolation was not used. The lower 10x interpolation was used instead. This will allow movements of about 10.3 radians per second and a resolution of 0.0003 degrees.

To gather force information, current sensors are included in the electrical panel that controls the ankle robot. If this proves inadequate for controller function, or if it is desired to gather more data on forces and torques, resistive or capacitive force sensors can be placed under the foot. There are shoe inserts available off the shelf for this purpose. The problem with these units is that they tend to have a short life cycle. Strain gauges could also be placed on load carrying members of the robot, such as the foot connection piece, if desired. If it is desired only to detect gait events such as heel strike and toe off, switches could be placed on the patients heel and toe. These sensors are not included in the original prototype design but could be added without significant effort.

Chapter 7

Transmission

This chapter will discuss the selection of transmission components for the ankle module. As with other components, weight was a critical design factor is the selection process. As discussed in the previous section, the continuous stall torque of the selected motors is 0.25 N-m each. A gear reduction of 30:1 will produce a total output torque of 15 N-m to the mechanism. An addition torque amplification of approximately 1.5:1 (depending on the actual location of the patient's joints) will be produced in dorsi/plantar flexion due to mechanical advantage in the linkage. No such amplification will be produced in inversion/eversion. For this ratio, the maximum moments produced at the ankle joints will be approximately 23 N-m in dorsi/plantar flexion and 15 N-m in inversion/eversion. In addition, because of the simplicity of mounting the actuators vertically (parallel to the leg) the transmission should change the torque axis by 90 degrees to apply torques to the two links of the mechanism.

7.1 Modular Speed Reducers

Due to the large reduction required in a small space, modular speed reducers (gearheads) mounted to the output of the motors are a simple, feasible approach. A number of different types of gearheads are available. This section describes those that were considered for this application.

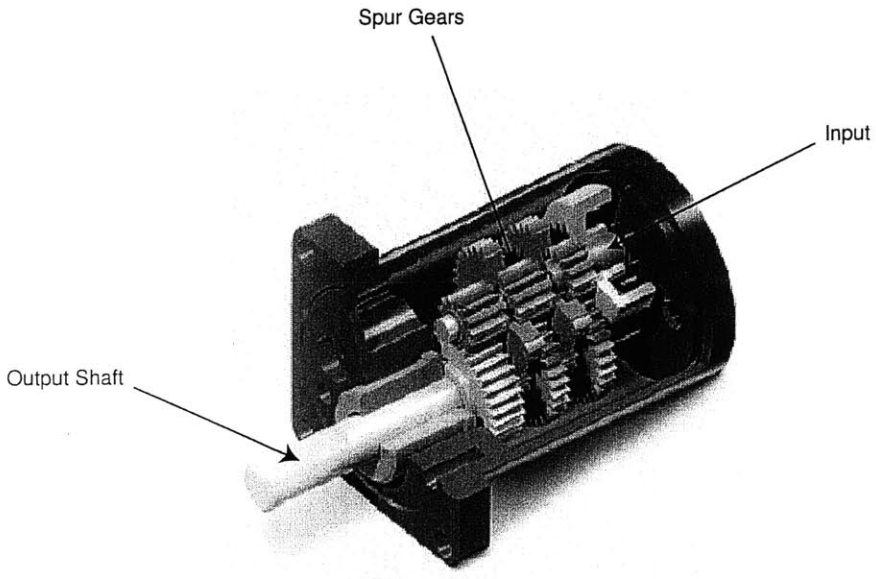

Figure 7-1: Spur gearhead construction [27].

7.1.1 Spur Gearheads

A spur gear is the simplest type of gear. A spur gearhead consists of one or more stages of spur gear reduction (Figure 7-1). Spur gearheads are typically simple and inexpensive but mostly used for low torque applications. This is because each gear in the train must support the entire torsional load. For this reason, these gearheads are often the largest and heaviest for a given torque. They also have more backlash than other types of gearheads. They typically have relatively high efficiencies and large gear reductions are available. The gear ratio of a spur gear stage is simply the ratio of the output gear diameter to the input gear diameter. The ratio of a spur gear train is the product of the ratio of the stages.

7.1.2 Planetary Gearheads

Planetary gearheads are another common modular speed reducer. A number of different configurations exist. The most common is shown in Figure 7-2. The stationary, outer gear is called the ring gear. The motor drives the planet arm which is connected to the small planet gears. As the arm rotates, the planet gears roll on the ring gear.

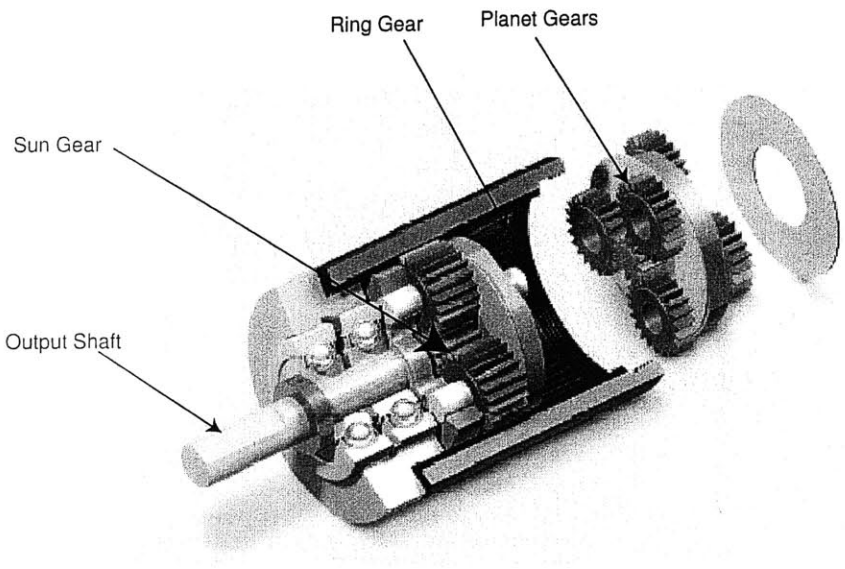

Figure 7-2: Planetary gearhead construction [27].

They roll a distance equal to the product of the rotation angle of the planet arm and the pitch diameter of the ring gear, D_{ring}. A sun gear with pitch diameter D_{sun} also meshes with the planet gears. The sun gear rotates due to the motion of the planet gears at a rate slower than the planet arm. The output of the gear stage is the rotation of the sun gear. The gear ratio, R_p for a planetary stage is

$$R_p = \frac{D_{sun}}{D_{ring} - D_{sun}} \tag{7.1}$$

The configuration of this type of gearhead makes it very simple to make multiple stages of reduction in a small space. The same ring gear can be used for a number of stages [23]. Another advantage of planetary gearheads over spur gearheads is a higher torque carrying capacity because the torsional loads are shared by multiple planet gears. Backlash is also typically lower for planetary gear systems than spur gearheads.

7.1.3 Harmonic Drive Gearheads

Harmonic drive gearheads operate much in the same way a planetary gearhead does but with different components which produce a much larger reduction. One possible

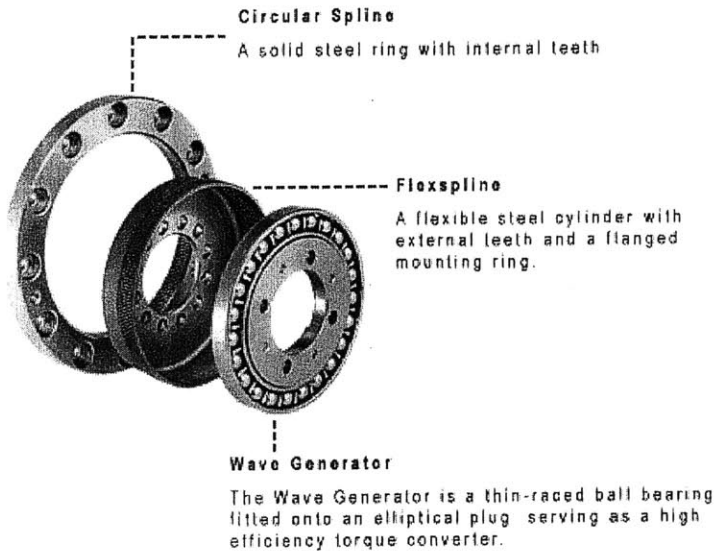

Figure 7-3: Harmonic gearhead components [30].

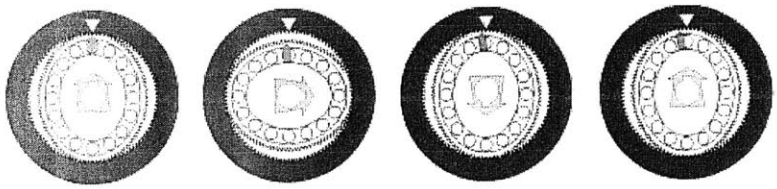

Figure 7-4: Harmonic gearhead principle of operation [30].

set of components is shown in Figure 7-3. A ring gear with inner teeth (circular spline) is used, as with the planetary gearhead. The planetary gears are replaced by a wave generator or cam rollers. The output sun gear is replaced with a flexible spline with external teeth (flexspline). The flexspline is of just smaller diameter (and has 2 fewer teeth) than the circular spline and is bent into an elliptical shape by the wave generator. It is connected to the output shaft or flange by a rigid back plate.

The principle of operation of a harmonic speed reducer is illustrated in Figure 7-4. The flexspline teeth on the major axis of the ellipse engage with the circular spline. As the wave generator rotates, the area of engagement on the circular spline changes. When the wave generator has rotated 180 degrees, the flexspline has regressed by one tooth relative to the circular spline. In each revolution, a relative rotation of two teeth is achieved.

This is equivalent to the planetary gearhead configuration described above where the sun and ring gears are of nearly the same diameter, resulting in a large gear reduction. The gear ratio of a harmonic stage, R_h can be expressed as a function of the number of teeth on the circular spline, N_{cs}, and the flexspline, N_{fs}.

$$R_h = \frac{N_{fs}}{N_{cs} - N_{fs}} \tag{7.2}$$

The denominator of Equation 7.2 is usually 2. Very high transmission ratios can be obtained in a single stage (50:1 to 200:1) [23]. They are typically ideal for robotic application where weight and space are critical. They can also handle relatively high loads. Backlash is very low in such a system because multiple teeth are in contact at any time. However, because of the preload forces on the teeth, they have high friction, especially at low speeds. They are not designed to be backdriven, as is required for this design.

Another type of speed reducer called a cycloidal gearhead has similar limitations.

7.2 Bevel Gears

Bevel gears allow torque to be transmitted through intersecting axes (see Figure 7-5). Most bevel gears transmit at right angles but they can be machined for other applications. For this design, the torque axis should be changed by 90 degrees. It is also possible to get additional gear reduction by using bevel gears of different pitch diameters (bevel gears sets with the same diameter are called miter gears). The reduction ratio of a set of bevel gears is simply the ratio of pitch diameters or number of teeth of the gear to the pinion.

Bevel gears can be made with straight or spiral cut teeth. Spiral bevel gears have a larger tooth contact area and are thus stronger, quieter and have less backlash with a slight increase in friction. When bevel gears rotate, forces are created in directions other than the direction of rotation. These forces depend on speed, torque applied, and tooth profile. The most important such force is the thrust force which tries to push the gears apart. This can increase backlash and noise. It can also damage

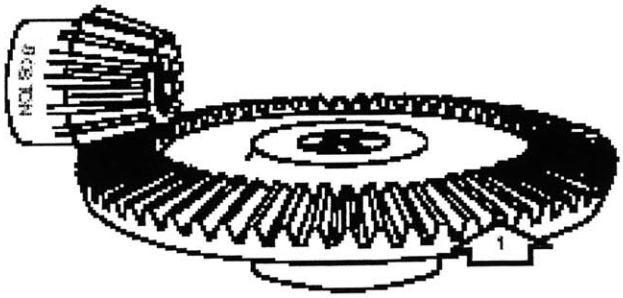

Figure 7-5: Straight tooth bevel gears [31].

bearings if not designed correctly. For straight tooth bevel gears, this force always acts in one direction but with spiral teeth, it can act in both directions depending on the direction of the motion and the tooth angle. Also, the sudden stopping of a spiral tooth bevel gear causes a momentary reversal of thrust. This aspect must be considered when selecting bearings for spiral bevel gears [15].

7.3 Other Transmission Options

There are some types of gears that can supply large reductions but are smaller and lighter than bevel gears and planetary gearheads. Some examples are worm gears and and hypoid gears. They can also work at right angles. However, the generally have much more friction and are not designed to be backdriven.

There are a number of alternatives to gears for torque amplification and speed reduction. These each have advantages and disadvantages. Some of these alternatives are; traction drives, wire capstan drives, belts, and cables.

There are possible configurations for devices that would have similar functionality to the chosen design that could incorporate one or more of these alternatives. The main advantage that could be gained is a significant weight reduction due to the elimination of metal gears. However, due to the time sensitive nature of the project, it was decided to pursue the more straightforward design alternative using standard gear components. The alternatives could be explored in future designs.

7.4 Selected Transmission Components

Based on the above discussion and a search of available components, a single stage planetary gearhead and a spiral bevel gear set were chosen to achieve the 30:1 reduction and torque axis change.

The selected gearhead is a Bayside PS 40-010 planetary module. The maximum reduction available in a single stage (each stage adds significant weight) was 10:1. One of these units will be mounted directly to each of the motors using a mounting kit supplied by the manufacturer. The gearheads have a 40 mm diameter, weigh 1 lb each, and have a maximum backlash of 10 arc minutes.

The additional 3:1 transmission ratio and the changing of the torque axis was achieved with a set of spiral bevel gears from Stock Drive Products. The pinion and gear have pitch diameters of 30 and 90 mm, respectively. The pinion has 15 teeth, while the gear has 45. The gears are made of steel and the teeth are hardened to HRC 48-53.

To reduce weight, gears of lighter materials were considered (e.g. plastic, brass) but were not strong or durable enough for this application. Because the pinion is the smaller but limiting gear in terms of strength, using a steel pinion with a gear of a lighter material was also considered. No available sets that could meet the requirements of this design were found, however. It was decided to use the steel gears but to remove material from the large gear to reduce weight. The hub length was decreased, and the bore was increased. Lightening holes were also added around the face of the gear just inside the tooth diameter. Detail drawings of these modifications are found in the appendix.

Another possibility to reduce the weight of the large gear is to remove material around the outside of the gear (including the teeth) over an angle of about 120 degrees as shown in Figure 7-6. This is possible because of the limited range of motion of the device. The links driven by this gear need to rotate no more than 180 degrees to meet the functional requirements. This was not done for the prototype but could be done in the future if needed.

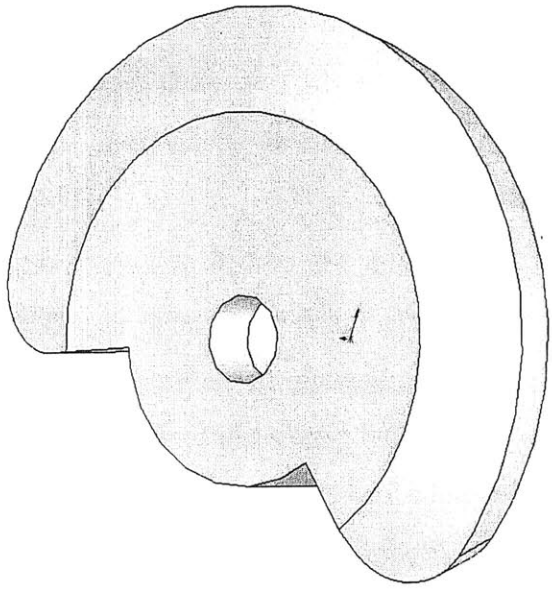

Figure 7-6: Possible material removal from large bevel gear.

These gears are expected to produce a thrust force of no more than 150 N at the maximum speed and torque expected for the ankle device.

Detailed specifications for the transmission components are found in the appendix.

Chapter 8

Patient Connection

One of the interesting challenges in the design of this device was determining how to connect the mechanical hardware to the patient in a safe and effective manner. It is important that the connection be rigid to ensure that the patient moves where the robot does and also to improve controller performance. At the same time, it must not restrict any movement of the patient or cause pain or injury. It is important that the patient interface not apply pressures large enough to restrict blood flow or cause skin damage. This is especially important considering the elderly patient population for which this device will be primarily used. This chapter will discuss the issues and component design for the connection components to the patient's leg and foot.

As mentioned previously, the connection would ideally work on either leg and on multiple sizes of patients with little or no modifications. It should also be easily attached and removed, taking no longer that 5 minutes.

8.1 Leg Connection

The leg connection piece is an interface between the patient's shank and the plate that the motors and gears mount on. Because this piece bears the weight of nearly the entire device, it is important that it be rigid and connect to the leg in such a way that it will not slide down the leg as the patient walks. To ensure this, a tight connection to the patient is required. It must not, however, apply too much pressure

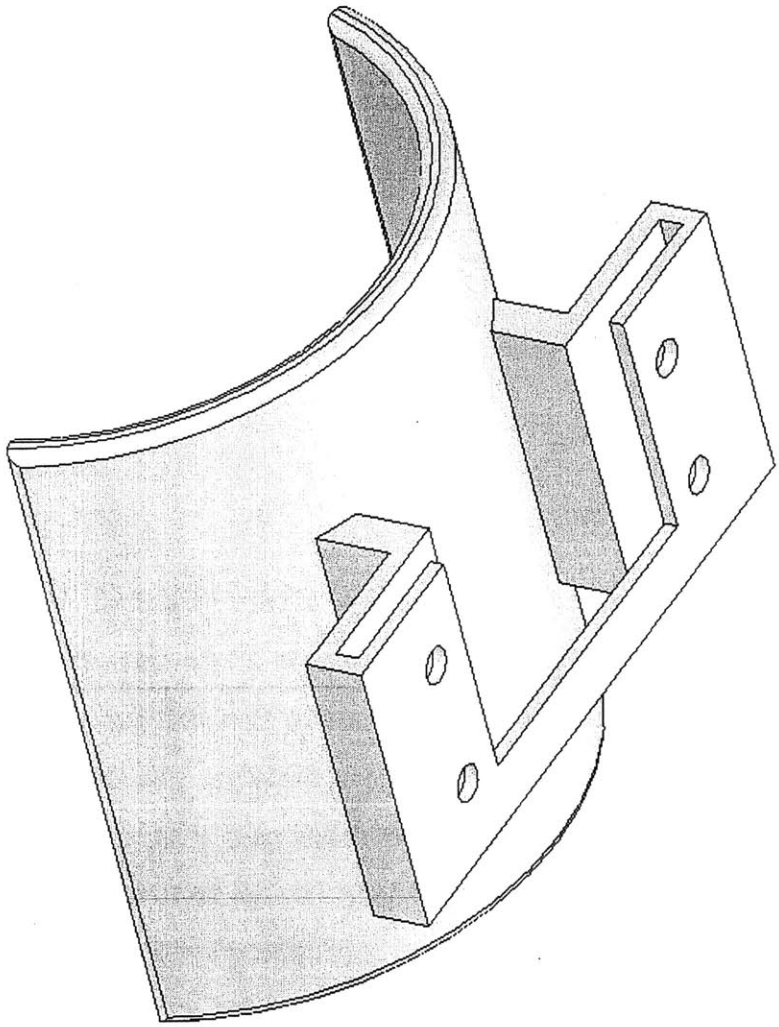

Figure 8-1: Leg connection (strap not shown).

to any part of the leg. For this reason, it was desired to distribute the force as much as possible along the leg.

The selected leg connection consists of 5 parts. An assembled view of the basic configuration is shown in Figure 8-1. The two main components are shown in Figures 8-2 and 8-3.

The cylindrical piece is made from High Density Polyethylene (HDPE). It is a 150 degree piece with rounded edges and slots with through holes for bolts to attach the mounting piece. The mounting piece is made from aluminum and has threaded holes to be bolted to the HDPE piece. The motor mounting plate of the robot slides into

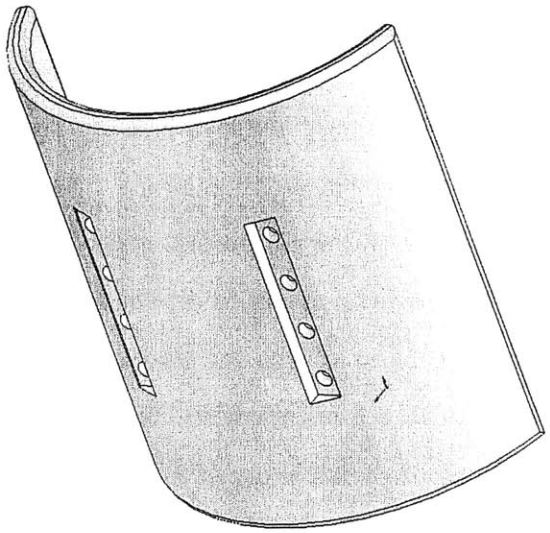

Figure 8-2: HDPE component of leg connection.

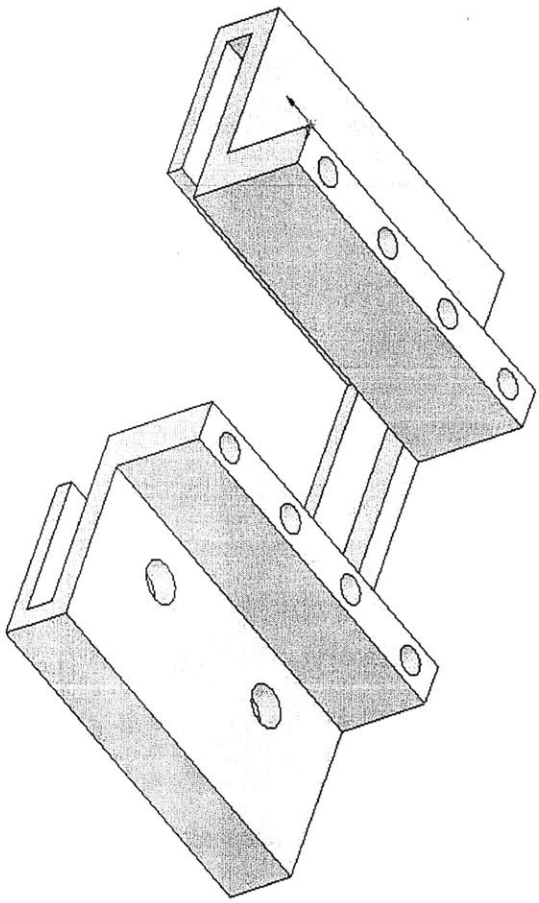

Figure 8-3: Aluminum component of leg connection.

the slot on this piece. It is held in place by 4 quick release bolts for easy removal if other sizes or adjustments are needed. Wedge shaped aluminum bolt plates go on the inside of the HDPE cylinder to distribute the bolt head force. Round head bolts will be used here to eliminate any sharp edges.

To ensure a good fit for a wide variety of patient sizes and for comfort and safety, an air bladder in a fabric sleeve will be attached on the inside of the HDPE cylinder. This system will inflate on the front of the leg and a large fabric strap will wrap around the rear of the leg and attach with velcro. It will be constructed of a blood pressure cuff designed to fit adults with arms of 12 to 22 inch circumference. This sleeve will be riveted to the inside of the HDPE piece. A schematic sketch of the top view of this setup is shown in Figure 8-4. The bladder pressure can be easily measured to ensure that an appropriate pressure is applied. Experiments with blood pressure cuffs have shown that pressures as low as 60 mm Hg were sufficient to support the weight of the device. This is an acceptable pressure that will not restrict blood flow. This system is also very easy to attach and detach from the patient. Only a single velcro strap is used.

8.2 Foot Connection

The foot connection pieces must attach rigidly to the hind-foot of the patient, as well as the rods of the robotic mechanism. It will be placed over the shoe and should allow the patient to roll over on their foot during stance. Because of the uncertainty in what the exact dimensions should be to feel comfortable during walking, experiments were done using a modified snowboard binding. The part of the binding that attaches to the fore-foot was removed, as well as the piece that goes behind the leg. It was then placed on a number of normal subject of different sizes and they were asked to walk and describe any discomfort. If discomfort of impedance to normal walking was reported, more material was removed until a comfortable connection was reached. The parts were then designed to similar dimensions. An assembled drawing of the concept without the strap is shown in Figure 8-5. The components are shown unassembled in

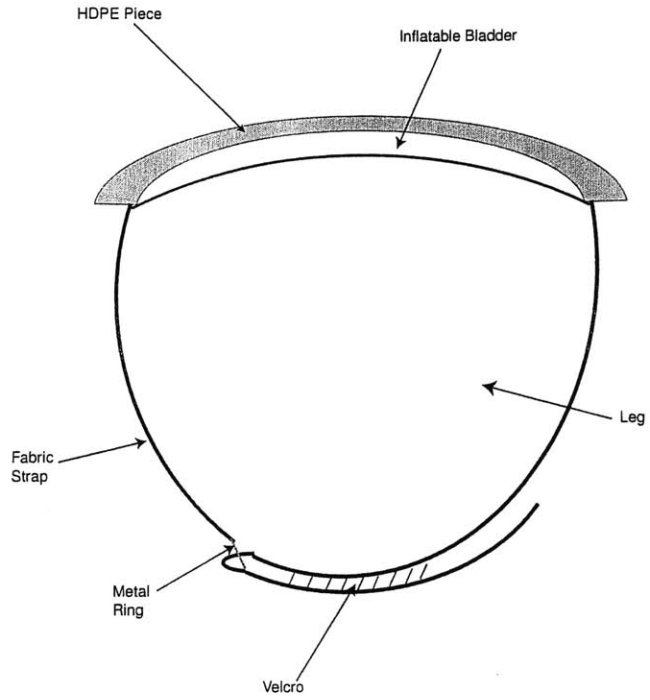

Figure 8-4: Schematic top view of air bladder and strap system.

Figures 8-6 and 8-7.

The piece under the foot is made of HDPE. The piece that goes around the heel is made from a piece of aluminum (see Figure 8.4) which is bent to the appropriate shape. A single strap (not shown in figure) goes over the hind foot. The strap is about 1.5 inches wide to distribute the force over a fairly large area on the foot and has a gel pad for comfort and to smooth any corners. The HDPE piece does not extend to the heel of the shoe. It also ends near the midtarsals to allow for rolling over onto the fore-foot. The rods of the robot connect through rod end spherical joints to the ends of the bent aluminum piece. Detailed drawing of these components are found in the appendix.

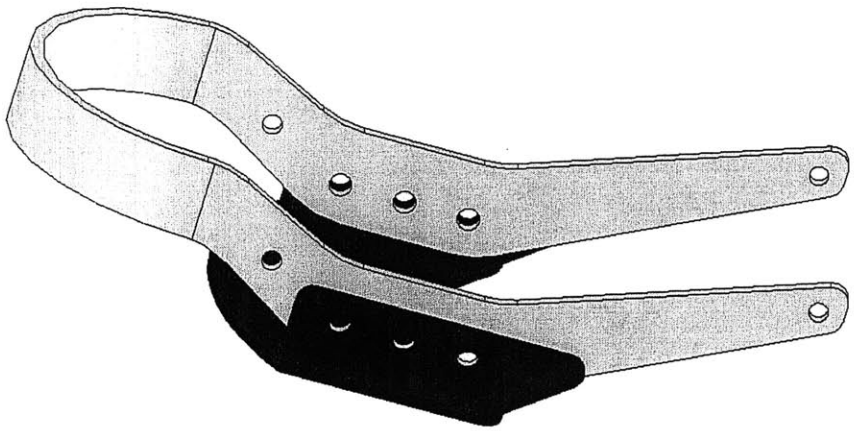

Figure 8-5: Foot connection (strap not shown).

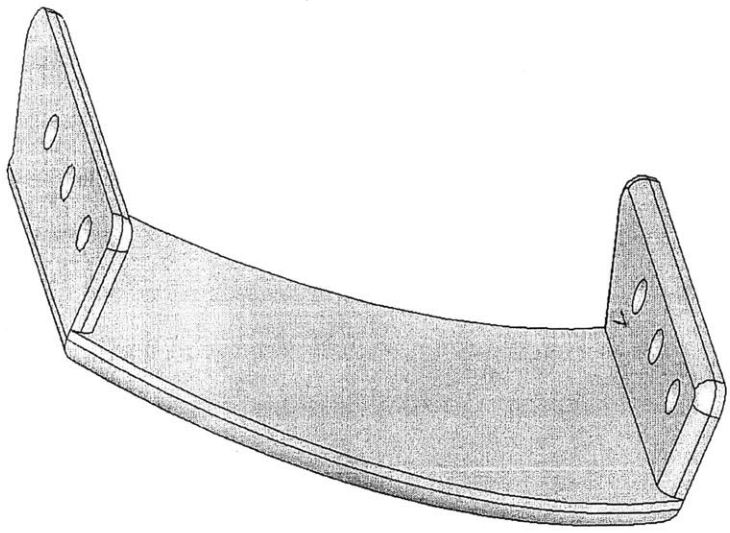

Figure 8-6: HDPE part of foot connection.

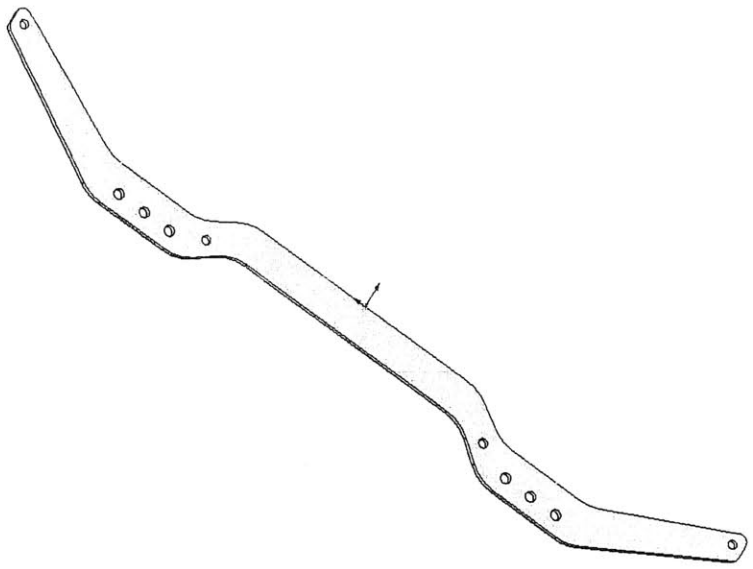

Figure 8-7: Aluminum piece of foot connection before bending.

Chapter 9

Design Overview

This chapter will discuss important aspects of the mechanical design of the ankle module. Selection of components such as bearings and sensors will be discussed. Actuator, transmission, and patient connection design and component selection were discussed in the previous three chapters and will not be revisited in detail here.

An important aspect of the design was that it be modular. Because the device being built is a prototype, some problems are likely to occur in clinical use that were not foreseen in the design. A modular design approach allows for changes to be made to components without major modifications to the entire device. Each component and part should be as independent as possible. A good example of this is the patient connection pieces. If they are found to be in need of modification, they simply need to have a connection to the robot that is similar to that of the current design and the rest could be altered as needed. No changes to the robot hardware would be required.

9.1 Assembly and Part Overview

An overview of the ankle module and some of its parts will be presented here using solid models created in SolidWorks. A solid model of the overall device concept is shown in Figure 9-1.

The motors are mounted parallel to the leg above the mechanism. This minimizes the inertia felt by the patient because most of the weight is near the knee. The

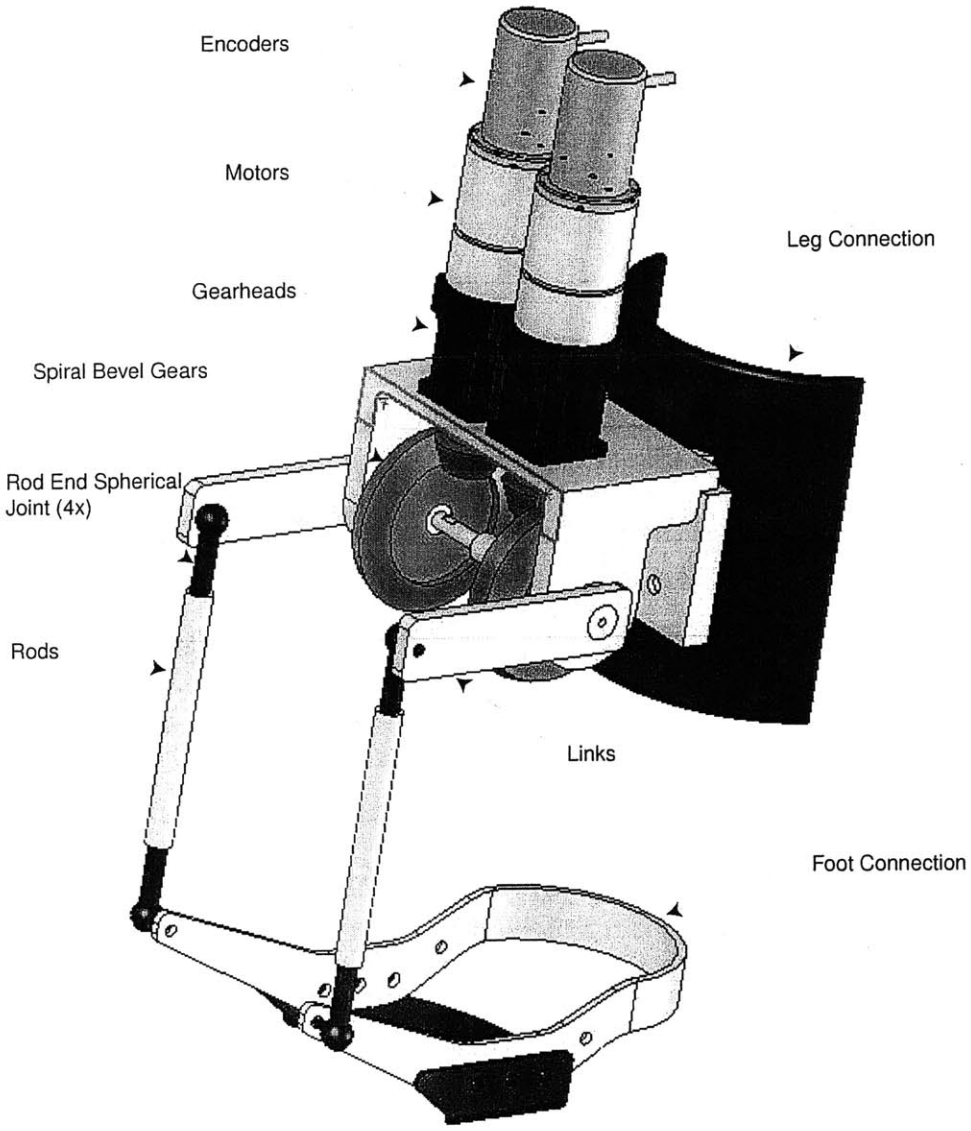

Figure 9-1: Ankle Module solid model.

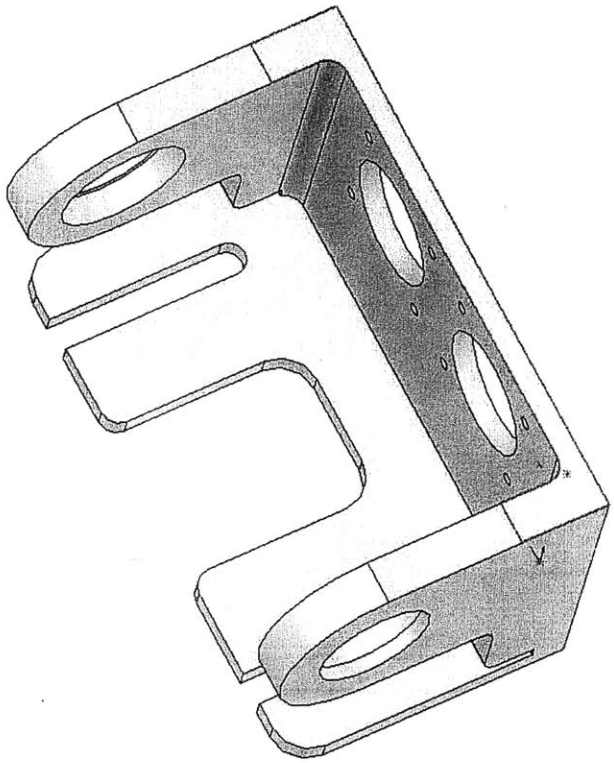

Figure 9-2: Solid model of mounting plate.

gearheads are mounted to one end of the motor and the encoders to the other. The bevel pinions are mounted to the output shaft of the gearhead. These components are located with a custom designed mounting plate that slides into the leg connection piece. A solid model of the mounting plate is shown in Figure 9-2.

The gearheads bolt into the top face of the plate and the bearings which support the gears mount in holes on either side. The thin piece in the rear slides into the leg connection piece. A section view of the assembly of gears and bearings is shown in Figure 9-3.

Torque is transmitted from the gearhead output shaft to the bevel pinion through a keyed shaft. Each of the large gears are mounted onto an aluminum shaft with a "polygon" profile which transmits torque with less stress concentration than a keyway. Each shaft is mounted to the mounting plate on a THK Cross Roller Ring Bearing which is discussed in more detail in a subsequent section. The inner race of these bearings is preloaded by a step in the shaft. The outer race is preloaded by a flange

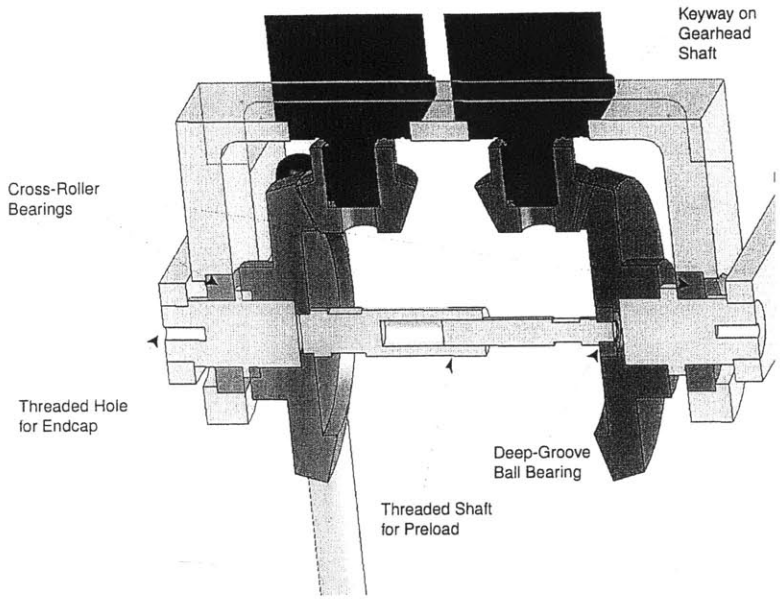

Figure 9-3: Bearing assembly section view.

on the mounting plate. A threaded shaft that runs between the two gears supplies the preload force. Flats for a wrench were added for convenience. Because the gears must rotate independently, another bearing was needed. An SKF deep-groove ball bearing is mounted in one of the gears and is preloaded on the inner race by the preload shaft and the outer race by a flange on the gear.

9.2 Link Dimensions

9.2.1 Link Lengths

It was important to determine the appropriate lengths of the mechanism links to allow full range of motion for patients of a variety of sizes. The distance between the two links that attach to the shank in the frontal plane was determined based on the width needed to mount the gears. It was also important that this distance not be great enough to put hardware inside the patient's leg.

To determine the appropriate length of the links and rods, a kinematic analysis was done in the sagittal plane, where the largest motions take place. Additional length was then added to allow for simultaneous movements in other planes. A diagram

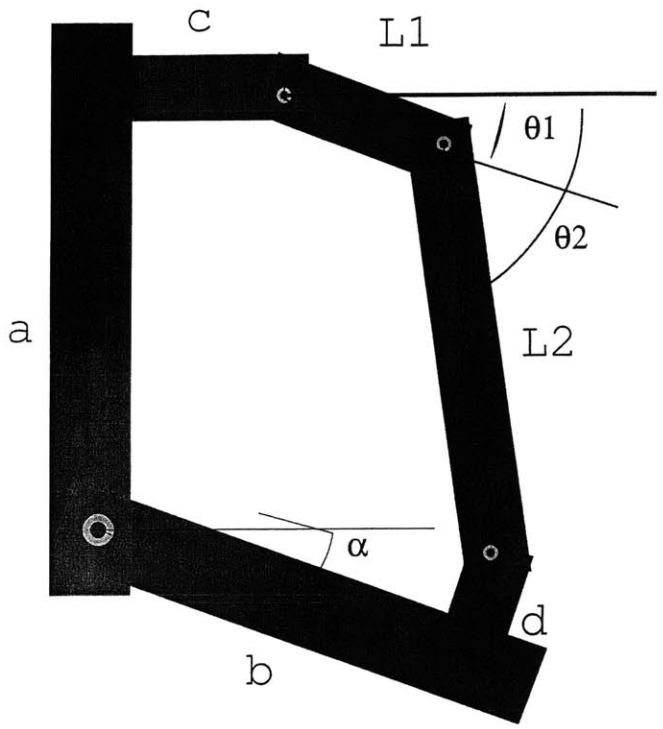

Figure 9-4: Sagittal plane linkage.

of the mechanism in the sagittal plane is shown in Figure 9-4. This is similar to a four-bar linkage with the leg, foot, links, and rods being the four links.

The kinematics of this mechanism can be expressed in the following equations.

$$c + L_1 \cos\Theta_1 + L_2 \cos\Theta_1 - d\sin\alpha - b\sin\alpha = 0 \tag{9.1}$$

$$a - L_1 \sin\Theta_1 - L_2 \sin\Theta_1 - d\cos\alpha + b\sin\alpha = 0 \tag{9.2}$$

Here, the inputs are a, the vertical distance from the ankle joint to the axis of the links, b, the horizontal distance from the ankle joint to the point of connection on the foot, c, the horizontal distance from the ankle joint to the axis of the links, d, the vertical distance from the ankle joint to the foot connection point, and α, the angle of the foot with respect to the leg. There are four unknowns in these equations, L_1 and L_2, the lengths of the links and rods respectively, and their respective rotations,

Θ_1 and Θ_2. To solve for these unknowns, two boundary conditions are needed. These can be based on the ranges of motion of the patient. To ensure that the links do not rotate too far, which could cause problems with interferences and controllability, Θ_1 was limited to plus or minus 45 degrees. At maximum plantar flexion (α = 45 degrees), Θ_1 should be 45 degrees. At maximum dorsiflexion (α = -25 degrees), Θ_1 should be -45 degrees. This allows us to solve these two equations for the appropriate links lengths to ensure an adequate range of motion.

Because the limiting case (longest required links) would occur with a large patient, these were the values used in the simulation. A custom designed spreadsheet was designed to solve this problem. The values used for the simulation were; a = 8 in., b = 6 in., c = 5 in., and d = 1 in.. When the boundary conditions were applied, equation 9.1 was solved for L2, which was then substituted into equation 9.2. The result was a single equation with only one true unknown, L1. Thee other three unknowns were all expressed in the spreadsheet as functions of L1. The single remaining equation was input to a cell in the spreadsheet and the Excel Solver function was used to minimize it while varying L1 subject to the boundary condition constraints. The required links lengths were found to be L_1 = 3.8 in. and L_2 = 7.7 in.. The actual links were sized just larger than this. Detailed drawings and dimensions are found in the appendix.

9.2.2 Link Cross-Sections

Once the lengths of the links and rods were known, the cross-section dimensions were chosen to ensure that the parts were strong enough to carry the required loads and that they had sufficient stiffness. A high stiffness was desired to allow force transmission with minimal deflection and also to provide favorable dynamics to improve controller performance.

The stiffness of the system was investigated using a beam model, again in the sagittal plane. For this calculation it was assumed that the links (that attach to the leg) were constrained so that they could not rotate (cantilevered). A simulated torque of 100 N-m was then applied at the ankle joint. This is larger than the torque that would be experienced in operation because the actuators cannot supply a torque

this large. This is a conservative estimate that would only occur if the motors were braked and a large external force was applied. This analysis only considers deflections in the links, rods, and foot connection piece. Compliance in shafts and gears are not considered here.

In such a loading condition, five significant deflections would occur; bending and torsion in the links, extension in the rods, and bending and torsion in the long members of the foot connection piece that attach to the rods. The torsional deflections are caused by the rod end joints being offset from the axis of the links by a small distance (about 1.5 cm). It was desired that the sum of these deflections be less than 0.4 mm. This corresponds to a total stiffness of 250 N-m/mm.

The deflection at the end of a beam, y, in bending with the load, F, applied at the end beam can be expressed as

$$y = \frac{Fl^3}{3EI} \tag{9.3}$$

where F is the force applied, l is the length, E is the modulus of elasticity of the material, and I is the cross sectional moment of inertia. The torsional deflection, Θ for a non-round beam with a torsional load, T, applied is

$$\Theta = \frac{Tl}{GK} \tag{9.4}$$

where G is the modulus of rigidity of the material and K is a geometric factor based on the cross sectional dimensions. For a rectangular cross section,

$$K = ab^3[\frac{16}{3} - 3.36\frac{b}{a}(1 - \frac{b^4}{12a^4})] \tag{9.5}$$

where $2a$ and $2b$ are the width and height of the beam, respectively.

The deflection of the rods, δ, in pure tension can be expressed as

$$\delta = \frac{Fl_r}{AE} \tag{9.6}$$

where l_r is the length, and A is the cross sectional area [22]. These equations can

be used to determine all five deflections of interest.

For this analysis, the parameters of interest are the width and height of the link cross section (a_l and b_l), the width and height of the foot connection piece members (a_c and b_c), and the diameter of the rods, d_r. The lengths of these members were determined in the previous section. The loads applied to each member due to the 100 N-m torque at the ankle is 330 N (on each side). This is applied to the rods by the leg connection and is in turn applied to the links. All of these components were made of aluminum (E = 72 GPa and G = 27 GPa).

Estimated cross section values were chosen and substituted into the above equations to determine the total deflection present. The chosen values were $a_l = 7.5$ mm, $b_l = 30$ mm, $a_c = 4.0$ mm, $b_c = 10$ mm, and $d_r = 12.5$ mm. The total deflection for the system was then calculated to be 0.24 mm. This translates to a stiffness of 417 N-m/mm. This was deemed adequate as it is stiffer than the requirement. The actual device dimensions are slightly larger than those listed here in many cases. This was done for convenience. See the appendix for exact part dimensions.

Static safety factors were also checked using a similar model and a load of 300 N-m. The smallest safety factor was 3.2, corresponding to the foot connection piece. Some of the parts could be made slightly smaller and lighter and still be adequately stiff but such measures would only reduce the total weight of the device by about 0.1 percent.

9.3 Bearings and Joints

This section describes the component selection for the joints of the robot. This includes the bearings discussed in the bearing assembly section above and the spherical joints that connect the rods to the links and the foot. Brief descriptions of selected bearings types are also included.

9.3.1 Rolling Element Bearings

The most important bearings in this device are those that support the shaft of the bevel gears. These bearings must support the static loads imposed by the mechanism as well as the dynamic loads caused by the rotating gears which were discussed in the previous chapter. This section will discuss some commonly used types of bearings that could possibly be used for this application. Only rolling element bearings were considered for practical reasons. Other types of bearing is (e.g. sliding contact, magnetic, hydrodynamic, and air) are not reasonable alternatives for this design.

There are two main classes of rolling element bearings, ball bearings and roller bearings. Ball bearings use spherical balls that roll in some sort of race. Roller bearings use cylindrical shaped rollers (sometimes tapered or spherical) instead of balls. There are a number of different types of ball and roller bearings, with either the shape of the roller or its orientation being unique. Only a few of the possible configurations are discussed here.

Deep groove radial contact bearings have balls mounted in grooves on the inner and outer bearing rings as shown in Figure 9-5. These bearings can handle large radial loads and moderate axial loads in both directions but generally require a pair mounted at some distance apart to support moments.

Angular contact bearings have balls that contact the races along a line inclined to plane orthogonal to the axis of rotation as shown in Figure 9-6. Radial load carrying capacity is similar to that of deep groove ball bearings but they can carry up to three times the axial loads (but only in one direction). These bearings are typically designed to be mounted in pairs (face to face or back to back) to support moment and bidirectional loads [23].

Thrust ball bearings (Figure 9-7) are designed to carry large, bidirectional thrust loads. Additional bearings are needed to maintain axial and moment stiffness.

Cylindrical roller bearings can have number of different race shapes as shown in Figure 9-8. They typically can carry very large radial loads and are ideal for heavily loaded shafts but require additional bearings to support axial and moment loads.

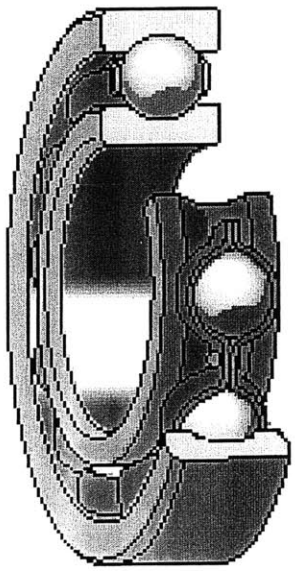

Figure 9-5: Deep groove radial contact ball bearings [28].

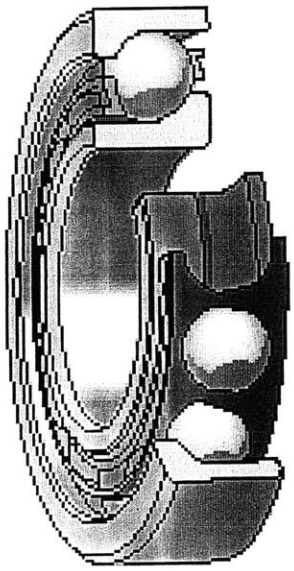

Figure 9-6: Angular contact ball bearings [28].

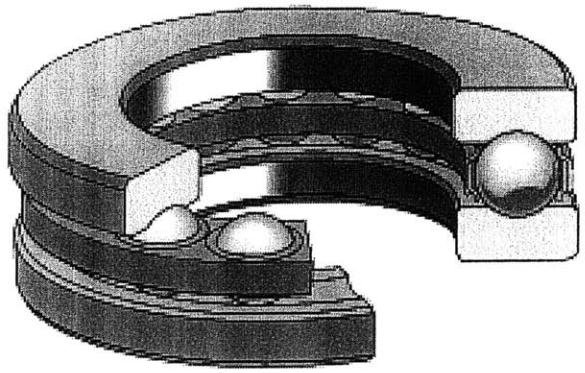

Figure 9-7: Thrust ball bearings [28].

Needle roller bearings (Figure 9-9) are similar but have smaller diameter rollers.

Tapered roller bearings have rollers mounted at an inclined angle to the axis of rotation as shown in Figure 9-10. They can support large radial and axial loads (unidirectional). Similar to angular contact bearings, they are designed to be used in pairs to support moment or bidirectional axial loads.

9.3.2 Cross Roller Ring Bearings

Due to the limited space for bearings in this design, it was desired to use a single bearing for each gear. As discussed above, most bearings are not designed to support radial, axial, and moment loads with a single bearing. A newer type of bearing, manufactured by THK, called a cross roller ring bearing is designed for such an application. This type of bearing has cylindrical rollers, each mounted orthogonal to the adjacent rollers as shown in Figure 9-11. These bearings can support high radial loads, bidirectional axial loads, and moderate moment loads with a single bearing. These bearings were chosen for mounting the gears for that reason. Specifically the RB 2008 model was chosen, dimensions and specifications are found in the appendix.

9.3.3 Bearing Life

The THK RB 2008 Bearing has a basic dynamic radial load rating, C, of 3.23 kN. It's basic static radial load rating, C_0, is 3.10 kN. The worst case loading conditions for

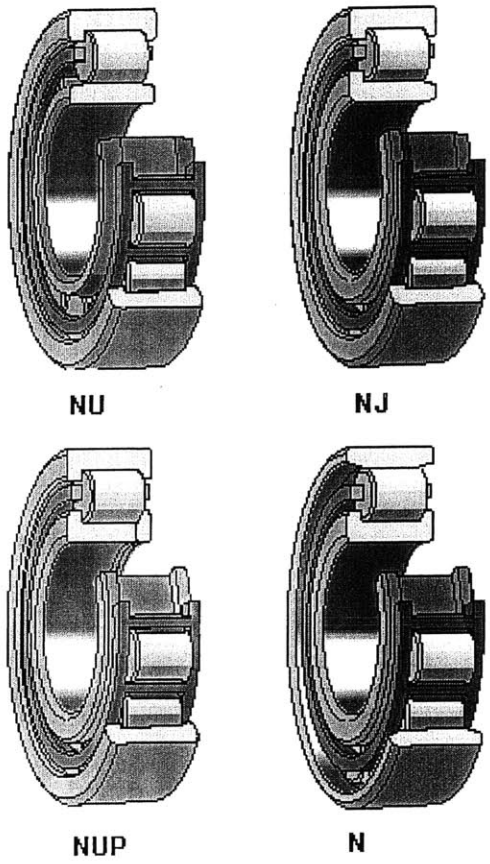

Figure 9-8: Cylindrical roller bearings [28].

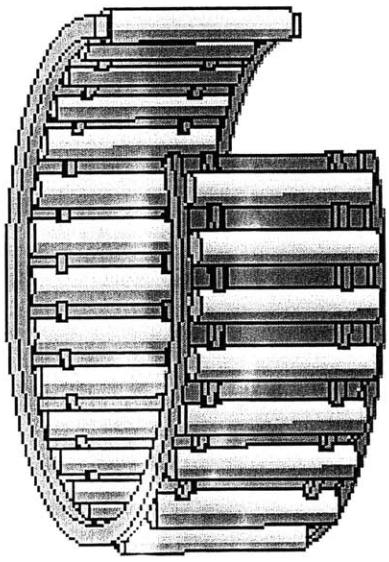

Figure 9-9: Needle roller bearings [28].

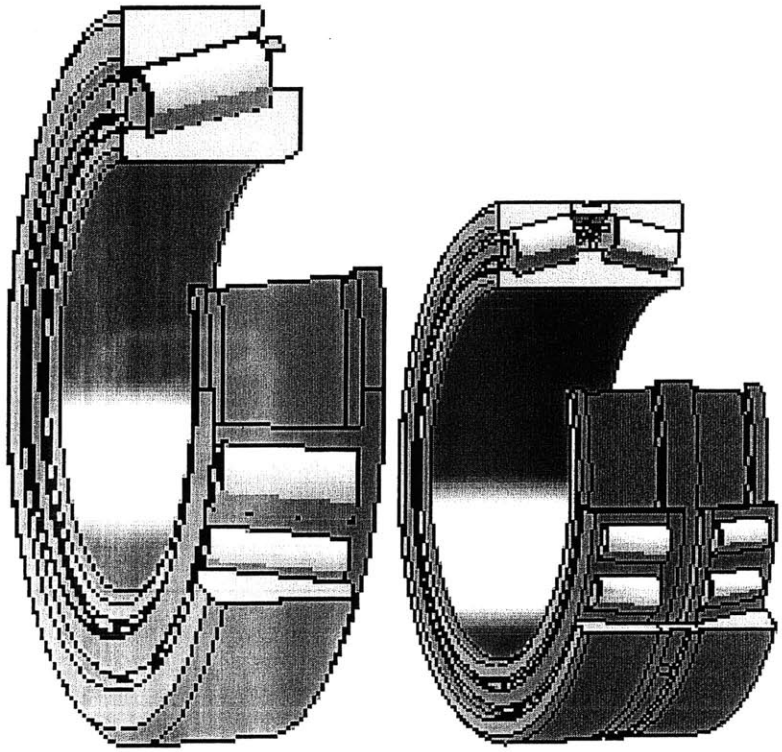

Figure 9-10: Single and double tapered roller bearings [28].

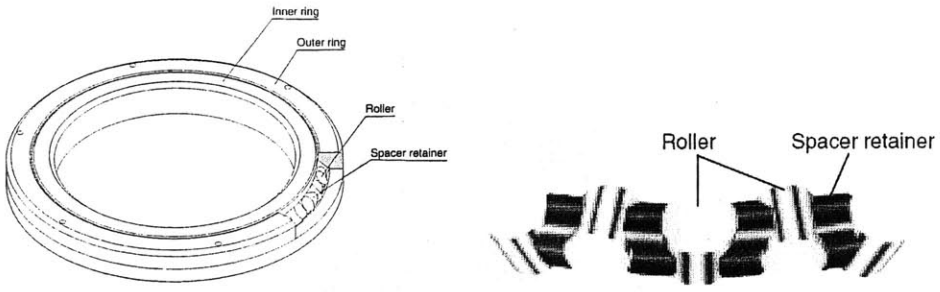

Figure 9-11: Cross roller ring bearing construction [29].

these bearings in operation would result in a radial force, Fr, of 250 N, an axial force, Fa, of 150 N, and a moment, M of 10 N-m. The dynamic equivalent radial load, Pc, is then

$$Pc = X * (Fr + \frac{2M}{dp}) + Y * Fa \tag{9.7}$$

where X is the dynamic radial factor, Y is the dynamic axial factor, and dp is the roller pitch circle diameter (27 mm). X and Y are functions of how the loads are primarily applied (axial or radial). For this case, X = 1 and Y = 0.45 so Pc = 1.06 kN. This can then be used to calculate the expected life, L, of the bearing [29].

$$L = (\frac{f_t * C}{f_w * Pc})^{10/3} \tag{9.8}$$

Here, f_t is the temperature factor and f_w is the load factor which relates to how much impact the bearing is expected to see. Values of $f_t = 1$ and $f_w = 2$ were used for this calculation, predicting a life of 4.1 million cycles.

If the ankle device were used each day for 8 hours at a frequency of 1 Hz, the bearings are predicted to last approximately 50 days. The actual duty cycle will be much less than this. This is also assuming constant worst case loading. The addition of the preload shaft with a deep groove bearing also decreases the load that these bearings are required to carry. This life estimate is very conservative.

9.4 Weight Budget

Once all the components were designed, a reasonable estimate of the overall weight of the ankle module could be determined. Table 9.1 shows the weight of each of the components. For component that were purchased, weight values were taken from the manufacturer's publications. For machined parts, weights were calculated based on volume data provided on the CAD models by SolidWorks.

The values presented here are conservative. For example, the weight listed for the bevel gears does not include the reduction caused by the addition of lightening

Component	Weight (lb)	Quantity	Total (lb)
Motor	0.88	2	1.75
Encoder	0.06	2	0.13
Gearhead	1.00	2	2.00
Bevel Pinion	0.17	2	0.35
Bevel Gear	1.12	2	2.25
Mounting Plate	1.24	1	1.24
Link	0.08	2	0.16
Rod	0.04	2	0.08
THK Bearing	0.09	2	0.18
SKF Bearing	0.04	1	0.04
Rod End	0.03	4	0.11
Preload Shaft	0.06	1	0.06
Foot Conn. 1	0.22	1	0.22
Foot Conn. 2	0.36	1	0.36
Leg Conn. 1	0.78	1	0.78
Leg Conn. 2	0.56	1	0.56
TOTAL			10.2

Table 9.1: Estimated weight budget.

holes. Other possible gear modifications were discussed in the transmission chapter. It is estimated that the addition of lightening holes and removing the material over an angle of 120 degrees, as discussed in Chapter 7, would reduce the weight of each bevel gear from 1.12 lbs to 0.88 lbs. This would reduce the total weight of the device to about 9.7 lbs.

As seen in the table, the heaviest components are the motors, gearheads, bevel gears, and the mounting plate. Of these, the easiest to modify in a future design would be the transmission components. As discussed earlier, there are other possible transmissions, other than gears that could potentially be used here.

Chapter 10

Conclusions and Future Work

The current design of the ankle module, as outlined in this document, provides a potentially useful tool to the rehabilitation community. The prototype meets the majority of the functional requirements outlined in Chapter 3, with the notable exception of the weight. The predicted weight is around 10 pounds, 2 pounds more than the requirement. Some suggestions for potential weight reduction are noted in this chapter and throughout the document.

10.1 Project Status

At the time of publication of this document, the ankle module was being prepared for assembly. The major components such as the motors, gearheads and bearings had been delivered and the machined parts are expected soon. The patient connection pieces and the electrical panel will also be completed soon. It is expected that all parts and components be in house and ready for assembly by mid-May 2004.

10.2 Future Work

This section describes additional work needed to prepare the ankle module for clinical use. It also discusses possible initial preclinical testing and applications.

10.2.1 Characterization and Control

Once the electrical panel is completed, the major components must be characterized. This includes the amplifiers and motors, with and without the gearheads attached. This characterization will provide transfer functions for each of the components to allow a controller to be designed. The characterization will be done using similar methods and equipment to that used in characterization of the wrist robot. This involves inputting waveforms of various frequencies to the components and measureing the response. The results are then analyzed using frequency domain processing tools. For a description of this process and results for the wrist device, see James Celestino's Thesis entitled "Characterization and Control of a Robot for Wrist Rehabilitation [24]."

A PC based controller can then be designed to run on an RT Linux operating system. This can be done using similar algorithms to those used in other robots in the lab. A critical decision in this design will be determining an appropriate trajectory of the foot during swing phase. The most likely function that the device will be required to perform is to position the foot during swing phase in preparation for heel strike. It should not simply move the patient, however, unless they are unable to move at all on their own. It should be an assistive controller that provides movements proportional to the impairment of the patient. The controller could have various levels of sophistication, but a simple controller is likely to be developed first for preclinical trials.

The other robots in the lab use a visual interface similar to a video game to prompt the patient to perform movements. This system will require a different approach, likely based on a series of events in the gait cycle. Some type of visual feedback could still be provided to the patient if desired. A control algorithm should also be developed that allows the pelvis and ankle modules to synchronize movements when both devices are attached to the patient.

10.2.2 Preclinical Testing

When the ankle robot is assembled, characterized, and functioning, tests need to be done to ensure that it is safe to be used in a clinical setting. This could involve attaching the device to other robots or testing on normal subjects in the lab. It may also be useful to repeat the tests done at the Bio-Motion Lab with the actual prototype to see the effect of the weight and friction on normal walking patterns. The tests could also be used to determine if symmetric loading (dummy weight on other leg) affects the gait pattern less than asymmetric loading and if the subjects tend to become accustomed to the device as time goes on. In any case, more trials should be run to gather enough data for statistical inferences to be made.

10.2.3 Improvements and Modifications

Because the device being constructed is an alpha prototype, problems are likely to occur that were not foreseen in the design process. The modular design of the prototype allows modifications to be made to components without a major redesign of the entire device. Preclinical testing should help determine what, if anything, is problematic in the design.

One area of particular concern is the weight of the device. If it proves too heavy to be effective for a large number of patients, significant weight reductions could possibly be made to the transmission. An increase in complexity and friction may result however. Simple modifications could also be made without a redesign of any of the major components. This could include using lighter materials (plastics or titanium) or modifying the patient connection components.

If time and resources permit, it may also be useful to design custom actuators and transmission components for the device. The components used in the prototype were chosen from readily available parts. An actuator and transmission system could be designed to maximize continuous stall torque while minimizing weight and impedance. There is also technology being developed in the Newman Lab involving remote actuation through flexible fluids lines that allow the bulk of the actuator weight to be

placed away from the device and the patient. This may be an appropriate application for such technology.

Another possible improvement is the addition of force sensors to the device. They could be placed under the foot or on the foot connection members. This would allow more clinical data to be gathered and more sophisticated controllers to be implemented.

10.3 Applications

The main use of this device will be to assist in stroke patient rehabilitation and perhaps eliminate the need for AFOs after therapy. It will provide a tool to address questions that have not been answered in this area due to the lack of therapist ability to target ankle function during gait training. This device can be a tool to determine to what extent ankle function can be regained after rehabilitation and whether results will be similar to those seen in upper extremity rehabilitation using the MIT-MANUS.

An important question that can be tested with the device is whether it is important to train inversion and eversion or if a single degree of freedom device is sufficient. If only one degree of freedom is trained, it is unknown if other impairments will still exist after therapy. The ankle module is a novel device that will allow many unanswered questions in this area to be addressed.

In addition to using the device while the patient is walking, it could be used to assist in stretching and strength training exercises, reducing therapist time and effort and perhaps providing the patient with visual feedback, similar to a video game. The ankle robot may also prove useful in correcting balance impairments in patients with neurological disorders or astronauts returning from space flight.

Appendix A

Component List and Specifications

Supplier/Description	Part Number	Quant.
Kollmorgen		
DC Brushless Motors	RBEH 00714	2
Bayside		
Planetary Gearhead	PS 40-010	2
Gurley		
Incremental Encoder	R120B01024Q5L10A18SP03MA	2
Coupler to Motor	SCD-03M-03M	2
Stock Drive		
Spiral Bevel Pinion	S13S4YMK20G15L10	2
Spiral Bevel Gear	S13S4YMK20G45R12	2
THK		
Cross Roller Ring Bearing	RB 2008 UU C0 P5	2
Link Ball Rod Ends	AL 6 D	4
SKF		
Deep Groove Ball Bearing	619/6	1

Table A.1: List of components.

Stealth® PS Advanced Series

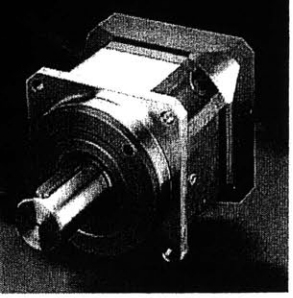

Performance Specifications

	Units	Ratio	Frame Size PS40	PS60	PS90	PS115	PS142	PS180	PS220	PS300
Nominal Output Torque, $T_{nom\ r}$	**Nm**	3-10	**5**	**25**	**74**	**170**	**294**	**735**	**1,413**	**3,616**
	in lb		42	220	650	1,500	2,600	6,500	12,500	32,000
	Nm	15-50	**9**	**34**	**107**	**226**	**396**	**1,017**	**1,808**	**4,520**
	in lb		75	300	950	2,000	3,500	9,000	16,000	40,000
	Nm	70-100	**8**	**28**	**90**	**203**	**339**	**893**	**1,582**	**4,181**
	in lb		67	250	800	1,800	3,000	7,900	14,000	37,000
Maximum Acceleration Output Torque, $T_{acc\ r}$	**Nm**	3-10, 70-100	**8**	**34**	**105**	**232**	**367**	**972**	**1,763**	**4,825**
	in lb		74	300	930	2,050	3,250	8,600	15,600	42,700
	Nm	15-50	**10**	**42**	**130**	**283**	**452**	**1,198**	**2,011**	**5,492**
	in lb		92	370	1,150	2,500	4,000	10,600	17,800	48,600
Emergency(1) Stop Output Torque, $T_{em\ r}$	**Nm**	3-10, 70-100	**19**	**78**	**243**	**537**	**853**	**2,237**	**4,068**	**11,119**
	in lb		170	690	2,150	4,750	7,550	19,800	36,000	98,400
	Nm	15-50	**24**	**96**	**299**	**655**	**1,040**	**2,757**	**4,520**	**12,656**
	in lb		210	850	2,650	5,800	9,200	24,400	40,000	112,000
Nominal Input Speed, $N_{nom\ r}$	RPM	3-5	3,600	3,200	2,800	2,400	2,000	1,600	1,200	1,000
	RPM	7-10	4,100	3,700	3,300	2,900	2,500	2,000	1,500	1,250
	RPM	15-50	4,600	4,200	3,800	3,400	3,000	2,400	1,800	1,500
	RPM	70-100	5,100	4,700	4,300	3,900	3,500	2,800	2,100	1,750
Max. Input Speed, N_{maxr}	RPM	3-100	6,000	6,000	5,300	4,500	3,800	3,000	2,300	1,900
Standard Backlash (2)	arc min	3-10	10	6	6	4	4	4	4	4
	arc min	15-100	14	8	8	6	6	6	6	6
Low Backlash (2)	arc min	3-10	—	4	4	3	3	3	3	3
	arc min	15-100	—	6	6	5	5	5	5	5
Efficiency at Nominal Torque	%	3-10	97	97	97	97	97	97	97	97
	%	15-100	94	94	94	94	94	94	94	94
Noise Level(3) at:										
3,000 RPM	dB	3-100	68	68	68	68	70	—	—	—
2,000 RPM	dB	3-100	—	—	—	—	—	70	70	70
Torsional Stiffness	**Nm / arc min**	3-100	**2**	**3**	**12**	**23**	**44**	**110**	**210**	**360**
	in lb / arc min		16	26	106	204	389	973	1,858	3,185
Maximum Weight	**kg**	3-10	**0.4**	**1.3**	**3**	**7**	**14**	**26**	**49**	**103**
	lb		1.0	2.8	7	15	30	57	108	228
	kg	15-100	**0.6**	**1.7**	**5**	**10**	**20**	**35**	**71**	**149**
	lb		1.4	3.7	10	22	43	77	157	330
Maximum Allowable Case Temperature	°C	3-100	← 100 →							
			For applications requiring lower case temperature, consult factory							

(1) Maximum of 1,000 stops
(2) Measured at 2% of rated torque
(3) Measured at 1 meter

(4) PS40 is available in Ratios of: 4, 5, 7, 10, 16, 20, 25, 40, 50, 70 & 100:1
PS300 is available in Ratios of: 4, 5, 7, 10, 20, 50, 70 & 100:1

Specification are subject to change without notice

Stealth® PS Advanced Series:
Get the Helical Advantage!

Stealth® Advanced in the PS / RS Models incorporates the latest enhancement in gearhead technology:

- Latest technology in seals...reduce heat and wear
- Oil lubrication...reduces friction and operating temperature
- Front output seal cover...captures and protects output seal

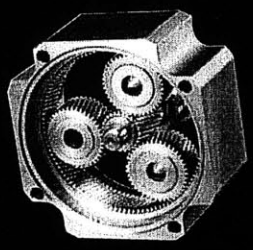

Helical Planetary Design - Helical gears have more tooth contact and greater face width than spur gears. This results in higher loads, smoother tooth engagement, quieter operation and lower backlash.

HeliCrown® - Bayside developed the HeliCrown gear tooth to further optimize Stealth's® performance. Since most vibration occurs at the entry and exit points of a gear tooth, HeliCrown eliminates metal only in these areas, *without sacrificing gear strength,* producing a quieter and stronger gear.

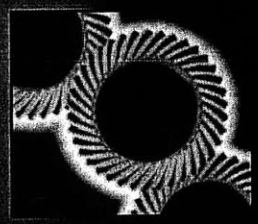

Plasma Nitriding - Bayside's in-house Plasma Nitriding process results in an ideal gear tooth. The surface is very hard (65 Rc) and the core is strong, but flexible (36 Rc). The result is a wear-resistant gear tooth that can withstand heavy shock, ensuring high accuracy for the life of the gearhead.

ServoMount® - Bayside's patented ServoMount design features a balanced input gear supported by a floating bearing. This unique design compensates for motor shaft runout and misalignment, ensuring TRUE alignment of the input sun gear with the planetary section, and allowing input speeds up to 6,000 RPM. ServoMount ensures error-free installation to any motor, in a matter of minutes.

Stealth's® superior design and construction deliver "The Helical Advantage":

- Strong...30% More Torque
- Fast...6,000 RPM Input Speeds
- Accurate...Less Than 3 Arc minutes Backlash
- Quiet...Less Than 68dB Noise **For Applications Requiring Lower dB, Consult Factory**

Plus... Over 97% Efficiency

11

Front Output Seal Cover
Completely captures and protects output seal and allows in-field seal replacement.

10

Output Wave Seal Technology
Creates a hydrodynamic film between seal and shaft and reducing heat and wear.

9

Magnetic Oil Fill Drain Plug
The magnetic plug attracts normal wear particles keeping them away from the gear mesh.

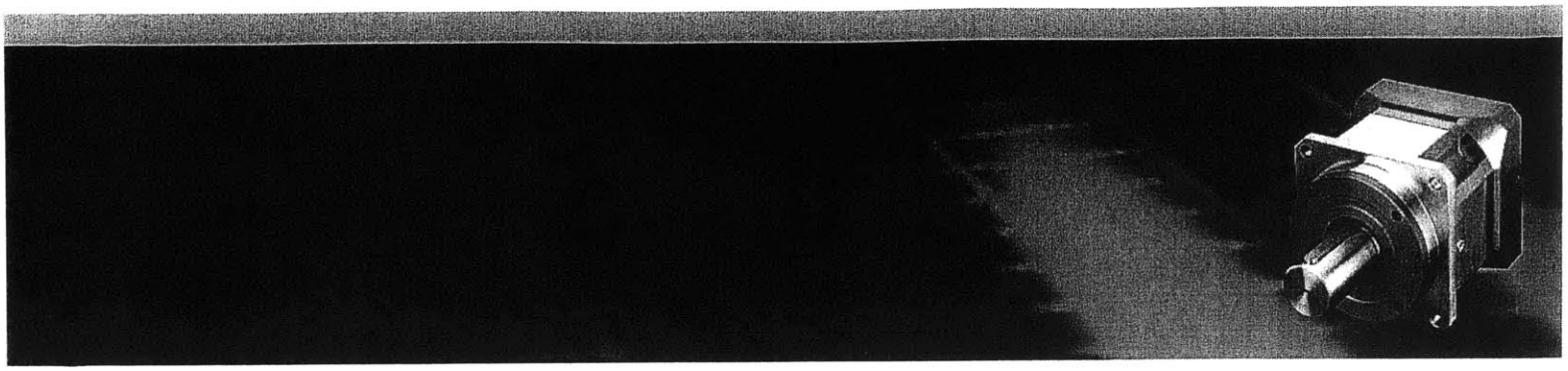

1

Helical Planetary
Provides smooth, quiet operation, high torque and high accuracy.

2

ServoMount®
Patented motor mounting design ensures error-free installation and the balanced pinion allows higher input speeds.

3

Precision Bearings
Large, deep groove bearings provide high speed capacity and radial loads.

4

HeliCrown®
Bayside's proprietary gear tooth geometry ensures quieter operation and higher loads than conventional gears.

5

Sealed Unit
Vition seals and O-Rings provide IP65 protection to prevent leaks and protect against harsh environments.

6

Rigid Sun Gear
Perfectly aligned between two large bearings for maximum stiffness and strength.

7

Integral Ring Gear
Cutting the ring gear directly into the housing allows for larger bearing and planet gears, delivering maximum power and stiffness in a minimum package.

8

Oil Lubrication
Oil provides better lubrication, reduces friction and operating temperatures.

Stealth® PS Advanced Series:
Moment of Inertia

MOMENT OF INERTIA

Specifications:	Units	Ratio	Frame Size							
			PS40	PS60	PS90	PS115	PS142	PS180	PS220	PS300
Small Motor Shaft Diameter Range	mm	3-100	3-8	6-12.7	6-16	9-19	12.7-24	15.9-35	24-48	28-65
	in		0.118-0.315	0.236-0.500	0.236-0.630	0.354-0.748	0.500-0.944	0.626-1.378	0.945-1.89	1.10-2.56
	gm cm sec²	3	—	0.176	0.784	2.34	7.81	28.6	—	—
	oz in sec²		—	0.002	0.011	0.033	0.109	0.397	—	—
	gm cm sec²	4,5	0.0140	0.101	0.486	1.87	4.92	17.6	62.6	284
	oz in sec²		0.0002	0.001	0.007	0.026	0.068	0.244	0.869	3.95
	gm cm sec²	7,10	0.0092	0.063	0.298	0.960	2.68	9.24	34.3	136
	oz in sec²		0.0001	0.001	0.004	0.013	0.037	0.128	0.476	1.88
	gm cm sec²	15	—	0.092	0.420	1.60	4.17	15.8	51.0	—
	oz in sec²		—	0.001	0.006	0.022	0.058	0.219	0.708	—
	gm cm sec²	16,20,25	0.0131	0.098	0.444	1.73	4.50	16.7	53.3	219
	oz in sec²		0.0002	0.001	0.006	0.024	0.063	0.232	0.741	3.05
	gm cm sec²	30-100	0.0083	0.054	0.247	0.760	2.18	7.450	27.1	93.9
	oz in sec²		0.0001	0.001	0.003	0.011	0.030	0.104	0.377	1.30
Large Motor Shaft Diameter Range	mm	3-100	8-10	12.7-16	16-19	19-24	24-35	35-42	48-55	—
	in		0.135-0.394	0.500-0.630	0.630-0.748	0.748-0.944	0.944-1.38	1.38-1.65	1.89-2.17	—
	gm cm sec²	3	—	0.253	1.07	3.25	10.6	37.8	111	—
	oz in sec²		—	0.004	0.015	0.045	0.148	0.526	1.54	—
	gm cm sec²	4,5	0.0483	0.185	0.745	2.70	7.51	25.6	72.4	—
	oz in sec²		0.0007	0.003	0.010	0.038	0.104	0.356	1.01	—
	gm cm sec²	7,10	0.0414	0.143	0.566	1.70	5.01	15.8	44.1	—
	oz in sec²		0.0006	0.002	0.008	0.024	0.070	0.219	0.613	—
	gm cm sec²	15	—	0.176	0.685	2.43	6.76	23.8	60.8	—
	oz in sec²		—	0.002	0.010	0.034	0.094	0.331	0.845	—
	gm cm sec²	16,20,25	0.0474	0.182	0.715	2.56	7.09	24.7	62.9	—
	oz in sec²		0.0007	0.003	0.010	0.036	0.099	0.344	0.874	—
	gm cm sec²	30-100	0.0405	0.134	0.507	1.50	4.50	14.0	37.0	—
	oz in sec²		0.0006	0.002	0.007	0.021	0.063	0.195	0.513	—

Note: All Moment of Inertia values are as reflected at the input shaft of the gearhead.

Specification are subject to change without notice

Stealth® PS Advanced Series:
Output Shaft Load Rating

PS40

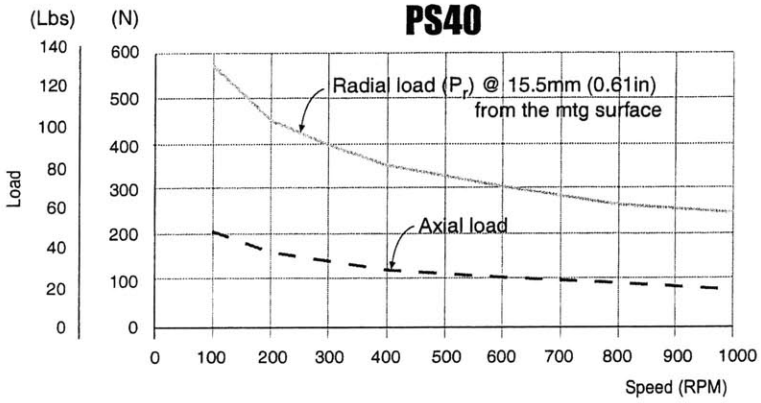

Formulas to calculate Radial Load (P_{rx}) at any distance "X" from the gearhead mounting surface.

$P_{rx} = (P_r)(\mathbf{37mm}) / (\mathbf{22mm} + X)$
$P_{rx} = (P_r)(1.46in) / (0.87in + X)$

PS60

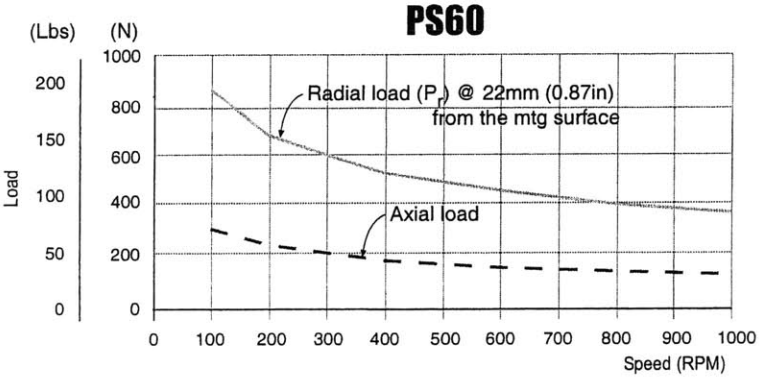

$P_{rx} = (P_r)(\mathbf{57mm}) / (\mathbf{35mm} + X)$
$P_{rx} = (P_r)(2.24in) / (1.38in + X)$

PS90

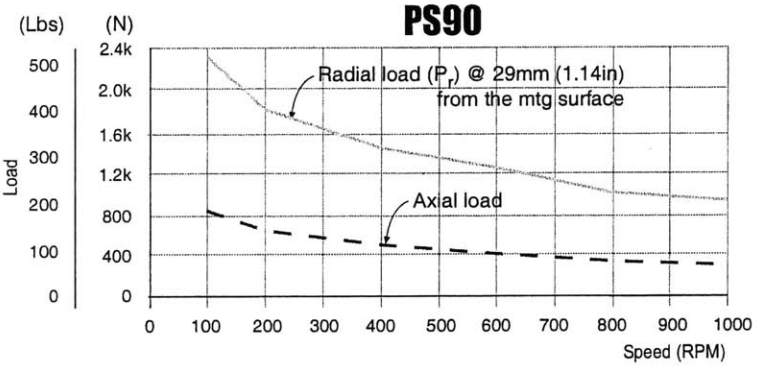

$P_{rx} = (P_r)(\mathbf{74mm}) / (\mathbf{45mm} + X)$
$P_{rx} = (P_r)(2.91in) / (1.77in + X)$

PS115

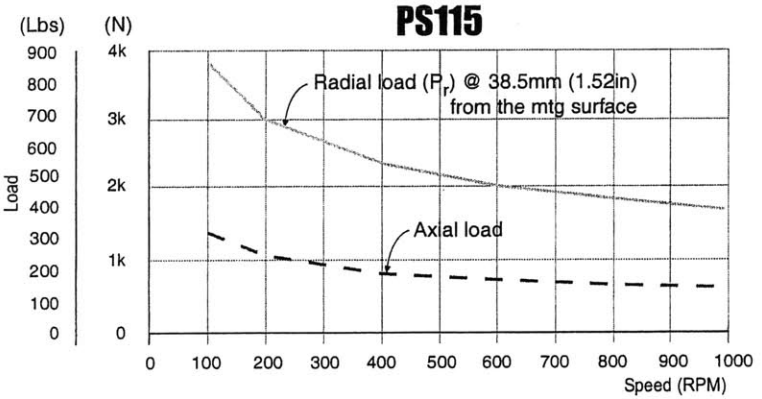

$P_{rx} = (P_r)(\mathbf{95mm}) / (\mathbf{57mm} + X)$
$P_{rx} = (P_r)(3.74in) / (2.24in + X)$

Stealth® PS Advanced Series

Dimensions

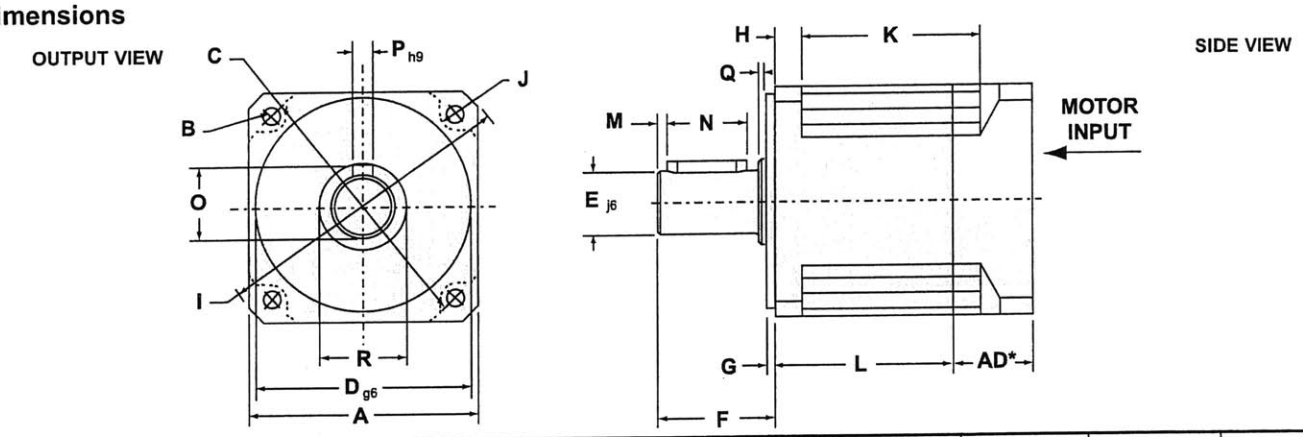

Frame Size	A Square Flange (mm)	A (in)	B Bolt Hole (mm)	B (in)	C Bolt Circle (mm)	C (in)	D Pilot Diameter (mm)	D (in)	E Output Shaft Diameter (mm)	E (in)	F Output Shaft Length (mm)	F (in)	G Pilot Thickness (mm)	G (in)	H Flange Thickness (mm)	H (in)	I Housing Diameter (mm)	I (in)	J Housing Recess (mm)	J (in)
PS40	42	1.654	3.4	0.134	50	1.969	35	1.378	13	0.512	26	1.024	5.5	0.217	5	0.197	56	2.205	3.5	0.138
PS60	60	2.362	5.5	0.217	70	2.756	50	1.969	16	0.630	37	1.457	8	0.315	8	0.315	80	3.150	5	0.197
PS90	90	3.543	6.5	0.256	100	3.937	80	3.150	22	0.866	48	1.890	11	0.433	10	0.394	116	4.567	6.5	0.256
PS115	115	4.528	8.5	0.335	130	5.118	110	4.331	32	1.260	65	2.559	13	0.512	14	0.551	152	5.984	7.5	0.295
PS142	142	5.591	11	0.433	165	6.496	130	5.118	40	1.575	97	3.819	15	0.591	15	0.591	185	7.283	10	0.394
PS180	182	7.165	13	0.512	215	8.465	160	6.299	55	2.165	105	4.134	20	0.787	16	0.630	240	9.449	16	0.630
PS220	220	8.661	17	0.669	250	9.843	180	7.087	75	2.953	138	5.433	30	1.181	22	0.866	290	11.417	16	0.630
PS300	305	12.008	21	0.827	350	13.780	250	9.843	100	3.937	190	7.480	35	1.378	26	1.024	400	15.748	18	0.709

Frame Size	K1 Recess Length For Ratio ≤ 10:1 (mm)	K1 (in)	K2 Recess Length For Ratio > 10:1 (mm)	K2 (in)	L1 Length For Ratio ≤ 10:1 (mm)	L1 (in)	L2 Length For Ratio > 10:1 (mm)	L2 (in)	M Dist. From Shaft End (mm)	M (in)	N Keyway Length (mm)	N (in)	O Key Height (mm)	O (in)	P Keyway Width (mm)	P (in)	Q Shoulder Height (mm)	Q (in)	R Shoulder Diameter (mm)	R (in)
PS40	32	1.260	53	2.087	30	1.181	50.7	1.996	2	0.079	16	0.630	15	0.591	5	0.197	1	0.039	15	0.591
PS60	37	1.457	67	2.638	36.7	1.445	66.7	2.626	2	0.079	25	0.984	18	0.709	5	0.197	0.5	0.020	22	0.866
PS90	48	1.890	88	3.465	49.5	1.949	89	3.504	3	0.118	32	1.260	24.5	0.965	6	0.236	0.5	0.020	35	1.378
PS115	62	2.441	110	4.331	61.7	2.429	109.5	4.311	5	0.197	40	1.575	35	1.378	10	0.394	1	0.039	45	1.772
PS142	82	3.228	143	5.630	76.5	3.012	138	5.433	5	0.197	63	2.480	43	1.693	12	0.472	3	0.118	55	2.165
PS180	88	3.465	158	6.220	83.5	3.287	153.5	6.043	6	0.236	70	2.756	59	2.323	16	0.630	3	0.118	70	2.756
PS220	116	4.567	218	8.583	108	4.252	210.5	8.287	6	0.236	90	3.543	79.5	3.130	20	0.787	3	0.118	95	3.740
PS300	160	6.299	332	13.071	158	6.220	292	11.496	7	0.276	140	5.512	106	4.173	28	1.102	3	0.118	140	5.512

*AD=Adapter Length. Adapter will vary, depending on motor.
Consult Internet (www.baysidemotion.com) for details or call Bayside.

Specifications are subject to change without notice.

How to Order

1. Pick frame size and ratio.
2. Pick backlash and orientation.
3. Specify motor make and model for mounting kit.

P	S	1	4	2	-	0	0	3	-	X	X	X	L	H

FRAME SIZE
40** 142
60 180
90 220
115 300***

RATIO
003 010 030
004 015 040
005 020 050
007 025 070
100

SPECIAL
(Factory Issued)

BACKLASH
L = Low
S = Standard

ORIENTATION
H = Horizontal orientation
U = Output shaft pointing up
D = Output shaft pointing down

(For other orientations consult the factory)

PS Gearheads are supported by a worldwide network of offices and local distributors. Call **1-800-305-4555** for application engineering assistance or for the name of your local distributor. Information can also be obtained at **www.baysidemotion.com**.

** PS40 is available in Ratios of : 4, 5, 7, 10, 16, 20, 25, 40, 50, 70 & 100:1*** PS300 is available in Ratios of: 4, 5, 7, 10, 20, 50, 70 & 100:1

RBE(H) Motor Series

RBE(H) 00710 MOTOR SERIES PERFORMANCE DATA

Motor Parameters	Symbols	Units	00710	00711	00712	00713	00714
Max Cont. Output Power	HP Rated	HP	0.0858	0.133	0.166	0.189	0.225
at 25°C amb.	P Rated	Watts	64	99	124	141	168
Speed at Rated Power	N Rated	RPM	17700	14110	12000	10800	9750
Max Mechanical Speed	N Max	RPM	20000	20000	20000	20000	20000
Continuous Stall Torque	Tc	oz-in	8.14	15.5	21.5	27.6	35.3
at 25°C amb.		N-m	0.057	0.109	0.152	0.195	0.249
Peak Torque	Tp	oz-in	22.7	43.8	63.3	84.5	114
		N-m	0.160	0.310	0.447	0.597	0.802
Max Torque	Tsl	oz-in	22.7	43.8	63.3	84.5	114
for Linear KT		N-m	0.160	0.310	0.447	0.597	0.802
Motor Constant	Km	oz-in/$\sqrt{W}$	2.36	4.05	5.38	6.67	8.25
		N-m/$\sqrt{W}$	0.0166	0.029	0.038	0.047	0.058
Thermal Resistance*	Rth	°C/Watt	5.90	4.91	4.47	4.19	3.94
Viscous Damping	Fi	oz-in/RPM	4.40E-05	8.39E-05	1.20E-04	1.56E-04	2.00E-04
		N-m/RPM	3.11E-07	5.93E-07	8.49-E-07	1.11E-06	1.41E-06
Max Static Friction	Tf	oz-in	0.90	1.54	2.12	2.70	3.40
		N-m	0.0064	0.011	0.015	0.019	0.024
Max Cogging Torque	Tcog	oz-in	0.75	1.38	1.95	2.52	3.20
Peak to Peak		N-m	0.0053	0.0097	0.0137	0.0178	0.023
Frameless Motor Inertia	Jmf	oz-in-sec^2	1.30E-04	2.00E-04	2.80E-04	3.50E-04	4.40E-04
		Kg-m^2	9.18E-07	1.41E-06	1.98E-06	2.47E-06	3.11E-06
Frameless Motor Weight	Wtf	oz	2.8	4.4	5.8	7.2	8.9
		Kg	7.94E-02	1.24E-01	1.64E-01	2.04E-01	2.52E-01
Housed Motor Inertia	Jmh	oz-in-sec^2	1.30E-04	2.00E-04	2.80E-04	3.60E-04	4.50E-04
		Kg-m^2	9.18E-07	1.41E-06	1.98E-06	2.54E-06	3.18E-06
Housed Motor Weight	Wth	oz	7.8	9.3	11	12	14
		Kg	2.21E-01	2.65E-01	3.04E-01	3.44E-01	3.91E-01
No. of poles	P		6	6	6	6	6

Winding Constants	Symbols	Units	A	B	C	A	B	C	A	B	C	A	B	C	A	B	C
Current at Cont. Torque	Ic	Amps	4.83	3.87	6.91	4.73	3.78	6.75	4.56	3.65	6.51	4.38	3.51	6.26	4.68	3.37	6.02
Current at Peak Torque	Ip	Amps	12.6	9.99	17.8	12.6	10.0	17.8	12.6	10.0	17.8	12.6	10.0	17.8	14.2	10.0	17.8
Torque Sensitivity	Kt	oz-in/Amp	1.87	2.34	1.31	3.60	4.50	2.52	5.19	6.49	3.63	6.92	8.65	4.85	8.26	11.5	6.43
		N-m/Amp	0.0132	0.0165	0.0092	0.0254	0.0318	0.0178	0.0367	0.0458	0.0257	0.0489	0.0611	0.0342	0.0584	0.0810	0.0454
Back EMF constant	Kb	V/KRPM	1.38	1.73	0.968	2.66	3.33	1.86	3.84	4.80	2.69	5.12	6.40	3.58	6.11	8.49	4.75
Motor Resistance	Rm	Ohms	0.629	0.991	0.311	0.790	1.24	0.390	0.933	1.47	0.461	1.08	1.70	0.533	1.00	1.97	0.618
Motor Inductance	Lm	mH	0.19	0.30	0.095	0.37	0.57	0.18	0.54	0.84	0.26	0.72	1.1	0.35	0.76	1.5	0.46

*Rth assumes a housed motor mounted to a 3.25" x 3.25" x 0.25" aluminum heatsink or equivalent

Continuous Duty Capability for 130°C Rise — RBE - 00710 Series

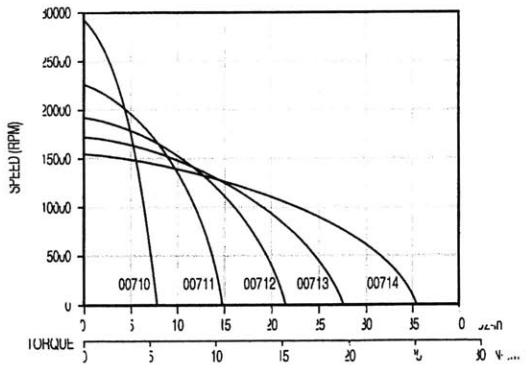

DIMENSIONS

RBE-0071X-X00

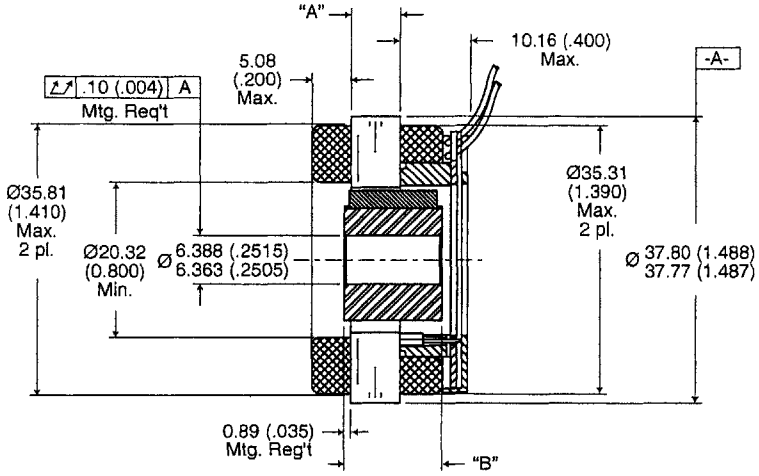

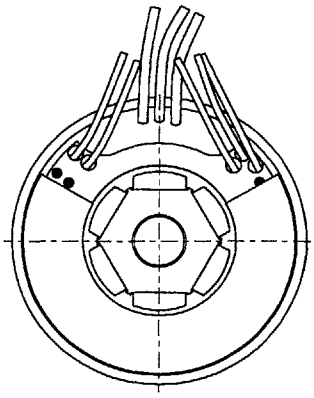

Dimensions in mm (inches).
Product designed in inches.
Metric conversions provided for reference only.

Notes:
1) For a C.W. rotation, as viewed from lead end, energize per excitation sequence table.
2) V-AB, V-BC and V-CA is back EMF of motor phases AB, BC and CA respectively, aligned with sensor output as shown for C.W. rotation only.
3) Mounting surface is between Ø 35.81 (1.410) and Ø 37.80 (1.488) on both sides.

MODEL NUMBER	RBE-00710	RBE-00711	RBE-00712	RBE-00713	RBE-00714
"A" Dimension	6.35 (0.250)	12.7 (0.500)	19.05 (0.750)	25.4 (1.000)	33.02 (1.300)
"B" Dimension	12.7 (0.500)	19.05 (0.750)	25.40 (1.000)	31.75 (1.250)	39.37 (1.550)
Tolerance ± .010 on "A" Dimension.					

RBEH-0071X-X00

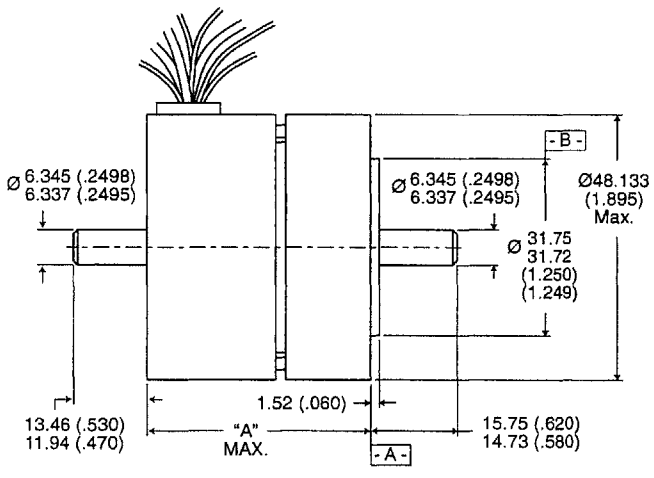

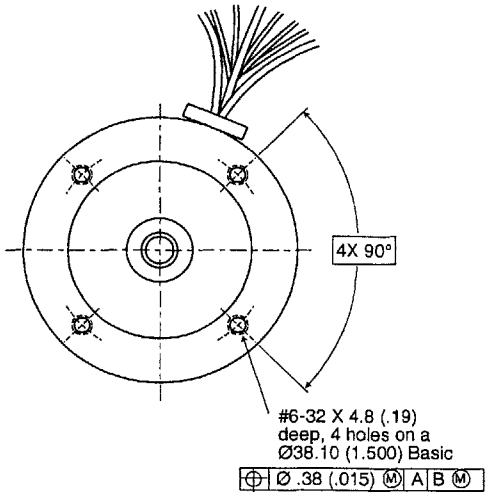

Dimensions in mm (inches).
Product designed in inches.
Metric conversions provided for reference only.

Notes:
1) Shaft end play: with a 6 lb reversing load, the axial displacement shall be .013-.15 (.0005-.006).
2) For a C.C.W. rotation, as viewed from pilot end, energize per excitation sequence table.
3) V-AB, V-BC and V-CA is back EMF of motor phases AB, BC and CA respectively, aligned with sensor output as shown for C.C.W. rotation only.

MODEL NUMBER	RBEH-00710	RBEH-00711	RBEH-00712	RBEH-00713	RBEH-00714
"A" Dimension	39.83 (1.568)	46.18 (1.818)	52.53 (2.068)	58.88 (2.318)	66.50 (2.618)

RBE/RBEH LEADWIRE

Motor Leads: #24 AWG Teflon coated per MIL-W-22759/11, 3 leads, 152 (6.00) min lg. ea. 1-black, 1-white, 1-red.

Sensor Leads: #26 AWG type "ET" Teflon coated per MIL-W-16878, 5 leads, 152 (6.00) min lg. ea. 1-blue, 1-brown, 1-green, 1-orange, 1-yellow.

Metric Metric Metric Metric Metric Metric Metric

SDP/SI Ground Spiral Bevel Gears - Module 2 to 4

Stock Drive Products/Sterling Instrument ■ Phone: 516-328-3300 ■ Fax: 516-326-8827

■ ISO CLASS 6 ■ 20° PRESSURE ANGLE ■ 35° SPIRAL ANGLE

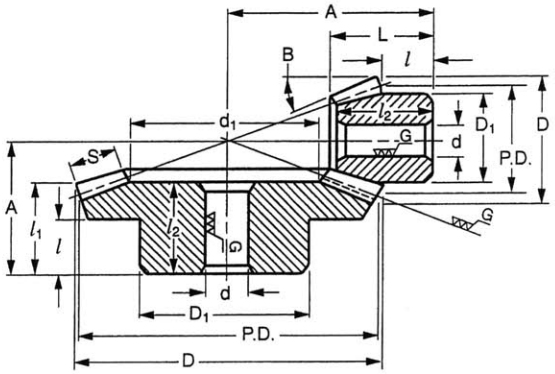

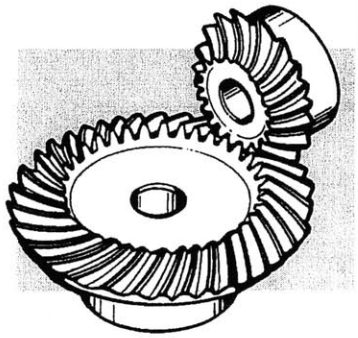

MATERIAL: AISI 1045 Steel, Tooth Surfaces Induction Hardened to HRC 48...53
FINISH: Black Oxide, except Ground Bore and Tooth Surfaces

Catalog Number	Mod.	No. of Teeth	d Bore H7	P.D.	D	S Face Width	L Length	D_1 Hub Dia.	l Hub Proj.	A Mtg. Dist.	d_1	l_1 Crown to Back	l_2 Length of Bore	B Face Angle
RATIO 2:3														
S13S2YMK20G20L10	2	20	10	40	43.55	11	24.91	30	11.67	45	21.34	16.18	22	37° 40'
S13S2YMK20G30R12		30	12	60	61.6		26.6	35	15	40	37.56	21.2	23	60° 43'
S13S2YMK25G20L12	2.5	20	12	50	54.43	15	30.88	40	14.17	55	27.42	18.98	28	37° 41'
S13S2YMK25G30R15		30	15	75	77.09		33.86	45	18	50	45.61	26.56	30	61° 01'
S13S2YMK30G20L16	3	20	16	60	65.58	17	40.17	45	20	70	34.71	26.86	37	38° 45'
S13S2YMK30G30R16		30	16	90	92.21		35.34	50	17	55	57.14	26.66	31	59° 20'
S13S2YMK40G20L20	4	20	20	80	87.34	20	48.17	60	23.33	90	46.89	32.45	43	38° 25'
S13S2YMK40G30R20		30	20	120	122.85		47.49	70	25	75	78.59	37.14	40	58° 52'
RATIO 1:2														
S13S3YMK20G20L12	2	20	12	40	44.1	15	34	32	18	60	21.11	21	32	29° 58'
S13S3YMK20G40R12		40	12	80	81		32.2	40	18	45	48.8	26	27	65° 20'
S13S3YMK25G20L12	2.5	20	12	50	55.2	20	43.61	40	22.5	75	20.53	26.3	40	30° 18'
S13S3YMK25G40R15		40	15	100	101.27		39.65	50	20	55	59.26	31.27	34	65° 50'
S13S3YMK30G20L16	3	20	16	60	66.07	22	50.63	50	27.5	90	29.63	31.52	47	29° 50'
S13S3YMK30G40R20		40	20	120	121.48		45.76	60	24	65	73.78	36.47	38	65° 03'
S13S3YMK40G20L20	4	20	20	80	88.5	28	66.24	60	35	120	42.8	42.12	62	30° 47'
S13S3YMK40G40R20		40	20	160	162.07		53.68	70	28	80	102.44	42.07	45	65° 30'
RATIO 1:3														
S13S4YMK20G15L10	2	15	10	30	34.78	15	29.66	24	14	60	19.15	15.8	29	22° 50'
S13S4YMK20G45R12		45	12	90	90.67		30.29	40	17	40	59.07	26.01	26	73° 25'
S13S4YMK25G15L12	2.5	15	12	37.5	43.36	20	38.27	30	17.5	75	20.48	19.73	37	22° 22'
S13S4YMK25G45R15		45	15	112.5	113.32		38.25	50	22	50	72.82	32.47	35	73° 13'
S13S4YMK30G15L15	3	15	15	45	52.08	23	44.98	38	21.33	90	28.52	23.68	44	22° 32'
S13S4YMK30G45R20		45	20	135	135.99		40.59	60	20	55	88.2	33.98	35	73° 18'

NOTE: R or L in catalog number indicates right- or left-hand direction of helix.

Gurley Models R119S and R120B Rotary Incremental Mini-Encoders

Motion Type:

Rotary

Usage Grade:

Light Industrial

Output:

Incremental

Max Resolution:

65,536 counts/rev

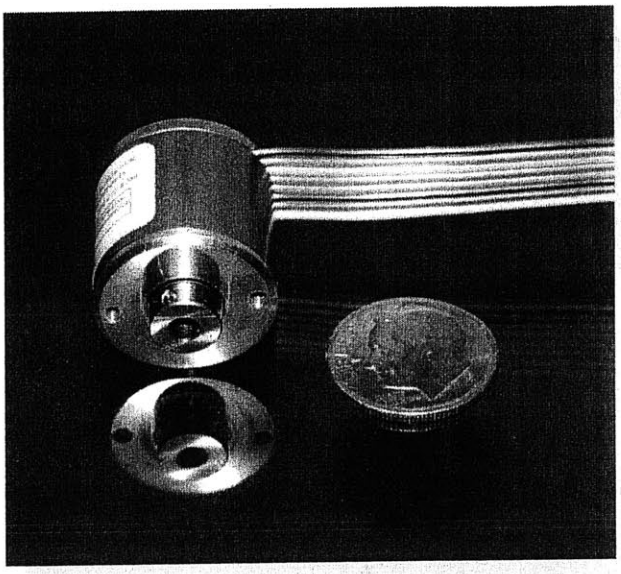

Smallest High-Resolution Encoder

The Models **R119** and **R120** optical incremental encoders are designed for light industrial applications that require high resolution in a very small package. The two models share these features:

- Represent either shafted or blind-hollow shaft version
- LED illumination for long life (>100,000 hours)
- Differential photo-detectors for signal stability
- Single-board, surface-mount electronics for reliability
- RS-422 differential line driver output for noise immunity
- Zero index signal
- Monolithic integrated ASIC for internally interpolated resolutions up to 16,384 cycles/rev (65,536 counts/rev)

R119: ϕ19-mm body; ribbon cable
R120: ϕ20-mm body; round cable with shielded twisted pairs

ingenuity@work®

ISO 9001 Certified

Gurley Precision Instruments
514 Fulton Street
Troy, NY 12180 U.S.A.
(800) 759-1844, (518) 272-6300, fax (518) 274-0336,
Online at www.gurley.com, e-mail: info@gurley.com

GPI

SPECIFICATIONS

	See Note	Models R112S and R112B
Maximum line count on disc		1024
Maximum cycles /rev (quad sq waves)		16,384
Max counts/rev (after quad decode)		65,536
Internal square wave interpolation		1x, 2x, 5x, 10x, or 16x
Instrument error, ±arcminutes	1, 2	4
Quadrature error, ±electrical degrees	1, 3	24
Interpolation error, ±quanta	1, 4	0.15
Maximum output frequency, kHz 1x square waves		100
2x square waves		150
5x square waves		300
10x, 16x square waves		500
Starting torque, in-oz (N-m) @20°C		0.07 (5×10^{-4})
Running torque, in-oz (N-m) @20°C		0.04 (2.9×10^{-4})
Moment of inertia, in-oz-s2 (g-cm^2)		5.7×10^{-6} (0.4)
Maximum weight, oz (g)		1 (30)
Sealing		IP50
Max. Radial or axial shaft load, lb (N)	5	0.7 (3)
Bearing life with 0.25 lb radial load	6	1×10^{10} rev
Operating temperature, °F (°C)		32 to 158 (0 to 70)
Storage temperature, °F(°C)		-22 to 185 (-30 to 85)
Humidity, % rh, non-condensing		98
Shock		30g (300m/s2)
Vibration		10g (100m/s2)

Notes:

1. Total Optical Encoder Error is the algebraic sum of *Instrument Error* + *Quadrature Error* + *Interpolation Error*. Typically, these error sources sum to a value less than the theoretical maximum. Error is defined at the signal transitions and therefore does not include quantization error, which is ±1/2 quantum. ("Quantum" is the final resolution of the encoder, after user's 4X quadrature decode.) Accuracy is guaranteed at 20°C.

2. *Instrument Error* is the sum of disc pattern errors, disc eccentricity, bearing runout and other mechanical imperfections within the encoder. This error tends to vary slowly around a revolution.

3. *Quadrature Error* is the combined effect of phasing and duty cycle tolerances and other variables in the basic analog signals. This error applies to data taken at all four transitions within a cycle; if data are extracted from 1X square waves on a 1X basis (i.e., at only one transition per cycle), this error can be ignored.

   Error in arcminutes = (60) x (error in electrical degrees) (disc line count)

4. *Interpolation Error* is present only when the resolution has been electronically increased to more than four data points per optical cycle. It is the sum of all the tolerances in the electronic interpolation circuitry.

   Error in arcminutes = (21600) x (error in quanta) (counts/rev)

5. The maximum recommended shaft load is based on bearing life considerations. If accuracy is critical, shaft loads should be kept as low as possible.

6. Bearing life is based on fatigue failure criteria. In many long-duration applications, lubrication retention becomes the determining factor.

As part of our continuing product improvement program, all specifications are subject to change without notice

Gurley Precision Instruments
514 Fulton Street
Troy, NY 12180 U.S.A.
(800) 759-1844, (518) 272-6300, fax (518) 274-0336,
Online at www.gurley.com, e-mail: info@gurley.com

SPECIFICATIONS

INPUT POWER
+5 VDC ±0.25 V @100 mA max.

SQUARE WAVE OUTPUT
Quadrature square waves at 1, 2, 5, 10, or 16 times the line count on the disc. On all channels: EIA/RS-422 balanced differential line driver, protected to survive an extended-duration short circuit across its output. May be used single-ended for TTL-compatible inputs. Index is ¼-cycle wide, gated with the high states of channels A and B.

OUTPUT WAVEFORMS (CW rotation shown)

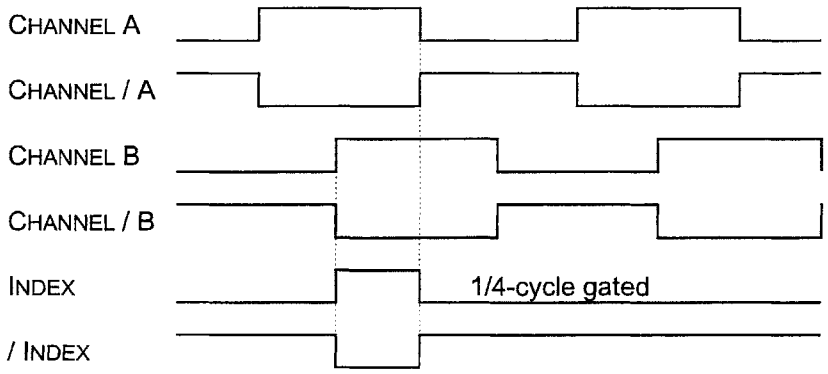

ELECTRICAL CONNECTIONS

	R119		R120	
Output Functions	Wire Colors Conn. Code **P**	Ribbon conn Conn. Code **Y**	Wire Colors Conn. Code **P**	Ribbon conn Conn. Code **Y**
A	Orange	2	Yellow	4
/ A	Yellow	3	Brown	8
B	Violet	6	Green	3
/ B	Gray	7	Orange	7
IND	Green	4	Blue	2
/ IND	Blue	5	White	6
+V	Red	1	Red	5
COMMON	White	8	Black	9
CASE			Bare (shield)	1

NOTE: Channel A leads Channel B for clockwise rotation, looking at the shaft end.

FLEXIBLE SHAFT COUPLINGS

	Tether Mount for **-B** version	**SCD** Coupling for **-S** version
Maximum parallel offset, in (mm)	0.002 (.05)	0.008 (0.2)
Maximum axial extension or compression, in (mm)	0.008 (0.2)	0.008 (0.2)
Maximum angular misalignment, degrees	2.0	0.5

See separate data sheet for specifications and ordering information for the Model **SCD** coupling.

NOTE: Flexible couplings are intended to absorb normal installation misalignments and run-outs in order to prevent undue loading of the encoder bearings. To realize all the accuracy inherent in the encoder, the user should minimize misalignments as much as possible.

Gurley Precision Instruments
514 Fulton Street
Troy, NY 12180 U.S.A.
(800) 759-1844, (518) 272-6300, fax (518) 274-0336,
Online at www.gurley.com, e-mail: info@gurley.com

R119 Dimensions

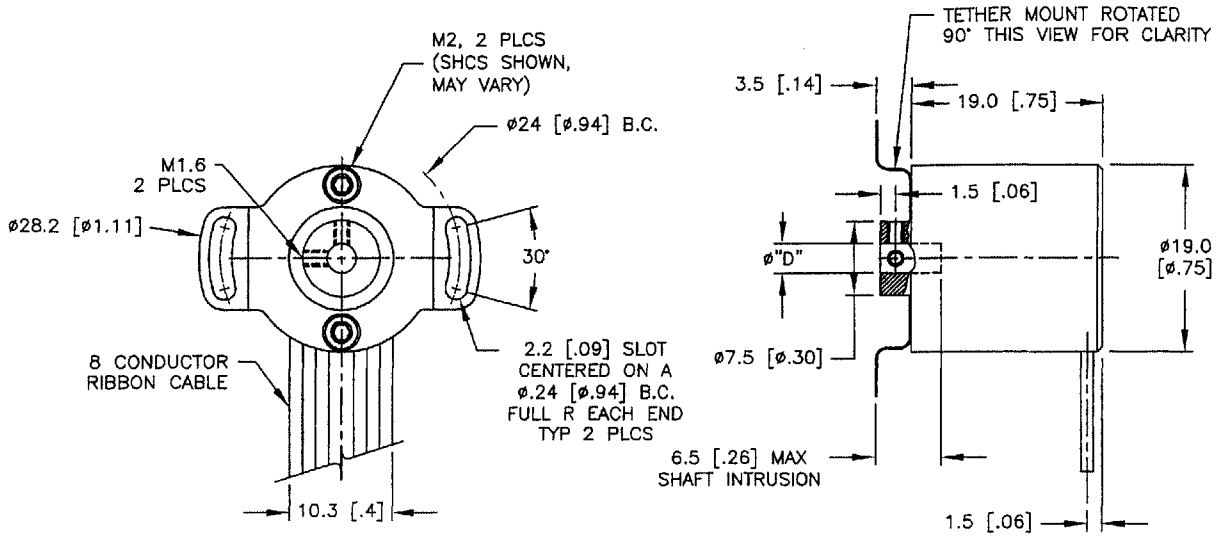

R119B (BASE CODE A)

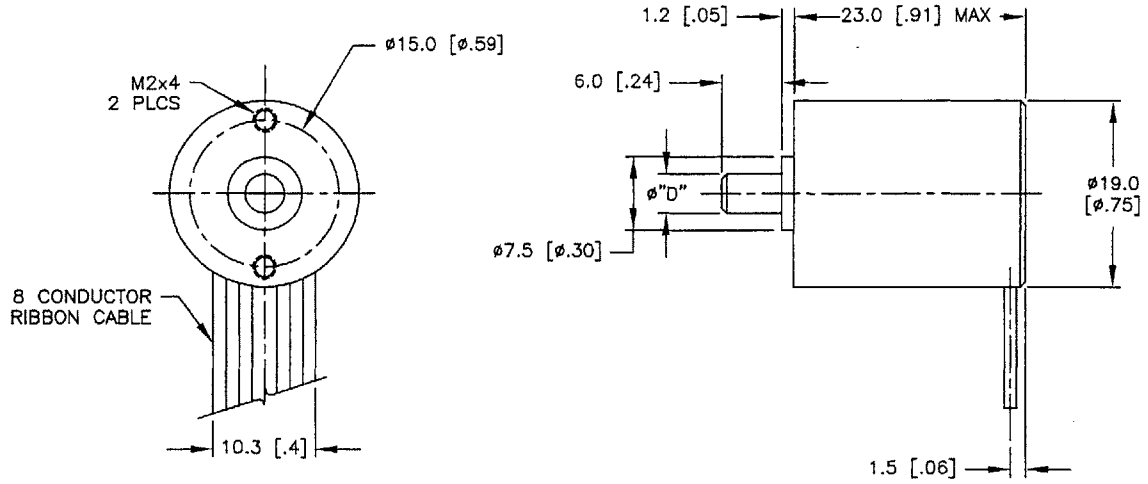

R119S (BASE CODE B)

ø"D" TABLE		
"DIA" CODE	R119S	R119B
04M	ø4mm h6	N/A
03M	ø3mm h6	ø3mm H7
02E	ø0.125" $^{+.0000}_{-.0003}$	ø0.125" $^{+.0005}_{-.0000}$

GPI0272 REV 3

ALL DIMENSIONS IN MM [INCHES]

Gurley Precision Instruments
514 Fulton Street
Troy, NY 12180 U.S.A.
(800) 759-1844, (518) 272-6300, fax (518) 274-0336,
Online at www.gurley.com, e-mail: info@gurley.com

R120 Dimensions

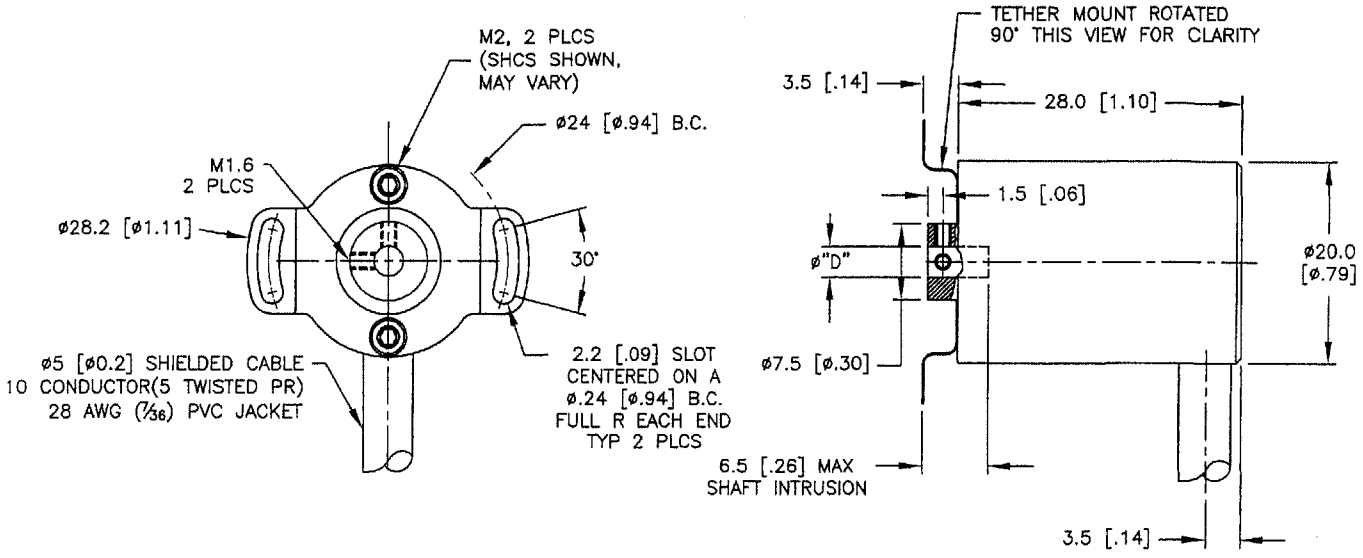

R120B (BASE CODE A)

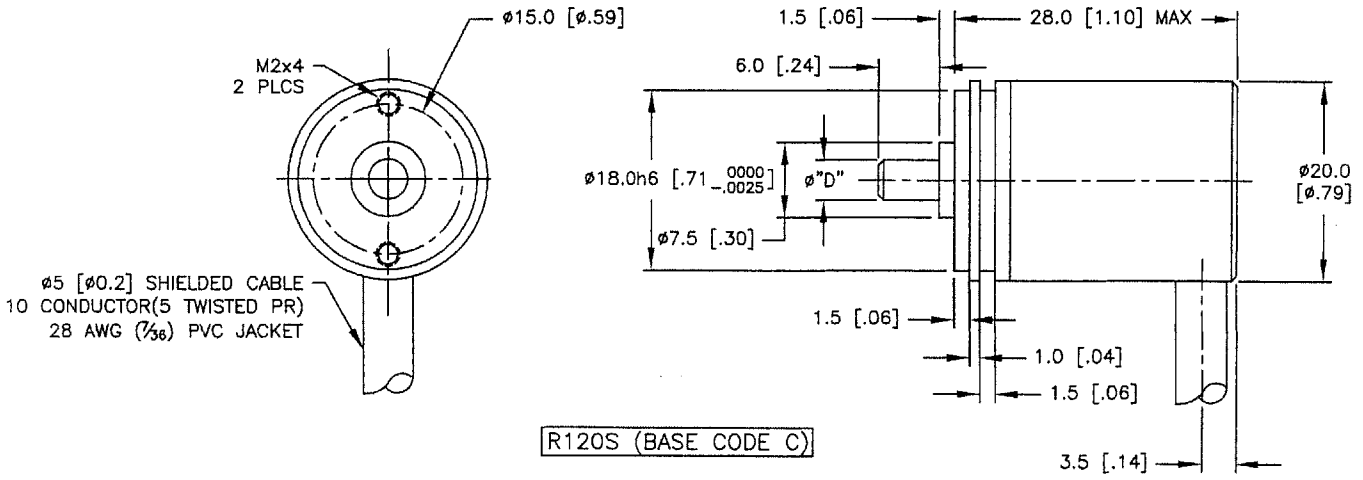

R120S (BASE CODE C)

ø"D" TABLE		
"DIA" CODE	R120S	R120B
04M	ø4mm h6	N/A
03M	ø3mm h6	ø3mm H7
02E	ø0.125" +.0000 -.0003	ø0.125" +.0005 -.0000

GPI0272 REV 5

ALL DIMENSIONS IN MM [INCHES]

Gurley Precision Instruments
514 Fulton Street
Troy, NY 12180 U.S.A.
(800) 759-1844, (518) 272-6300, fax (518) 274-0336,
Online at www.gurley.com, e-mail: info@gurley.com

Ordering Information

MODEL	SHAFT	LINES	IND		OUT	INTERP	BASE	CAB	EXIT	CONN	DIA	SPEC
				5								

MODEL
- **R119** ϕ19-mm body, ribbon cable
- **R120** ϕ20-mm body, round cable

SHAFT
- **B** Blind hollow shaft
- **S** Solid shaft

LINES - Disc line count
00360, 00500, 00512, 00900, 01000, 01024
Consult factory for other line counts

IND - Index format
- **Q** Quarter-cycle gated index

V - Input voltage
- **5** +5 Vdc

OUT – Output format
- **L** RS422 differential line driver

INTERP - Interpolation factor
01, 02, 05, 10, 16

BASE
- **A** Use with **R119B** or **R120B**
- **B** Use with **R119S**
- **C** Use with **R120S**

CAB - Cable length, inches
- **18** Standard

EXIT
- **S** Side-exit cable

CONN - Connector
- **P** Pigtails (no connector)
- **Y** 8-pos ribbon cable socket connector (Berg 71602-308 or equal) (**R119** only)
- **S** DE-9P (**R120** only)

DIA - Shaft diameter
- **02E** 1/8" (SHAFT = **S** or **B**)
- **03M** 3 mm (SHAFT = **S** or **B**)
- **04M** 4 mm (SHAFT = **S**)

SPEC- Special features
- **#** Issued at time of order to cover special customer requirements
- **N** No special features

ACCESSORIES (order separately)
- **SCD-xxx-xxx** Shaft coupling (see separate data sheet)
- **M06** Mating connector for DE-9P

SPECIAL CAPABILITIES

For special situations, we can optimize catalog encoders to provide higher frequency response, greater accuracy, wider temperature range, reduced torque, non-standard line counts, or other modified characteristics. In addition, we regularly design and manufacture custom encoders for user-specific requirements. These range from high-volume, low-cost, limited-performance commercial applications to encoders for military, aerospace and similar high-performance, high-reliability conditions. We would welcome the opportunity to help you with your encoder needs.

WARRANTY

Gurley Precision Instruments offers a limited warranty against defects in material and workmanship for a period of one year from the date of shipment.

Gurley Precision Instruments
514 Fulton Street
Troy, NY 12180 U.S.A.
(800) 759-1844, (518) 272-6300, fax (518) 274-0336,
Online at www.gurley.com, e-mail: info@gurley.com

Model No.	External dimensions, mm			Thread	Holder dimensions, mm					
	Length	Diameter	Height	S	L_1	L_2	L_3	D	D_1	W
	L	D_2	ℓ	JIS Class 2						$^{0}_{-0.3}$
AL 4D	24.5	13	20	M 4×0.7	18	8	4	7.5	9.5	8
AL 5D	34.5	15	26.7	M 5×0.8	27	15	4	9	12	10
AL 6D	38.5	17	32.6	M 6×1	30	16	5	10	13	11
AL 8D	46	20	38.6	M 8×1.25	36	19	6	13	16	14
AL10D	56	26	46.3	M10×1.25	43	23	7	15.5	19	17
AL10BD	56	26	52.3	M10×1.5	43	23	7	15.5	19	17

1. Material
   Holder : A-1 Alloy (See Page H-22)
   Ball shank : Bearing steel ball with a hardness of Hv650 or higher
   Shank : S35C (H_RC20 to 28)
   Color-chromate-treated
   Boot : NBR-based special synthetic rubber
2. Spherical clearance
   Direction perpendicular to the axis
   : 0.02 to 0.06 mm max.
   Axial direction : 0.3 mm max.
3. The recommended tolerance for the hole into which the ball shank is inserted is H10.
4. Yield strength : Strength in the direction shown below

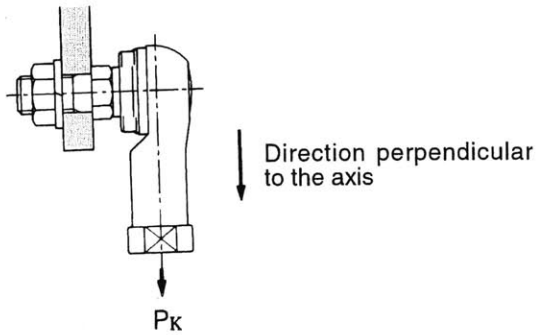

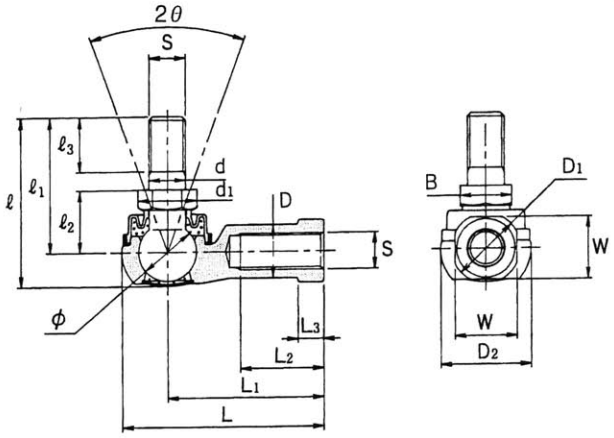

Ball-shank dimensions, mm						Ball diameter	Permissible tilting angle	Static-load-carrying capability	Yield strength	Mass
d	ℓ_1	ℓ_2	ℓ_3	Hexagon B	d_1	ϕ		C_s	P_K	
h9		±0.3		$^{0}_{-0.3}$		mm	2θ	N	N	g
4	15	7	6	7	8.1	7.938	40°	4510	1370	7
5	21	10	8	8	9.2	9.525	40°	6470	2250	12
6	26	11	11	10	11.6	11.112	40°	9900	3920	18
8	31	14	12	12	13.8	12.7	40°	12500	6570	32
10	37	17	15	14	16.2	15.875	40°	18300	11300	65
10	43	17	21	14	16.2	15.875	40°	18300	11300	68

5. Lithium soap-based grease No. 2 is sealed in the boot and cap.
6. The left-hand internal thread should be identified by its cap color and impression.

[Ex.] Type AL 6 D L
- L: Left-hand thread
- D: Boot provided
- AL 6: Model No.

Thread	Identification	
	Cap color	Impression on the cap
Right-hand	White	—
Left-hand	Yellow	Impress "L"

1 N≒0.102 kgf

RB (outer-ring-separable type)

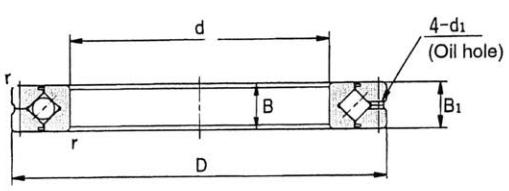

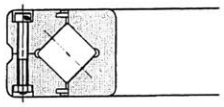
Type RB

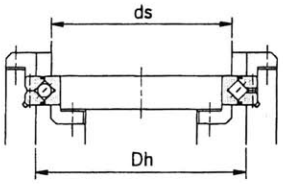

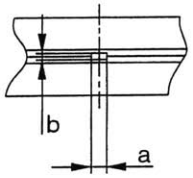

Oil hole detail

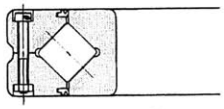
Type RB-UU

Unit: mm

Shaft diameter	Model No.	Major daimensions ID d	OD D	Roller pitch circle diameter dp	Width B	B_1	Oil hole a	b	r	Shoulder dimensions ds	Dh	Basic load rating (radial) C kN	C_0 kN	Mass kg
20	RB 2008	20	36	27	8		2	0.8	0.8	23.5	30.5	3.23	3.10	0.04
25	RB 2508	25	41	32	8		2	0.8	0.8	28.5	35.5	3.63	3.83	0.05
30	RB 3010	30	55	41.5	10		2.5	1	1	37	47	7.35	8.36	0.12
35	RB 3510	35	60	46.5	10		2.5	1	1	41	51.5	7.64	9.12	0.13
40	RB 4010	40	65	51.5	10		2.5	1	1	47.5	57.5	8.33	10.6	0.16
45	RB 4510	45	70	56.5	10		2.5	1	1	51	61.5	8.62	11.3	0.17
50	RB 5013	50	80	64	13		2.5	1.6	1	57.4	72	16.7	20.9	0.27
60	RB 6013	60	90	74	13		2.5	1.6	1	68	82	18.0	24.3	0.3
70	RB 7013	70	100	84	13		2.5	1.6	1	78	92	19.4	27.7	0.35
80	RB 8016	80	120	98	16		3	1.6	1	91	111	30.1	42.1	0.7
90	RB 9016	90	130	108	16		3	1.6	1.5	98	118	31.4	45.3	0.75
100	RB 10016	100	140	119.3	16		3.5	1.6	1.5	109	129	31.7	48.6	0.83
	RB 10020		150	123	20		3.5	1.6	1.5	113	133	33.1	50.9	1.45
110	RB 11012	110	135	121.8	12		2.5	1	1	117	127	12.5	24.1	0.4
	RB 11015		145	126.5	15		3.5	1.6	1	122	136	23.7	41.5	0.75
	RB 11020		160	133	20		3.5	1.6	1.5	120	140	34.0	54.0	1.56
120	RB 12016	120	150	134.2	16		3.5	1.6	1	127	141	24.2	43.2	0.72
	RB 12025		180	148.7	25		3.5	2	2	133	164	66.9	100	2.62
130	RB 13015	130	160	144.5	15		3.5	1.6	1	137	152	25.0	46.7	0.72
	RB 13025		190	158	25		3.5	2	2	143	174	69.5	107	2.82

Notes:
- Models with seals are denoted "RB-UU."
- When accuracy is required, use this type to rotate the inner ring.

Appendix B

Detailed Drawings

Part Description	Number of Sheets
Assembly Solid Model	1
Motor Mounting Plate	5
Gear and Link Shaft	1
Links	1
Rods	1
Preload Shaft 1	1
Preload Shaft 2	1
Spiral Bevel Gear Modifications 1	1
Spiral Bevel Gear Modifications 2	1
Spiral Bevel Pinion Modifications	1
Leg Connection Part 1	1
Leg Connection Part 2	2
Foot Connection Part 1	1
Foot Connection Part 2	1

Table B.1: List of drawings.

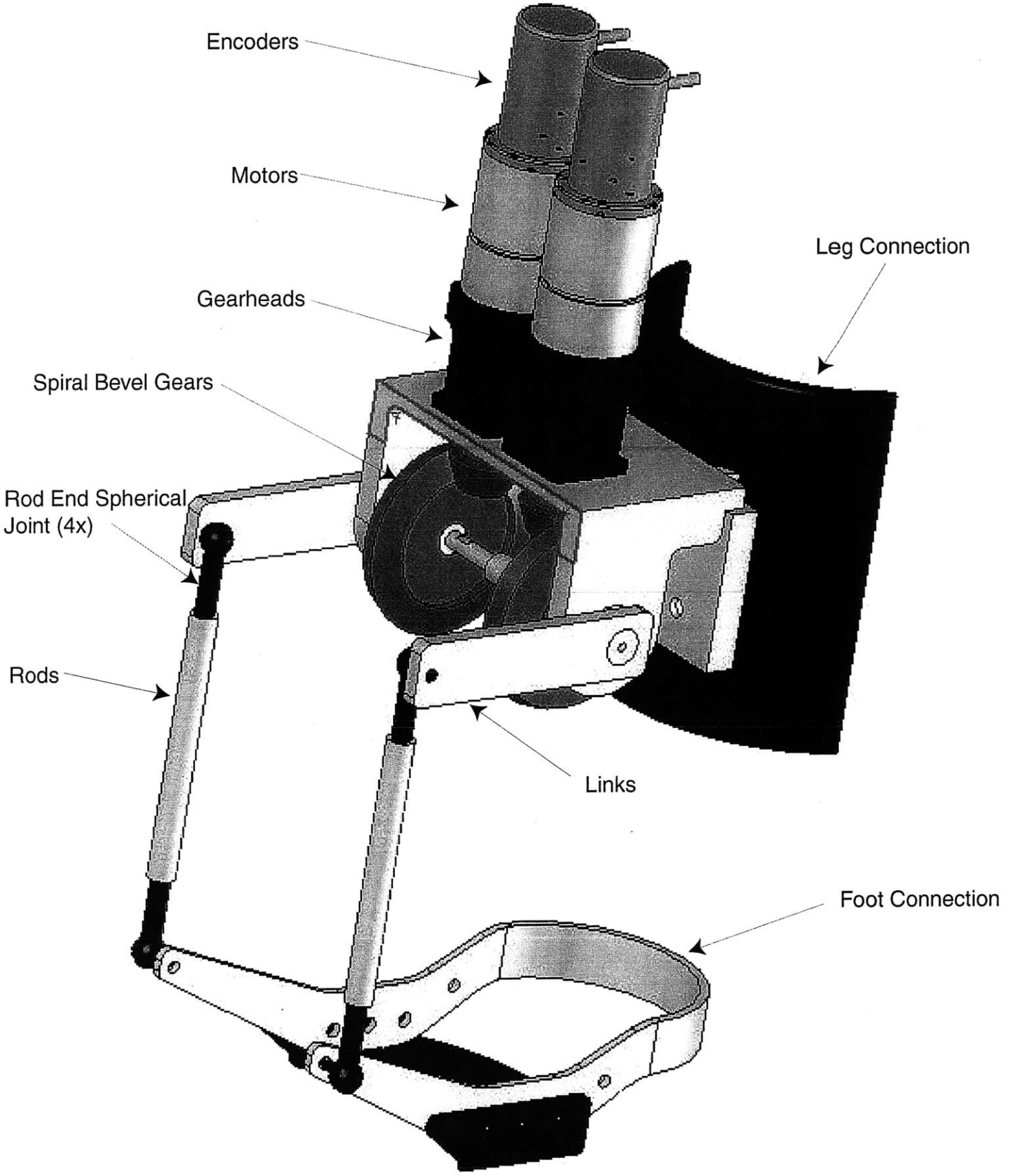
Encoders
Motors
Leg Connection
Gearheads
Spiral Bevel Gears
Rod End Spherical Joint (4x)
Rods
Links
Foot Connection

		REVISIONS		
ZONE	REV.	DESCRIPTION	DATE	APPROVED

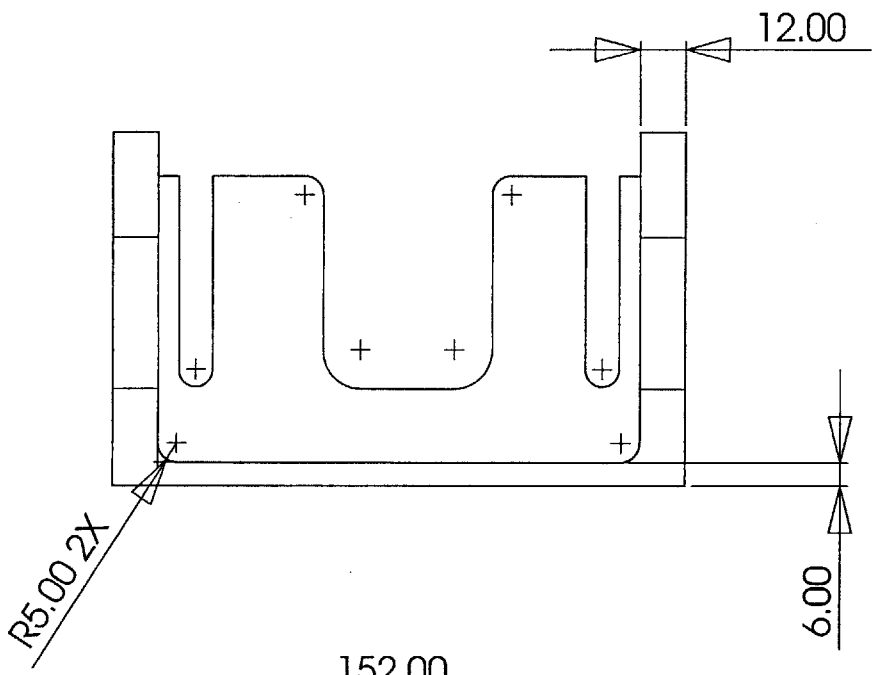

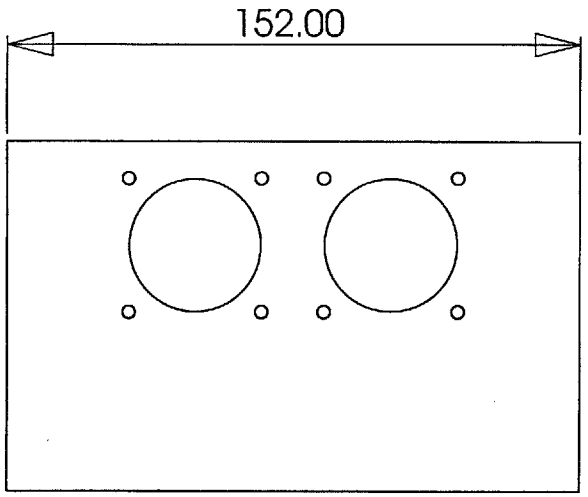

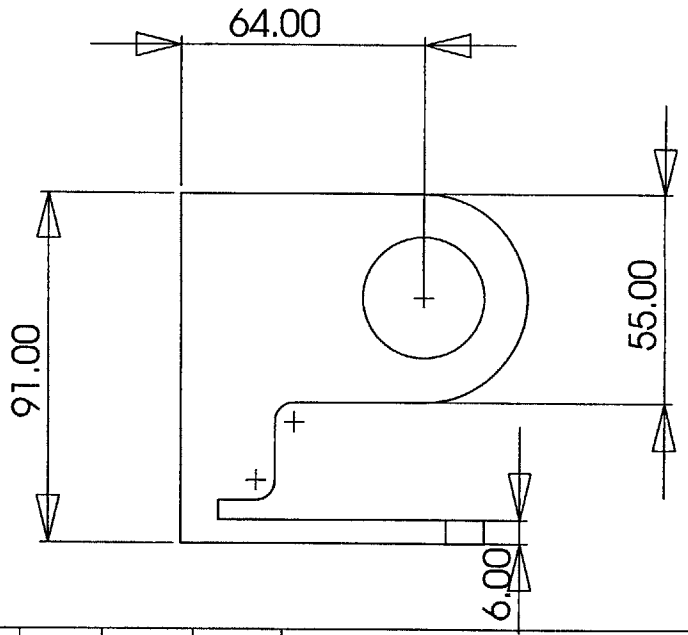

NEXT ASSY	USED ON
APPLICATION	

DIMENSIONS ARE IN MILLIMETERS
TOLERANCES:
ANGULAR: ± 0.5 DEG
TWO PLACE DECIMAL ±0.1
THREE PLACE DECIMAL ±0.01

MATERIAL AL 6061-T6

FINISH --

DO NOT SCALE DRAWING

	NAME	DATE
DRAWN	JWW	
CHECKED		
ENG APPR.		
MFG APPR.		
Q.A.		

COMMENTS:

MIT Newman Lab

Mounting Plate
Make 1 Piece
Major Dims

SIZE	DWG. NO.	REV.
A		
SCALE: 1:2	WEIGHT:	SHEET 1 OF 5

ZONE	REV.	REVISIONS DESCRIPTION	DATE	APPROVED

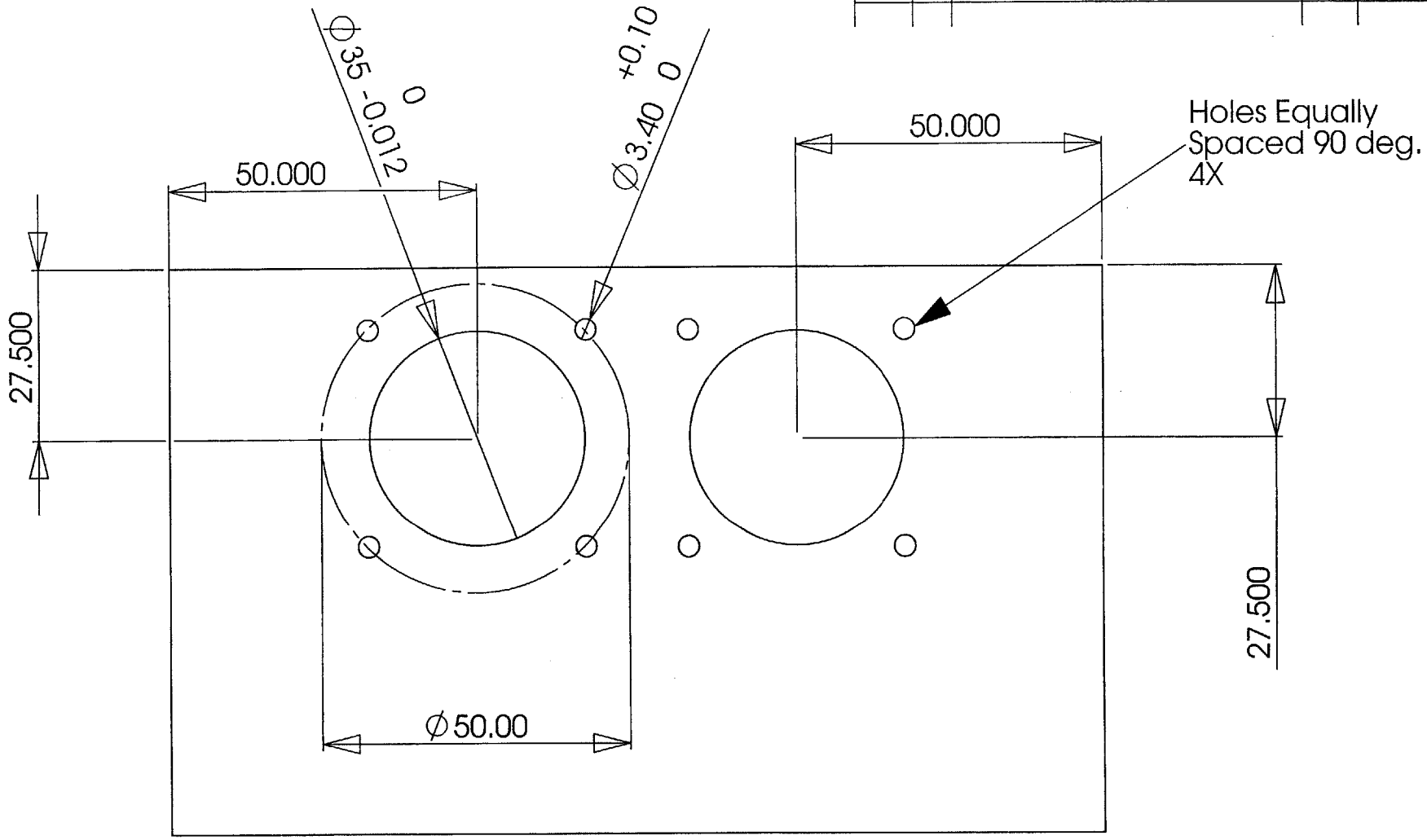

NEXT ASSY	USED ON
APPLICATION	

DIMENSIONS ARE IN MILLIMETERS
TOLERANCES:
ANGULAR: ± 0.5 DEG
TWO PLACE DECIMAL ±0.1
THREE PLACE DECIMAL ±0.01

MATERIAL AL 6061-T6

FINISH --

DO NOT SCALE DRAWING

	NAME	DATE
DRAWN	JWW	
CHECKED		
ENG APPR.		
MFG APPR.		
Q.A.		

COMMENTS:

MIT Newman Lab

Mounting Plate Make 1 Piece Top Detail

SIZE	DWG. NO.	REV.
A		

SCALE:1:2 | WEIGHT: | SHEET 2 OF 5

ZONE	REV.	REVISIONS DESCRIPTION	DATE	APPROVED

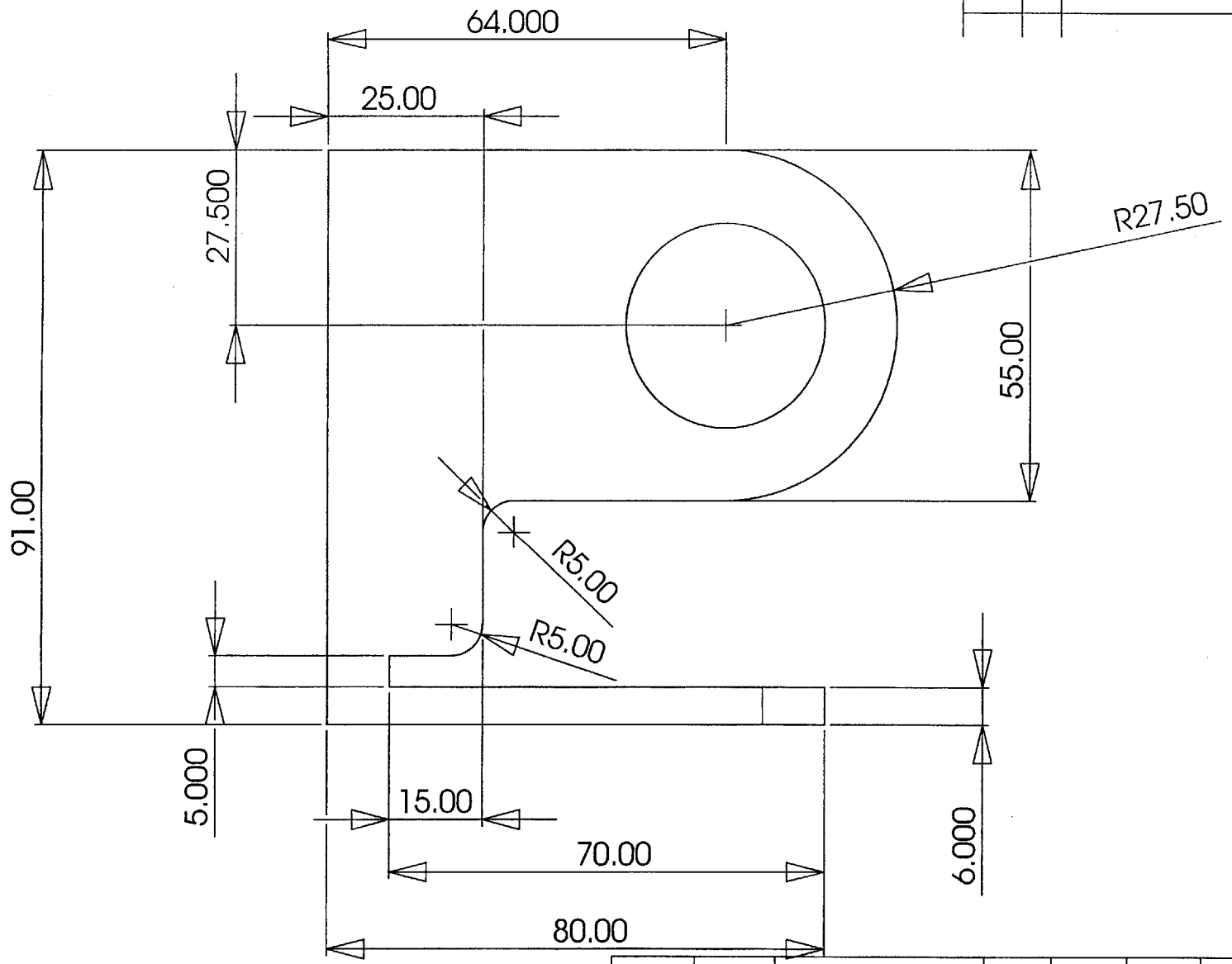

NEXT ASSY	USED ON
APPLICATION	

DIMENSIONS ARE IN MILLIMETERS
TOLERANCES:
ANGULAR: ± 0.5 DEG
TWO PLACE DECIMAL ±0.1
THREE PLACE DECIMAL ±0.01

MATERIAL AL 6061-T6

FINISH --

DO NOT SCALE DRAWING

	NAME	DATE
DRAWN	JWW	
CHECKED		
ENG APPR.		
MFG APPR.		
Q.A.		

COMMENTS:

MIT Newman Lab

Mounting Plate
Make 1 Piece
Side Detail

SIZE	DWG. NO.	REV.
A		
SCALE:1:2	WEIGHT:	SHEET 3 OF 5

ZONE	REV.	REVISIONS DESCRIPTION	DATE	APPROVED

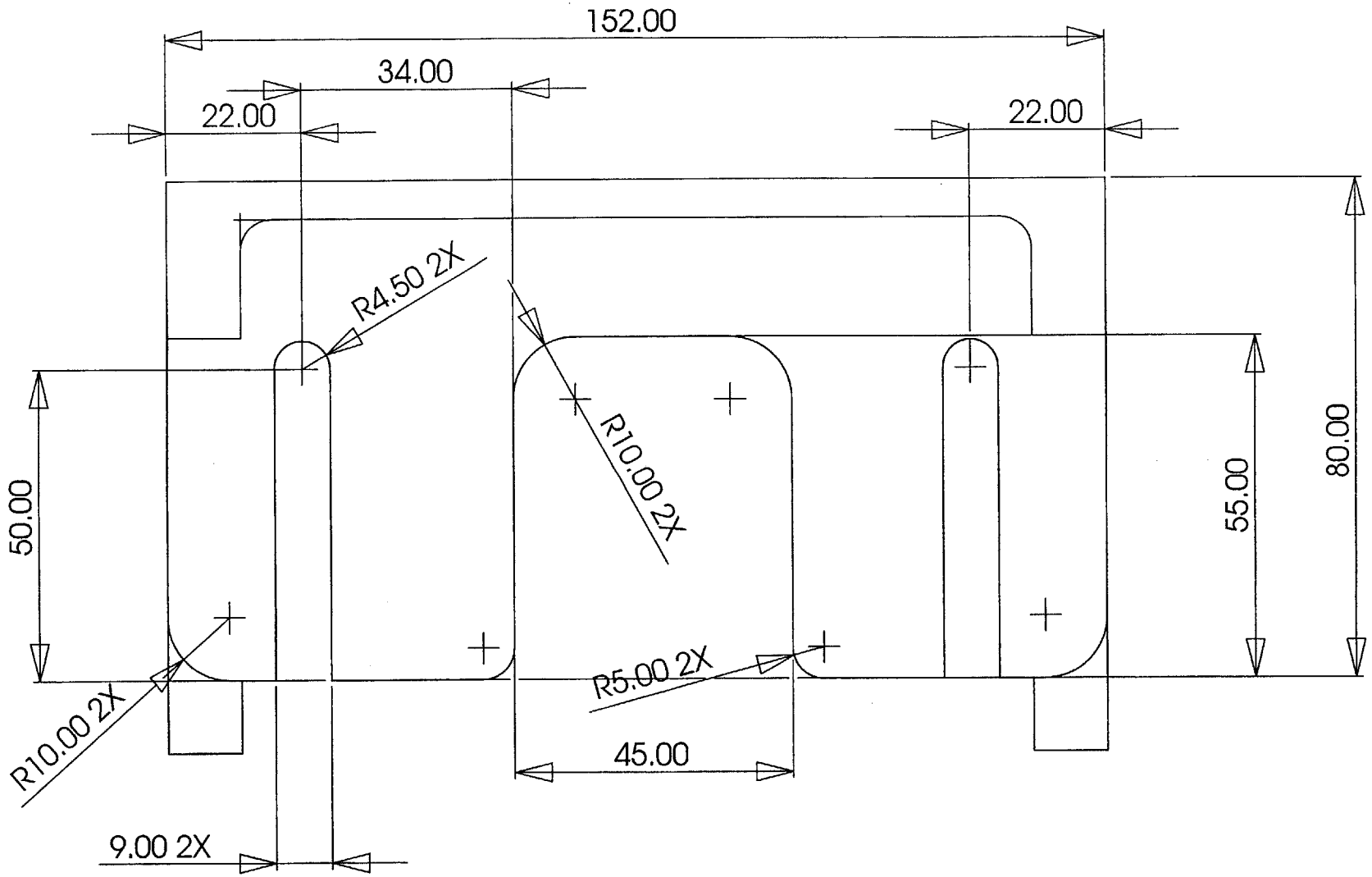

NEXT ASSY	USED ON
APPLICATION	

DIMENSIONS ARE IN MILLIMETERS
TOLERANCES:
ANGULAR: ± 0.5 DEG
TWO PLACE DECIMAL ±0.1
THREE PLACE DECIMAL ±0.01

MATERIAL AL 6061-T6

FINISH --

DO NOT SCALE DRAWING

	NAME	DATE
DRAWN	JWW	
CHECKED		
ENG APPR.		
MFG APPR.		
Q.A.		

COMMENTS:

MIT Newman Lab

Mounting Plate
Make 1 Piece
Rear Detail

SIZE	DWG. NO.	REV.
A		
SCALE:1:2	WEIGHT:	SHEET 4 OF 5

		REVISIONS		
ZONE	REV.	DESCRIPTION	DATE	APPROVED

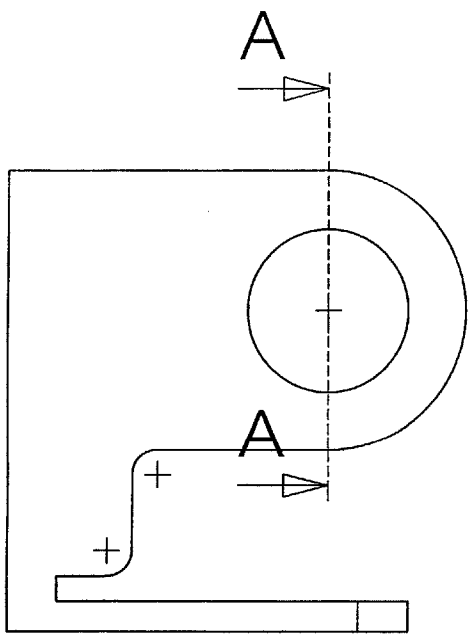

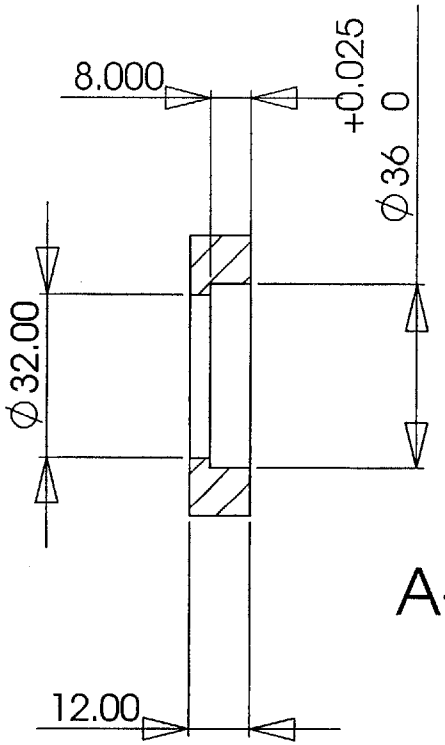

A-A (1 : 1.5)

NEXT ASSY	USED ON
APPLICATION	

DIMENSIONS ARE IN MILLIMETERS
TOLERANCES:
ANGULAR: ± 0.5 DEG
TWO PLACE DECIMAL ±0.1
THREE PLACE DECIMAL ±0.01

MATERIAL AL 6061-T6

FINISH --

DO NOT SCALE DRAWING

	NAME	DATE
DRAWN	JWW	
CHECKED		
ENG APPR.		
MFG APPR.		
Q.A.		

COMMENTS:

MIT Newman Lab

Mounting Plate Make 1 Piece Bearing Hole Sec.

SIZE	DWG. NO.	REV.
A		
SCALE:1:2	WEIGHT:	SHEET 5 OF 5

ZONE	REV.	REVISIONS DESCRIPTION	DATE	APPROVED

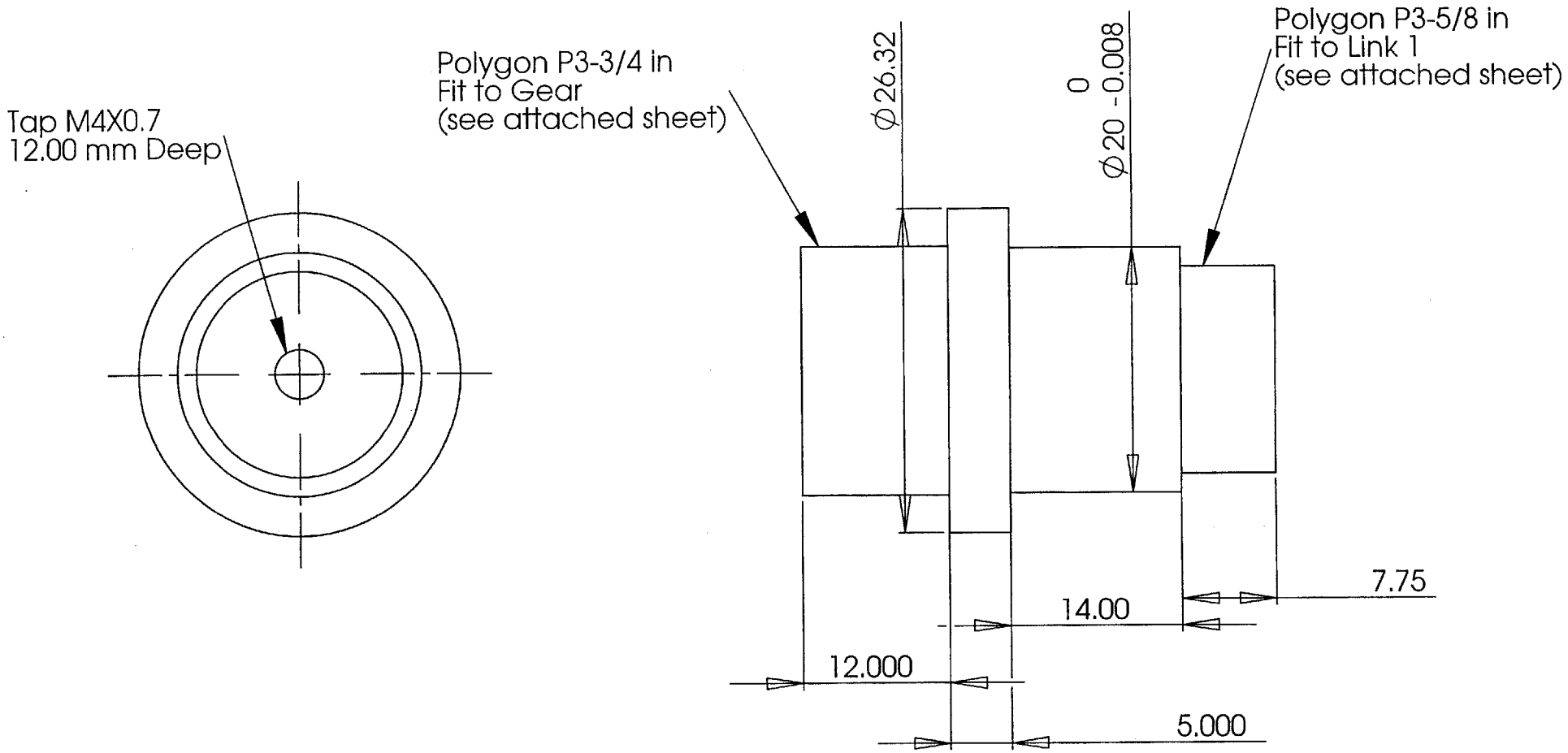

NEXT ASSY	USED ON
APPLICATION	

DIMENSIONS ARE IN MILLIMETERS
TOLERANCES:
TWO PLACE DECIMAL ±0.1
THREE PLACE DECIMAL ±0.01

MATERIAL AL 6061-T6

FINISH --

DO NOT SCALE DRAWING

	NAME	DATE
DRAWN	JWW	
CHECKED		
ENG APPR.		
MFG APPR.		
Q.A.		

COMMENTS:

MIT Newman Lab

Shaft
Make 2 Pieces

SIZE	DWG. NO.	REV.
A		
SCALE:2:1	WEIGHT:	SHEET 1 OF 1

REVISIONS				
ZONE	REV.	DESCRIPTION	DATE	APPROVED

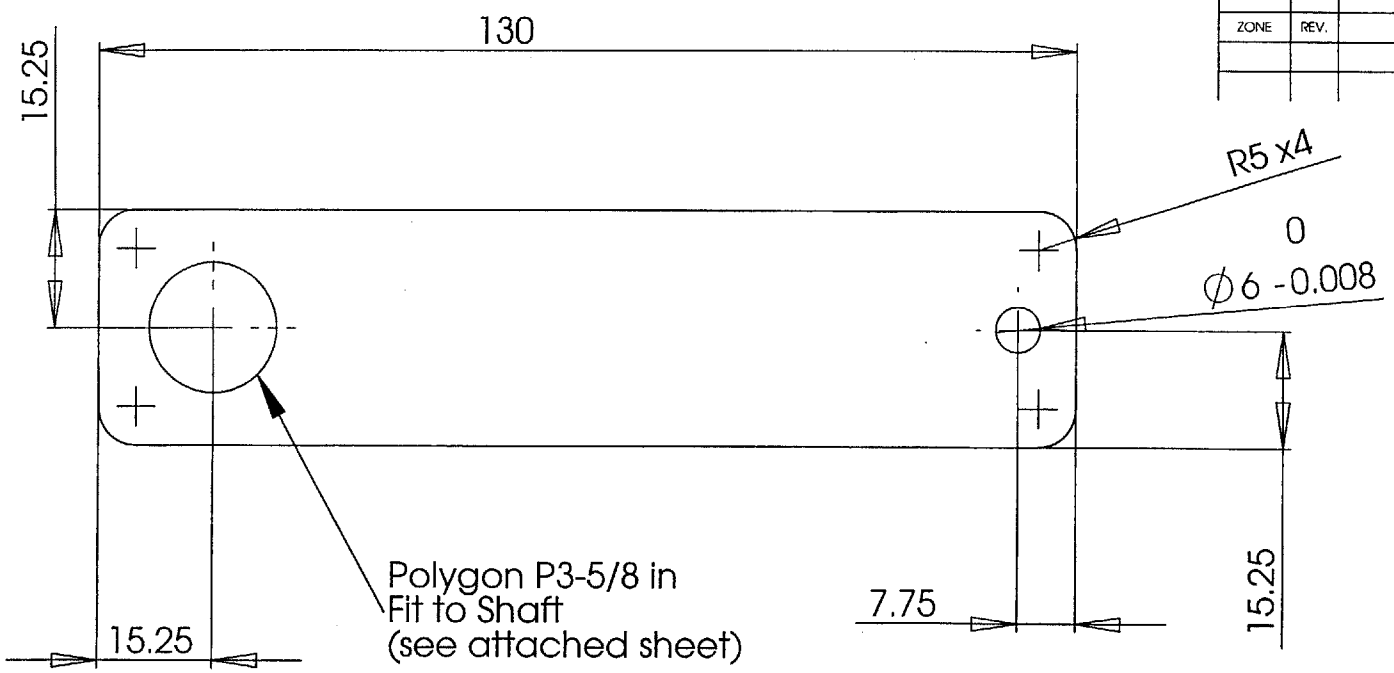

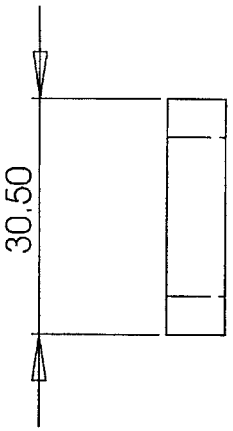

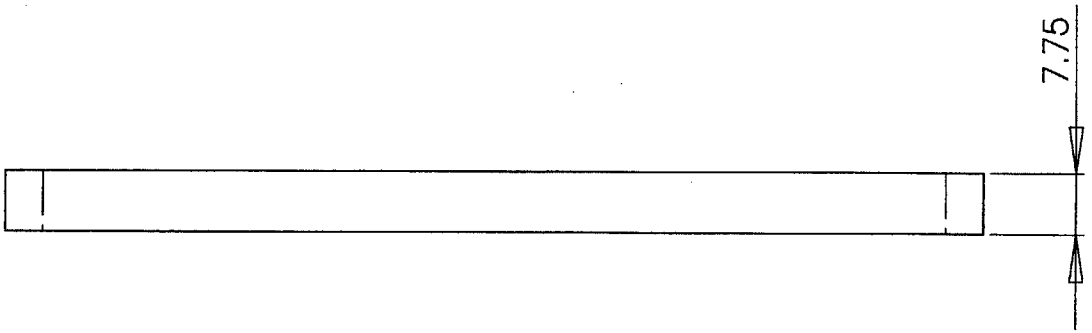

NEXT ASSY	USED ON
APPLICATION	DO NOT SCALE DRAWING

DIMENSIONS ARE IN MILLIMETERS
TOLERANCES:
TWO PLACE DECIMAL ±0.1
THREE PLACE DECIMAL ±0.01

MATERIAL AL 6061-T6
FINISH --

	NAME	DATE
DRAWN	JWW	
CHECKED		
ENG APPR.		
MFG APPR.		
Q.A.		

COMMENTS:

MIT Newman Lab

Link 1
Make 2 Pieces

SIZE	DWG. NO.	REV.
A		
SCALE:1:2	WEIGHT:	SHEET 1 OF 1

REVISIONS				
ZONE	REV.	DESCRIPTION	DATE	APPROVED

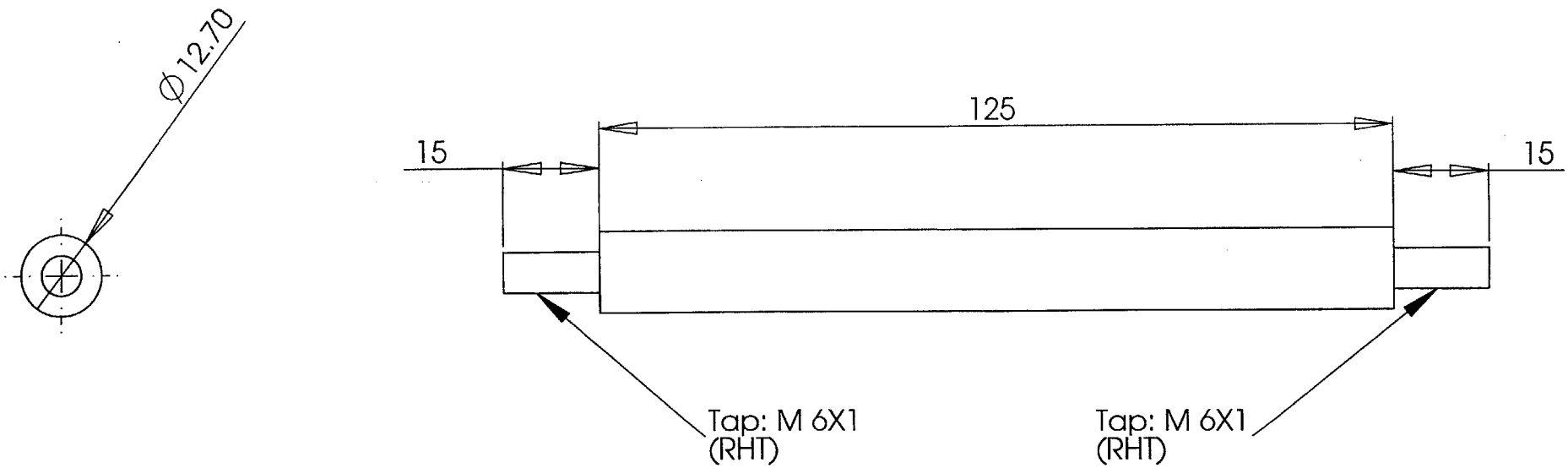

NEXT ASSY	USED ON
APPLICATION	

DIMENSIONS ARE IN MILLIMETERS
TOLERANCES:
TWO PLACE DECIMAL ± 0.1
THREE PLACE DECIMAL ± 0.01

MATERIAL AL 6061-T6

FINISH --

DO NOT SCALE DRAWING

	NAME	DATE
DRAWN	JWW	
CHECKED		
ENG APPR.		
MFG APPR.		
Q.A.		

COMMENTS:

MIT Newman Lab

Linkage Rod
Make 2 Pieces

SIZE	DWG. NO.	REV.
A		
SCALE:1:2	WEIGHT:	SHEET 1 OF 1

REVISIONS				
ZONE	REV.	DESCRIPTION	DATE	APPROVED

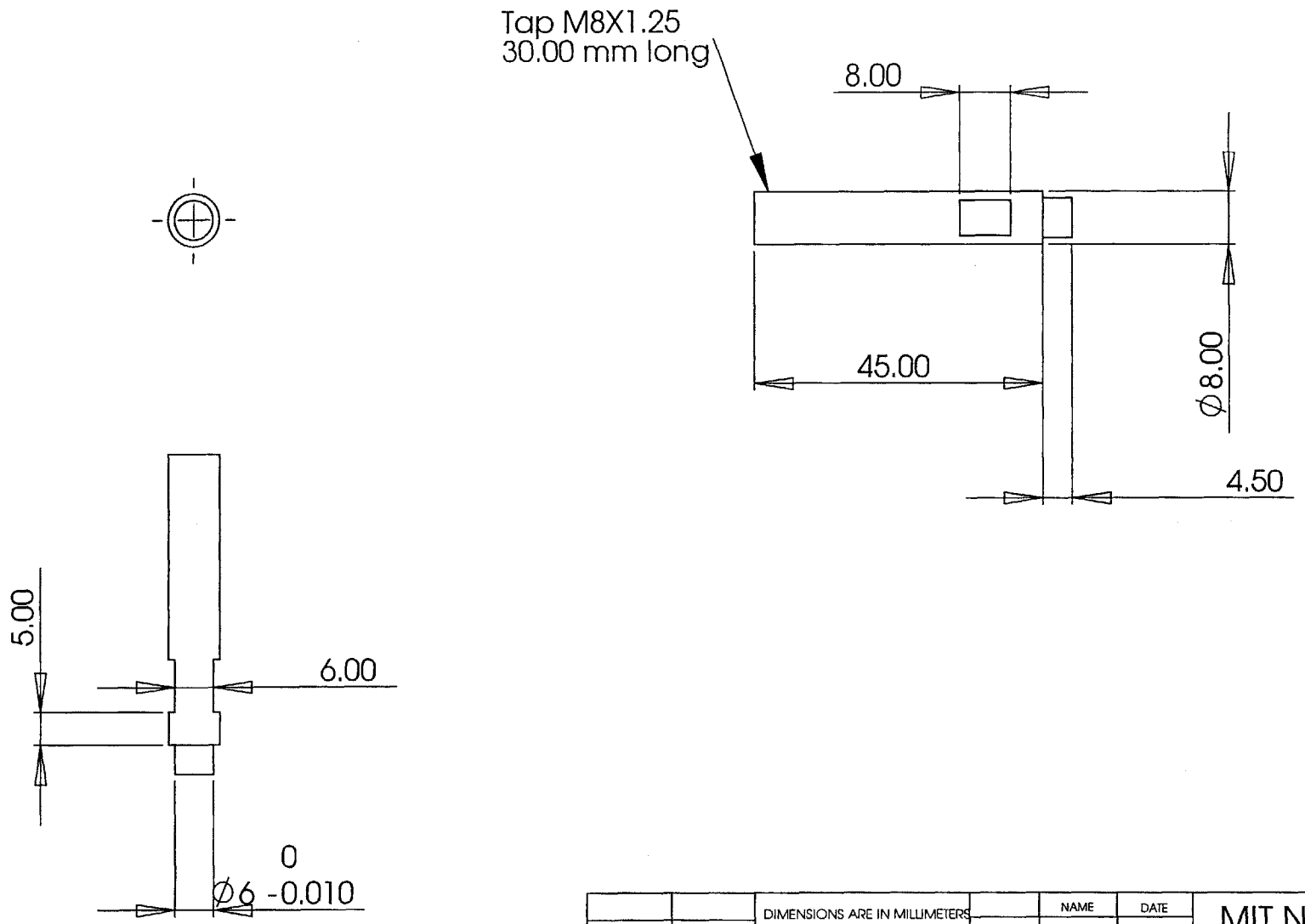

PROPRIETARY AND CONFIDENTIAL
THE INFORMATION CONTAINED IN THIS DRAWING IS THE SOLE PROPERTY OF MIT. ANY REPRODUCTION IN PART OR AS A WHOLEWITHOUT THE WRITTEN PERMISSION OF MIT IS PROHIBITED.

NEXT ASSY	USED ON
APPLICATION	

DIMENSIONS ARE IN MILLIMETERS
TOLERANCES:
ANGULAR: ± 0.5 DEG
TWO PLACE DECIMAL ±0.1
THREE PLACE DECIMAL ±0.01

MATERIAL AL 6061-T6

FINISH --

DO NOT SCALE DRAWING

	NAME	DATE
DRAWN	JWW	
CHECKED		
ENG APPR.		
MFG APPR.		
Q.A.		

COMMENTS:

MIT Newman Lab

PL Shaft 1
Make 1 Piece

SIZE	DWG. NO.	REV.
A		
SCALE:1:1	WEIGHT:	SHEET 1 OF 1

REVISIONS				
ZONE	REV.	DESCRIPTION	DATE	APPROVED

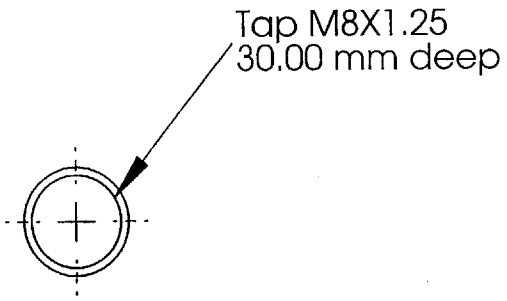

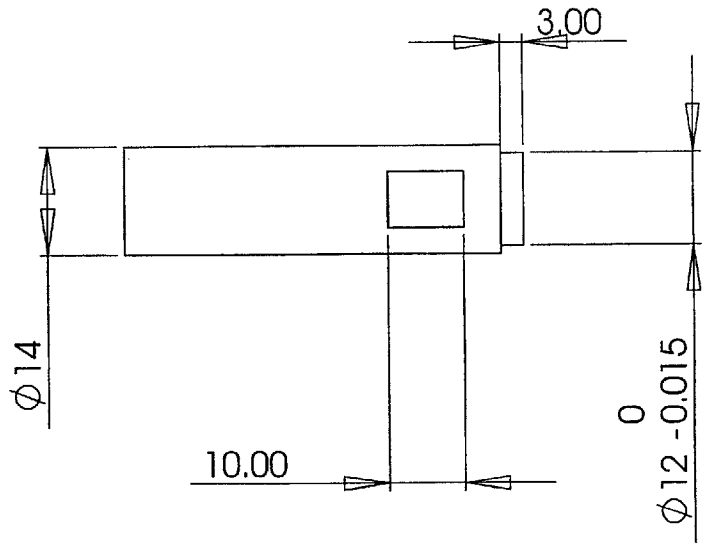

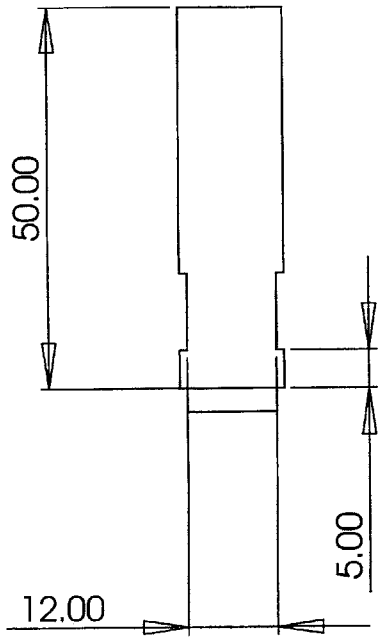

NEXT ASSY	USED ON
APPLICATION	

DIMENSIONS ARE IN MILLIMETERS
TOLERANCES:
ANGULAR: ± 0.5 DEG
TWO PLACE DECIMAL ±0.1
THREE PLACE DECIMAL ±0.01

MATERIAL AL 6061-T6

FINISH --

DO NOT SCALE DRAWING

	NAME	DATE
DRAWN	JWW	
CHECKED		
ENG APPR.		
MFG APPR.		
Q.A.		

COMMENTS:

MIT Newman Lab

PL Shaft 2
Make 1 Piece

SIZE	DWG. NO.	REV.
A		
SCALE:1:1	WEIGHT:	SHEET 1 OF 1

ZONE	REV.	REVISIONS DESCRIPTION	DATE	APPROVED

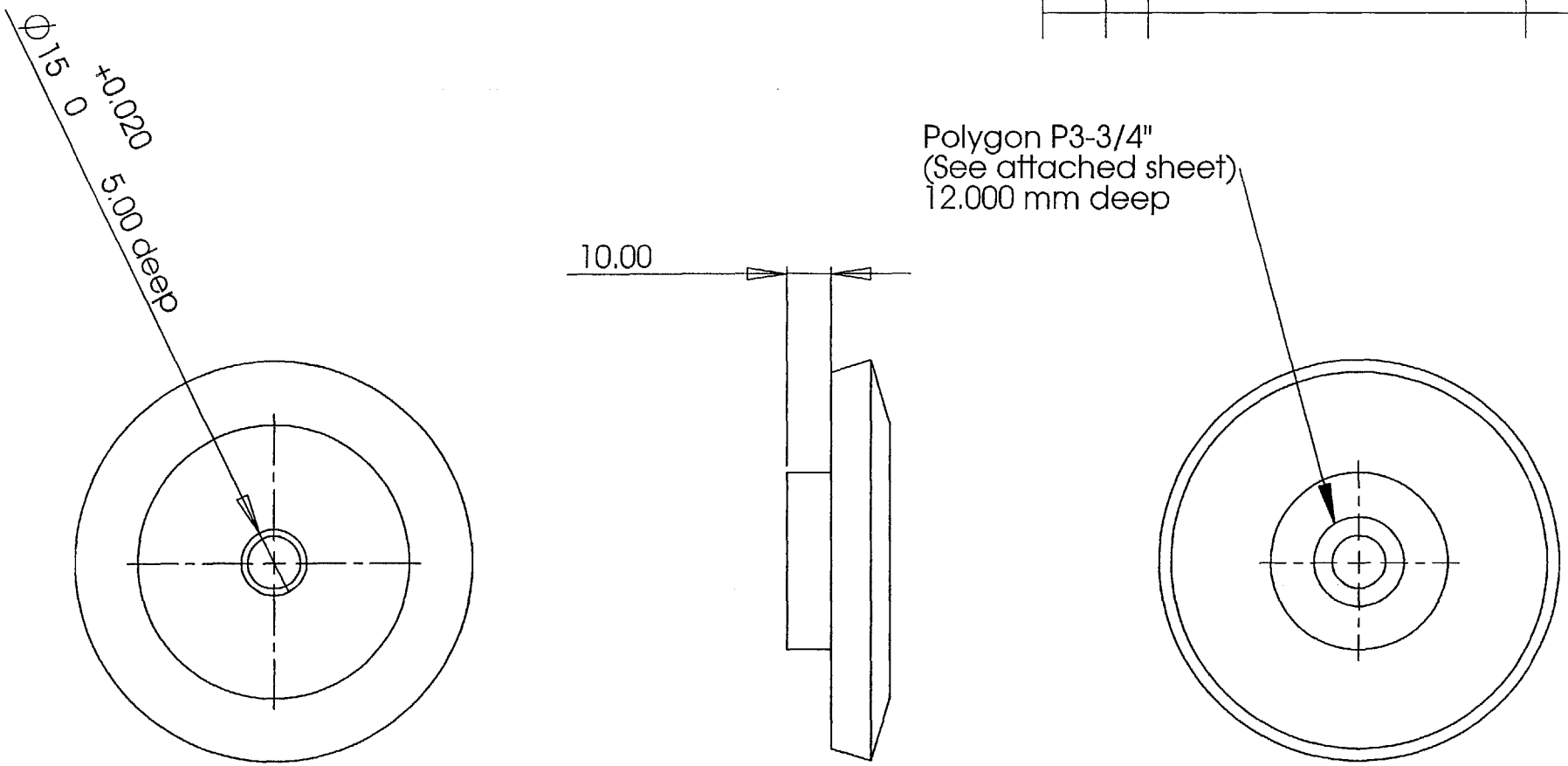

NEXT ASSY	USED ON
APPLICATION	

DIMENSIONS ARE IN MILLIMETERS
TOLERANCES:
TWO PLACE DECIMAL ±0.1
THREE PLACE DECIMAL ±0.01

MATERIAL Steel

FINISH --

DO NOT SCALE DRAWING

	NAME	DATE
DRAWN	JWW	
CHECKED		
ENG APPR.		
MFG APPR.		
Q.A.		

COMMENTS:

MIT Newman Lab

Gear Modifications
1 Piece

SIZE	DWG. NO.	REV.
A		
SCALE:1:2	WEIGHT:	SHEET 1 OF 1

ZONE	REV.	REVISIONS DESCRIPTION	DATE	APPROVED

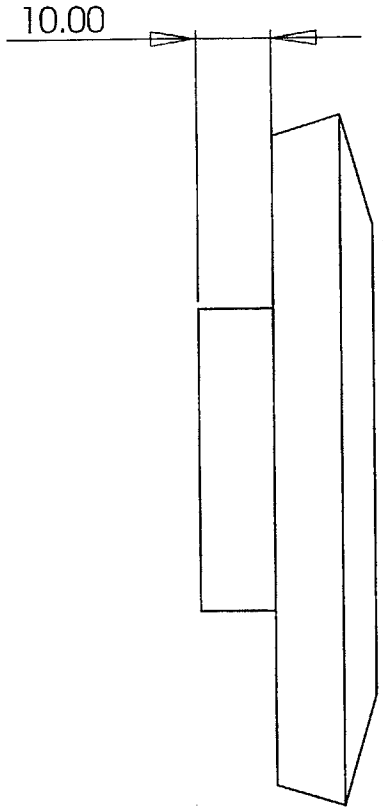

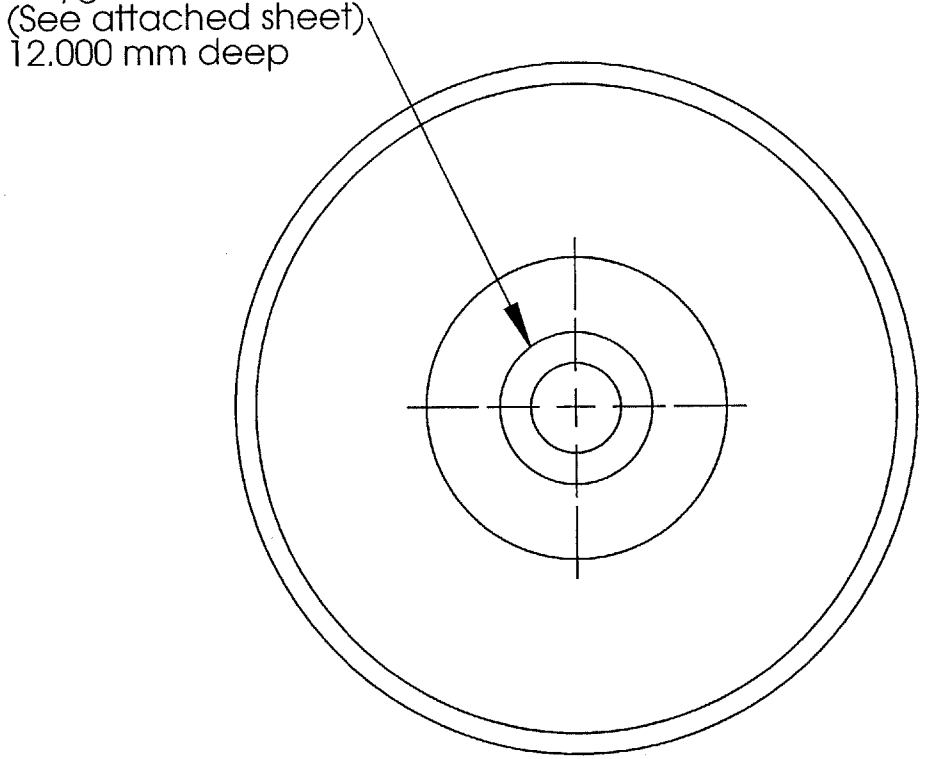

NEXT ASSY	USED ON	
APPLICATION		

DIMENSIONS ARE IN MILLIMETERS
TOLERANCES:
ANGULAR: ± 0.5 DEG
TWO PLACE DECIMAL ±0.1
THREE PLACE DECIMAL ±0.01

MATERIAL Steel

FINISH --

DO NOT SCALE DRAWING

	NAME	DATE
DRAWN	JWW	
CHECKED		
ENG APPR.		
MFG APPR.		
Q.A.		

COMMENTS:

MIT Newman Lab

Gear Modifications 2
1 Piece

SIZE	DWG. NO.	REV.
A		

SCALE:1:2 | WEIGHT: | SHEET 1 OF 1

ZONE	REV.	REVISIONS DESCRIPTION	DATE	APPROVED

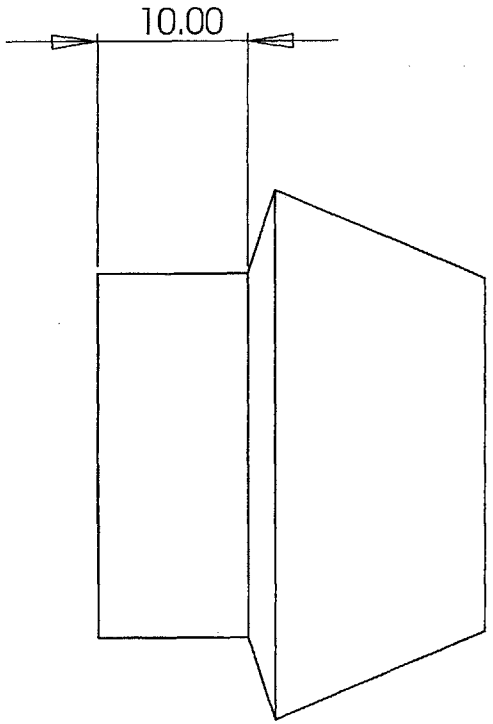

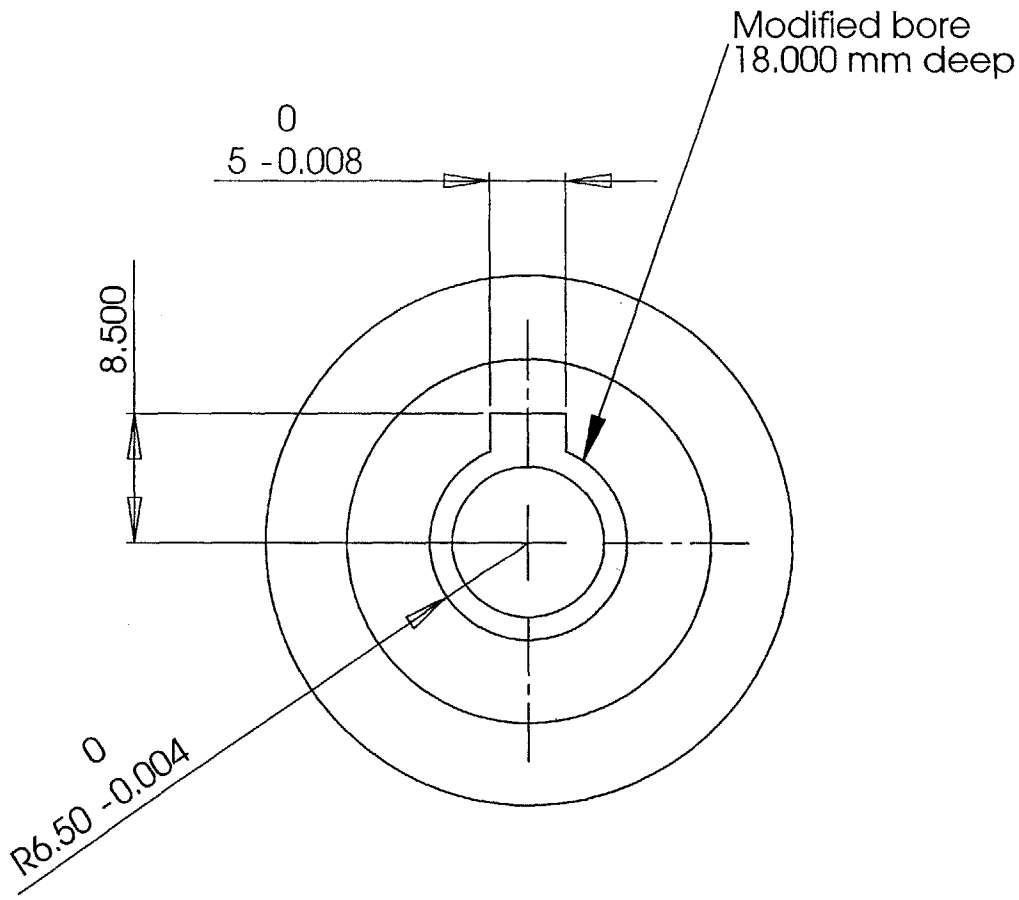

NEXT ASSY	USED ON
APPLICATION	

DIMENSIONS ARE IN MILLIMETERS
TOLERANCES:
TWO PLACE DECIMAL ±0.1
THREE PLACE DECIMAL ±0.01

MATERIAL Steel

FINISH --

DO NOT SCALE DRAWING

	NAME	DATE
DRAWN	JWW	
CHECKED		
ENG APPR.		
MFG APPR.		
Q.A.		

COMMENTS:

MIT Newman Lab

Pinion Modifications
2 Pieces

SIZE	DWG. NO.	REV.
A		
SCALE:2:1	WEIGHT:	SHEET 1 OF 1

REVISIONS				
ZONE	REV.	DESCRIPTION	DATE	APPROVED

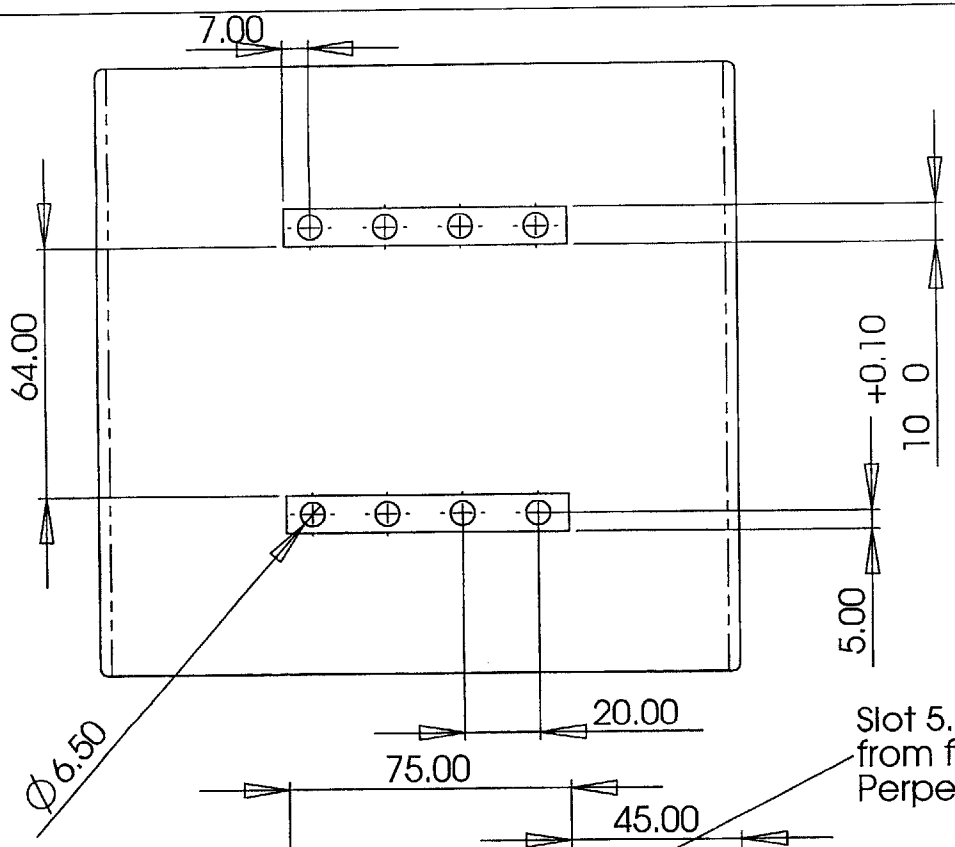

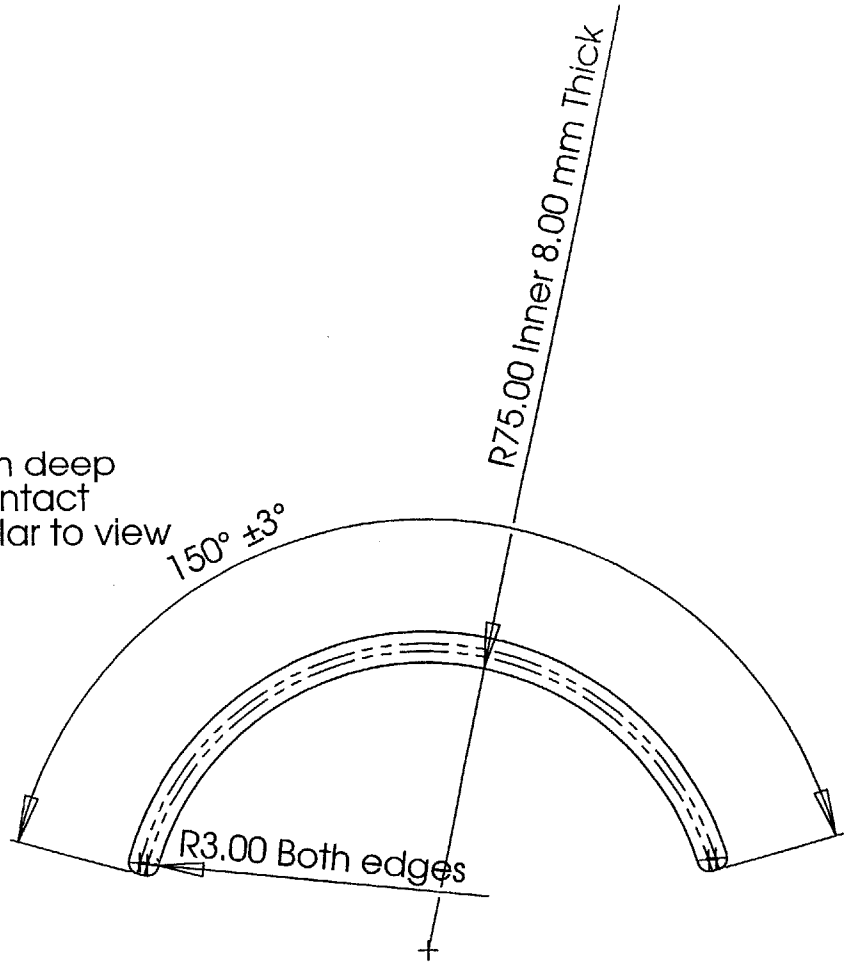

PROPRIETARY AND CONFIDENTIAL

THE INFORMATION CONTAINED IN THIS DRAWING IS THE SOLE PROPERTY OF MIT. ANY REPRODUCTION IN PART OR AS A WHOLEWITHOUT THE WRITTEN PERMISSION OF MIT IS PROHIBITED.

NEXT ASSY	USED ON	
APPLICATION		

DIMENSIONS ARE IN MILLIMETERS
TOLERANCES:
ANGULAR: ± 0.5 DEG
TWO PLACE DECIMAL ±0.1
THREE PLACE DECIMAL ±0.01

MATERIAL: HDPE

FINISH: --

DO NOT SCALE DRAWING

	NAME	DATE
DRAWN	JWW	
CHECKED		
ENG APPR.		
MFG APPR.		
Q.A.		

COMMENTS:

MIT Newman Lab

Leg Connection 1
Make 1 Piece

SIZE	DWG. NO.	REV.
A		
SCALE:1:2	WEIGHT:	SHEET 1 OF 1

ZONE	REV.	REVISIONS DESCRIPTION	DATE	APPROVED

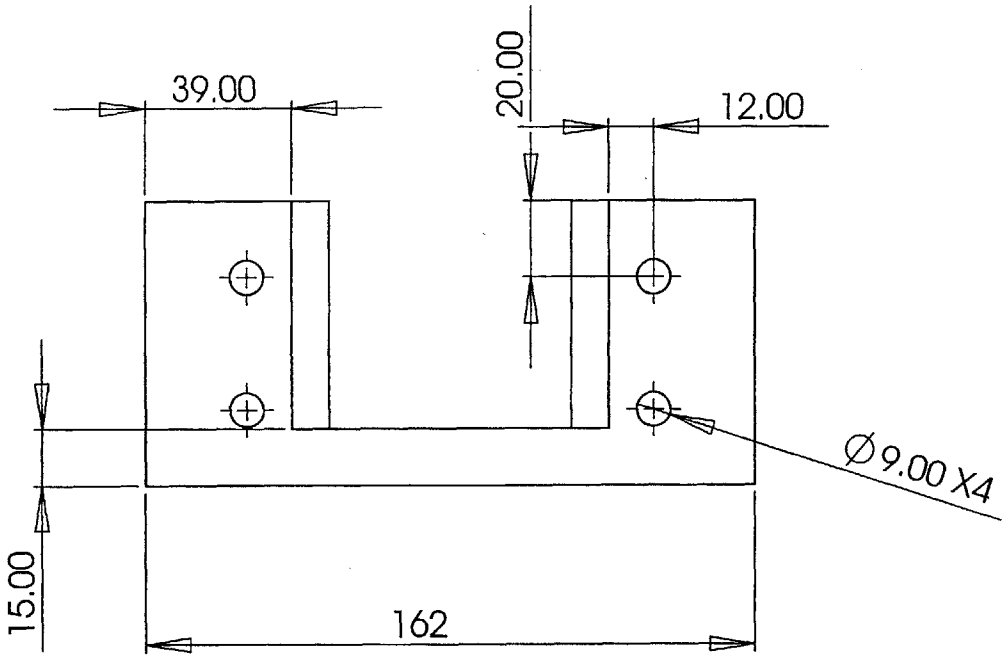

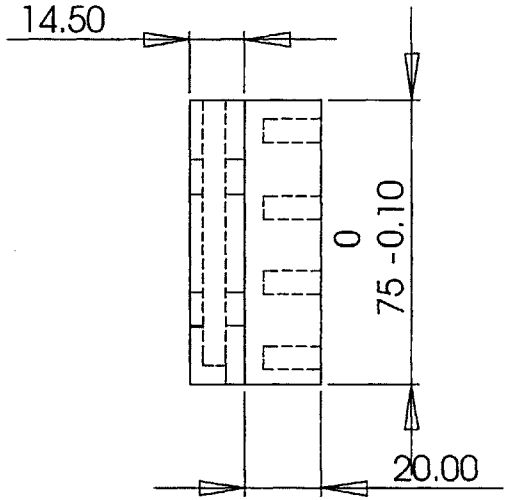

NEXT ASSY	USED ON
APPLICATION	

DIMENSIONS ARE IN MILLIMETERS
TOLERANCES:
ANGULAR: ± 0.5 DEG
TWO PLACE DECIMAL ±0.1
THREE PLACE DECIMAL ±0.01

MATERIAL AL 6061-T6

FINISH --

DO NOT SCALE DRAWING

	NAME	DATE
DRAWN	JWW	
CHECKED		
ENG APPR.		
MFG APPR.		
Q.A.		

COMMENTS:

MIT Newman Lab

Leg Connection 2
Make 1 Piece

SIZE	DWG. NO.	REV.
A		
SCALE:1:2	WEIGHT:	SHEET 1 OF 2

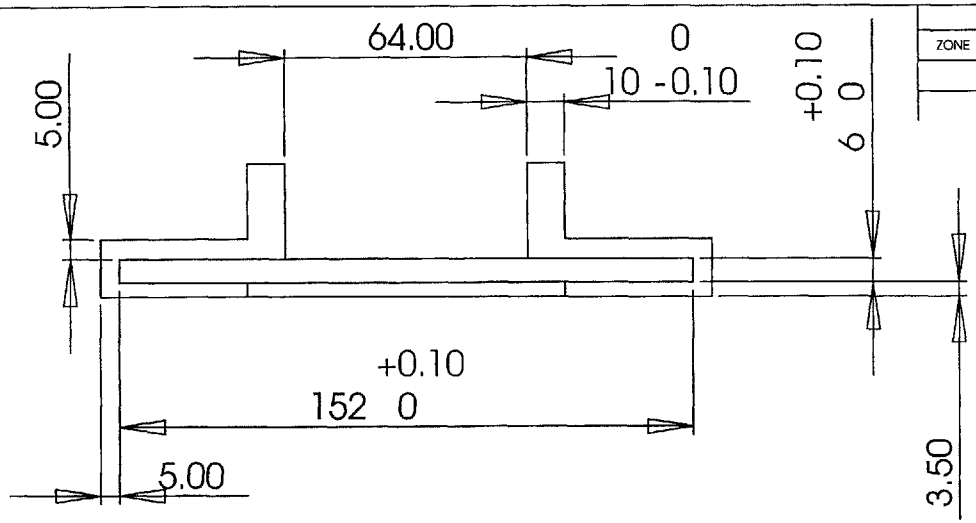

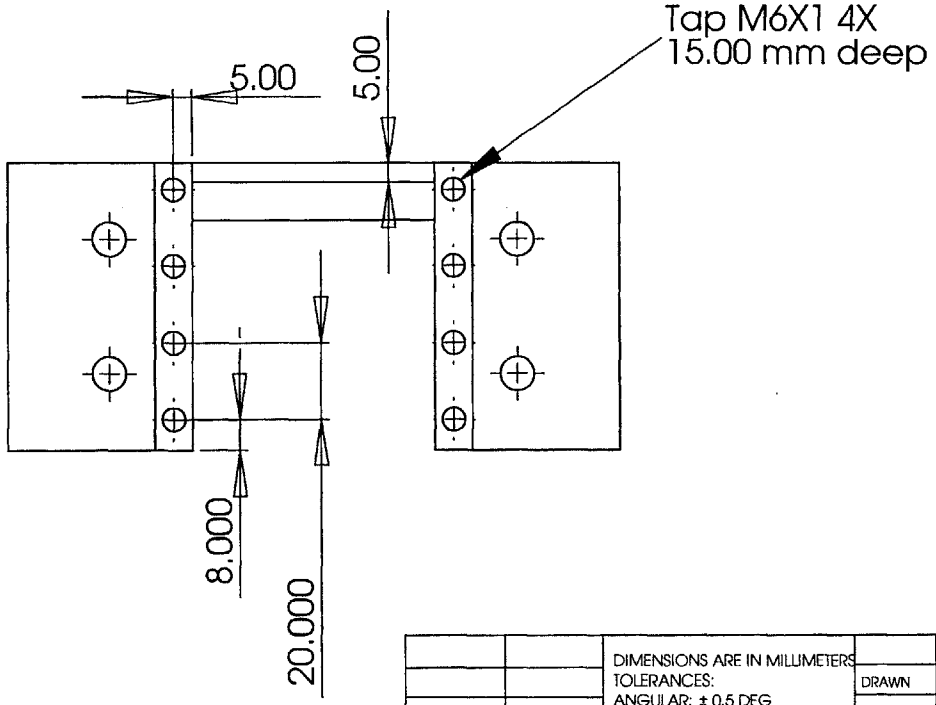

REVISIONS				
ZONE	REV.	DESCRIPTION	DATE	APPROVED

NEXT ASSY	USED ON	
APPLICATION		DO NOT SCALE DRAWING

DIMENSIONS ARE IN MILLIMETERS
TOLERANCES:
ANGULAR: ± 0.5 DEG
TWO PLACE DECIMAL ±0.1
THREE PLACE DECIMAL ±0.01

MATERIAL AL 6061-T6

FINISH --

	NAME	DATE
DRAWN	JWW	
CHECKED		
ENG APPR.		
MFG APPR.		
Q.A.		

COMMENTS:

MIT Newman Lab

Leg Connection 2
Make 1 Piece

SIZE	DWG. NO.	REV.
A		
SCALE:1:2	WEIGHT:	SHEET 2 OF 2

REVISIONS				
ZONE	REV.	DESCRIPTION	DATE	APPROVED

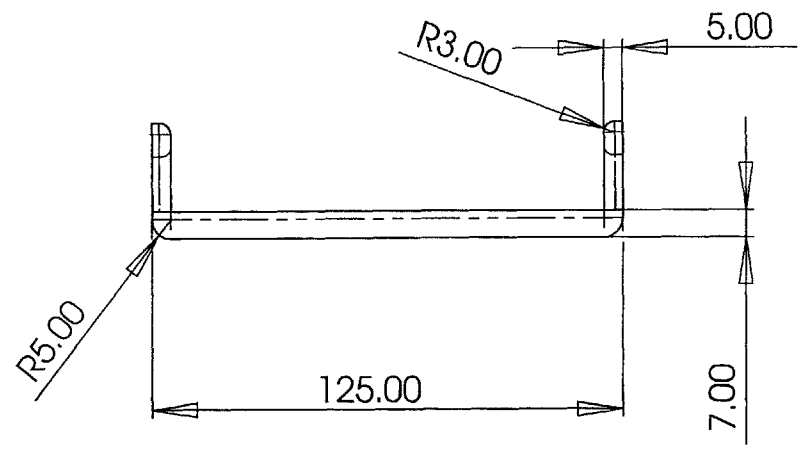

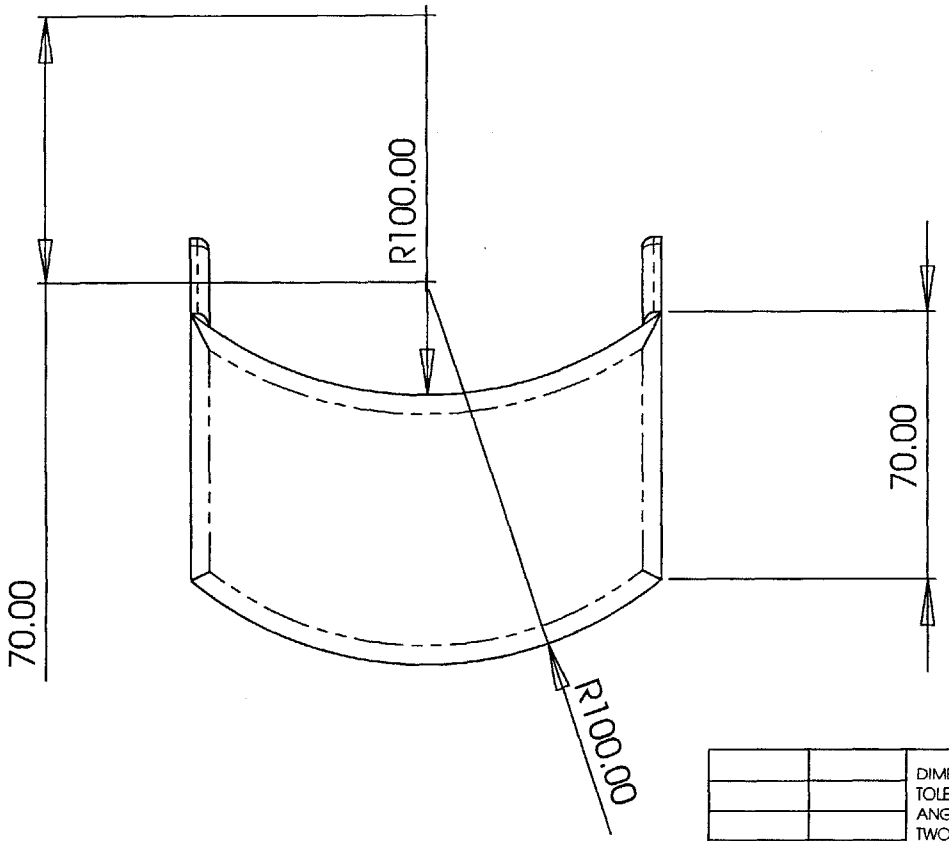

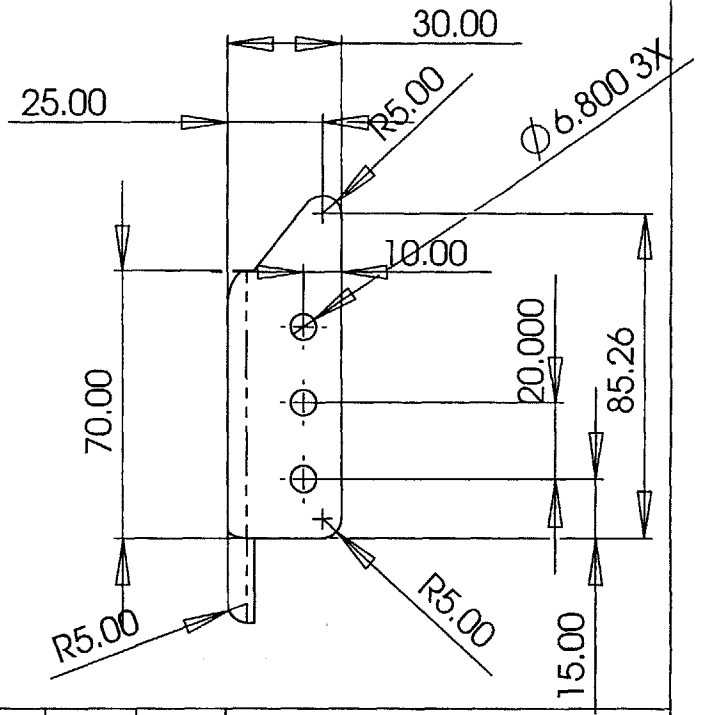

PROPRIETARY AND CONFIDENTIAL

THE INFORMATION CONTAINED IN THIS DRAWING IS THE SOLE PROPERTY OF MIT. ANY REPRODUCTION IN PART OR AS A WHOLEWITHOUT THE WRITTEN PERMISSION OF MIT IS PROHIBITED.

NEXT ASSY	USED ON
APPLICATION	

DIMENSIONS ARE IN MILLIMETERS
TOLERANCES:
ANGULAR: ± 0.5 DEG
TWO PLACE DECIMAL ±0.5
THREE PLACE DECIMAL ±0.1

MATERIAL HDPE

FINISH ---

DO NOT SCALE DRAWING

	NAME	DATE
DRAWN	JWW	
CHECKED		
ENG APPR.		
MFG APPR.		
Q.A.		

COMMENTS:

MIT Newman Lab

Foot Connection 1
Make 1 Piece

SIZE	DWG. NO.	REV.
A		
SCALE: 1:2	WEIGHT:	SHEET 1 OF 1

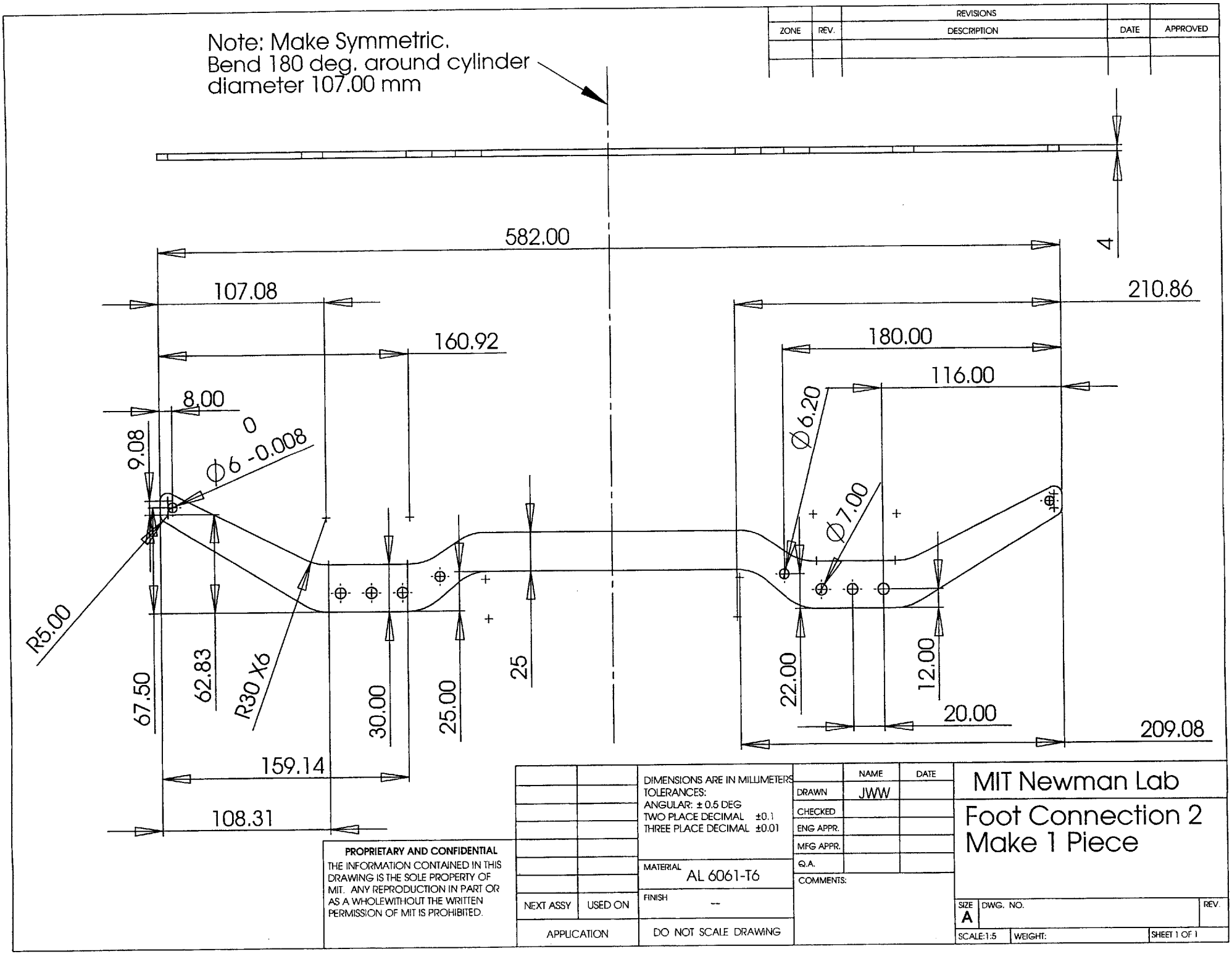

REVISIONS				
ZONE	REV.	DESCRIPTION	DATE	APPROVED

PROPRIETARY AND CONFIDENTIAL

THE INFORMATION CONTAINED IN THIS DRAWING IS THE SOLE PROPERTY OF MIT. ANY REPRODUCTION IN PART OR AS A WHOLEWITHOUT THE WRITTEN PERMISSION OF MIT IS PROHIBITED.

NEXT ASSY	USED ON
APPLICATION	

DIMENSIONS ARE IN MILLIMETERS
TOLERANCES:
ANGULAR: ± 0.5 DEG
TWO PLACE DECIMAL ±0.1
THREE PLACE DECIMAL ±0.01

MATERIAL AL 6061-T6

FINISH --

DO NOT SCALE DRAWING

	NAME	DATE
DRAWN	JWW	
CHECKED		
ENG APPR.		
MFG APPR.		
Q.A.		

COMMENTS:

MIT Newman Lab

Foot Connection 2
Make 1 Piece

SIZE	DWG. NO.	REV.
A		
SCALE:1:5	WEIGHT:	SHEET 1 OF 1

Bibliography

[1] Aisen, M. L., H. I. Krebs, N. Hogan, F. McDowell, and B. T. Volpe. 1997. The Effect of Robot-Assisted Therapy and Rehabilitative Training on Motor Recovery Following Stroke. *Archives of Neurology* 54:443-446.

[2] H. I. Krebs, N. Hogan, Aisen, M. L., and B. T. Volpe. 1998. Robot-aided neurorehabilitation. *IEEE Transactions on Rehabilitation Engineering* 6:75-87.

[3] About Stroke — Internet Stroke Center: http://www.strokecenter.org/pat/about.htm.

[4] Smidt G.L. 1990. Gait in Rehabilitation. New York, Churchill Livingstone.

[5] Whittle, Michael. 2001. Gait Analysis: An Introduction. Butterworth-Heinemann; 3rd edition.

[6] Perry, Jacqueline. 1992. Gait Analysis: Normal and Pathological Function. Slack.

[7] Seliktar, Rami and Bo, Lin. 1994. "The Theory of Kinetic Analysis in Human Gait." Gait Analysis: Theoty and Application. Edited by Craik and Oatis. St. Louis. Mosby.

[8] M. J. Kandel, I. A. Kapandji, 1987. The Physiology of the Joints: Annotated Diagrams of the Mechanics of the Human Joints: Lower Limb, 5th Ed. Edinburgh: Churchill Livingstone.

[9] Wooley, Sandra M. "Characteristics of Gait in Hemiplegia." Topics in Stroke Rehabilitation, 71:4. Winter 2001. Thomas Land Publications.

[10] Bassille, Clare and Bock, Connie. 1994. "Gait Training." Gait Analysis: Theory and Application. Edited by Craik and Oatis. St. Louis. Mosby.

[11] Zhang, L-Q, S.G. Chung, Zhiqiang Bai, Dali Xu, E. van Rey, M.W. Rogers, M.E. Johnson, E.J. Roth. 2002. Intelligent stretching of ankle joints with contracture/spasticity. IEEE Trans. Rehab. Eng, 10:149-157, 2002.

[12] Wu, Kent K. 1990. Foot Orthoses: Principles and Clinical Applications. Lippincott, Williams and Wilkins.

[13] Blaya, Joaquin A. 2003. Force-Controllable Ankle Foot Orthosis (AFO) to Assist Drop Foot Gait. MSME Thesis, Massachusetts Institute of Technology.

[14] Norton, Robert L., 1999. Design of Machinery: An Introduction to the Synthesis and Analysis of Mechanisms and Machines. McGraw-Hill, New York.

[15] Stock Drive Products Metric Drive Handbook of Components 2003, technical section.

[16] Wright, I.C., R.R. Neptune, A.J. van den Bogert, B.M. Nigg, 2000. The Influence of Foot Positioning on Ankle Sprains. Journal of Biomechanics 33:513-519.

[17] Colombo G, Joerg M, Schreier R, Dietz V. 2000. Treadmill training of paraplegic patients using a robotic orthosis. Journal of Rehabilitation Research and Development. 37(6):693-700.

[18] Hesse, Stefan and Uhlenbrock, Dietmar. 2000. A mechanized gait trainer for restoration of gait. Journal of Rehabilitation Research and Development 37:6, November/December.

[19] Krebs, H. I., B. T. Volpe, M. L. Aisen, and N. Hogan. 2000. Increasing productivity and quality of care: Robot-aided neuro-rehabiltation. *Journal of Rehabiltation Research and Development* 37:639-652.

[20] National Stroke Association. 2002. *http://www.stroke.org.*

[21] Shigley, Joseph E. and C. R. Mischke. 1989. *Mechanical Engineering Design.* 5th ed. New York, NY: McGraw-Hill.

[22] Norton, Robert L. 1998. *Machine Design: An Integrated Approach.* Saddle River, NJ: Prentice-Hall.

[23] Slocum, Alexander H. 1992. *Precision machine design.* Dearborn, MI: Society of Manufacturing Engineers.

[24] Celestino, J. 2003. Characterization and Control of a Robot for Wrist Rehabilitation. MSME Thesis, Massachusetts Institute of Technology.

[25] D.A. Winter. J. J. Eng, M. G. Ishac, 1995. "A review of Kinetic Parameters in Human Wlaking," in Gait Analysis: Theory and Application, R.L. Craik and C. A. Oatis, St. Louis: Mosby.

[26] Kollmorgen Motors. 2004. *http://www.motionvillage.com/products/motors/*

[27] Moxon Motors. 2004. *http://www.maxonmotor.com/*

[28] SKF Bearings. 2004. *http://www.skf.com/*

[29] THK Motion Products. 2004. *http://www.thk.com/*

[30] Harmonic Drive AG. 2004. *http://www.harmonicdrive.de/*

[31] Boston Gear. 2004. *http://www.bostongear.com/*

[32] Jones, Lynette A. 2003. Perceptual Constancy and the perceived magnitude of muscle forces. *Experimental Brain Research* 151:197-203.